NTNU – Trondheim
Norwegian University of
Science and Technology

Application of Extended Elastic Impedance (EEI) to improve Reservoir Characterization

Seyed Ali Gharaee Shahri

Petroleum Geosciences
Submission date: June 2013
Supervisor: Per Åge Avseth, IPT

Norwegian University of Science and Technology
Department of Petroleum Engineering and Applied Geophysics

Preface

This thesis is prepared as part of fulfillment for the degree of Master of Science in Petroleum Geosciences (TPG 4925-Petroleum Geophysics) at the Norwegian University of Science and Technology (NTNU) at the Department of Petroleum Engineering and Applied Geophysics.

Acknowledgements

I wish to express my sincere thanks to Norwegian University of Science and Technology (NTNU) for providing the opportunity to pursue my Master degree in this university and providing all the necessary facilities to carry out this project.

I place on record, my sincere gratitude to Professor Per Avseth, my teaching supervisor at NTNU, for suggesting the research topic and his constant help and encouragement.

I take this opportunity to express my sincere thanks to all the faculty members of the Department of Petroleum Engineering and Applied Geophysics for their help and encouragement.

I also place on record, my sincere gratitude to Spring Energy and Tullow Oil plc for providing the necessary data and their support.

Abstract

The Extended Elastic Impedance (EEI) as a seismic attribute was first introduced by Whitcombe (2002) as a method for fluid and lithology prediction. EEI is the application of angle rotation in the conventional acoustic impedance under certain approximation. It essentially works by projecting intercept and gradient together with different angles which highlights different features.

EEI has capability to estimate elastic parameters such as S-wave impedance, V_P/V_S ratio, bulk modulus, shear modulus, Poisson`s ratio and so on. It also provides reservoir physical properties like porosity, clay content and water saturation.

EEI is an interesting subject in Geosciences and is very useful seismic reconnaissance attribute. Its ability to predict fluids and lithology is well proven especially in the area where the acoustic impedance of gas saturated sands and surrounding shale are almost equal. This approach allows a better distinction between seismic anomaly caused by lithology and those caused by fluid content (hydrocarbon).

In this study, the concept of extended elastic impedance inversion is used to derived petrophysical properties and distribution of reservoir facies to create relationship between these attributes and well log data. The results show that EEI is worthy effort to highlight the difference between reservoir and non-reservoir to identify hydrocarbon area.

Keywords: Well log analysis, Rock physics, Seismic inversion, Elastic impedance, Extended elastic impedance (EEI)

Contents

List of Figures

List of Tables

1. Introduction

1.1 Problem description

While we can claim that all of easily exploited hydrocarbon fields have already been discovered, the global energy market is still striving for more oil and gas. Higher demands for hydrocarbon in recent years caused oil and gas industry players to focus on deep water, and frigid/hot regions around the world. Even by overcoming the geographical challenges there still remain serious problematic areas to deal with.

Another challenge in the world of seismic exploration is the subsurface ambiguities, which can be a difficult task in most regions in addition to gathering and analyzing data quickly and efficiently. We are always looking for the best image of subsurface for more accurate and low risk decision making to reduce drilling risk (dry wells) and increasing yield. Advanced techniques provide vast amount of information that can help to address the challenges which improves our interpretation of subsurface structures and also reveal more information about hydrocarbon prospects. Global competition for hydrocarbon continues to drive the need to increase exploration and enhance recovery rate; however the cost of the operation is critically important.

The seismic reflection method was used initially as a useful tool for structure identification; some kind of structures could act as trap (such as anticline) for hydrocarbon reservoir (Russell, Brian., Hampson, Dan., Bankhead, Bradley, 2006). So much effort has been made to improve our understanding of the amplitudes of the seismic reflection. It has been proved that a considerable amount of information is contained in seismic amplitude reflection that could be connected with porosity, lithology and even fluid change within the subsurface (Russell et al, 2006). Although seismic amplitude is fairly good indicator in the subsurface; however, several case studies show that it is an ambiguous indicator of hydrocarbon.

To overcome the limitation, amplitude versus offset (AVO) was born and developed as a commercial tool to analysis the pre-stack seismic data for reservoir prediction and hydrocarbon indication in petroleum industry. An AVO response is stemmed from a change in subsurface

reflectivity as a function of angle of incidence exhibited by seismic reflection events (Russell, 1999). A consequence of increase in offset/angle is the reflectivity change. This reflectivity variation depending on the P-wave velocity, S-wave velocity (shear wave velocity) and density contrast over an interface. It has been proved that change in fluid or lithology can give rise to variation in these properties and therefore vary AVO response (Russell et al, 2006).

In order to obtain more accurate seismic reservoir characterization (also known as reservoir geophysics) we should integrate all available seismic, petrophysical and geological information into the volumetric distribution of reservoir properties like porosity and saturation. Each of them has a piece of information which assists us to delineating or describing a reservoir or monitoring the change (Walls, Joel., Dvorkin, Jack., Carr, Matt, 2004).

“Wells can measure several reservoir properties at high vertical resolution, but offer only sparse sampling laterally”, often at considerable cost (Russell, 1988). In addition difficulties arise; however, when we encounter poor wellbore condition or unexpected lithology or complexities related to subsurface structure. On the other hand, “seismic data provides nearly continuous lateral sampling at relatively low expense but with much less vertical resolution” (Russell, 1988). To address the challenges, seismic inversion for estimating the elastic properties was introduced. It is the latest advancement in an integration approach which is the inverse modeling of the logs from seismic data.

By inversion, we convert seismic reflection amplitude to impedance profile (rock property information) and estimate model parameters (in term of impedance instead of reflectivity). Using inversion process, we try to “reduce discrepancies between observed and modeled seismic data” (Russell, 1988). The main objective here is to extract underlying geology and reservoir properties from some set of observed seismic data to use for better lithology and fluid prediction and prospect delineation (Russell, 1999). That is to say, the purpose is to obtain reliable estimate of P-wave velocity, S-wave velocity and density to calculate the physical properties and the earth`s structure.

With more complex geological conditions and rise in cost of hydrocarbon explorations, the inversion technique has become more popular and is widely used in the seismic industry for exploration and development of existing field. Inversion technique is a useful tool to derive

elastic properties such as P-impedance, bulk modulus, Poisson`s ratio and so forth, which largely control the seismic response. As a result the outcomes we obtain from seismic inversion make up better volumetric estimation (hydrocarbon anomalies are better predicted) than seismic attributes derived from band limited seismic data (Connolly, 1999).

It has been suggested to integrate inversion results with AVO and other attributes to improve interpretation accuracy and get more valuable results for reservoir modeling and characterization.

1.2 Motivation

The main idea of this research is to use application of extended elastic impedance inversion (EEI) to improve reservoir characterization and enhance lithology and fluid discrimination. The aim of this study is to determine the sensitivity of elastic parameters to seismic anomaly and show that extended elastic impedance is an effective way for lithology and fluid differentiation in clastic reservoir. The output of this work can be beneficial for static model building and volumetric calculation; therefore it might be advantageous in future field development.

1.3 Available dataset

In this study, exported 2D seismic inversion data has been used along with a random line (including AI, V_P/V_S and density) intersecting 2 wells located in Norwegian Sea. The data set is listed below:

Seismic information	
Type of seismic data	**Format**
AI inversion	SEG-Y
V_P/V_S inversion	SEG-Y
Density	SEG-Y

Well log information						
Type of well log / **Well name**	Gamma ray	Resistivity	Density	P-wave sonic	S-wave sonic	Check shot
6507/11-8	×	×	×	×	×	×
6507/11-9	×	×	×	×	×	×

Table 1.1: Available data

1.4 Method

The workflow used in this study is divided into three main phases with petrophysical analysis as the starting point. Rock physics of the formation will be examined to establish the relationship between petrophysical data and elastic properties. This step involves preparing the well logs to generate new log attributes, namely, V_P/V_S, bulk modulus, shear modulus, Poisson`s ratio, LMR, etc. It is followed by well base cross plot analysis for lithology and fluid determination together with identification of reservoir.

The second step will consider cross correlation study to determine best chi project angle for different elastic parameters and extended elastic impedance (EEI) analysis.

The third and final step consists of implementation and processing of extended elastic impedance on seismic inversion data and interpretation of the outcomes of EEI inversion. This stage involves making new seismic inversion attributes for different petrophysical and elastic parameters (EEI seismic inversion attributes) to understand the key characteristic of reservoir, which enables us to distinguish different lithology and fluid content efficiently.

2. Background Theory

This chapter provides a brief summary of seismic inversion algorithm and describes several basic background topics necessary for understanding this thesis. Section 2.1 summarize the concept of inversion algorithm and two different categories used for inversion is discussed. Section 2.2 describes the elastic impedance inversion method with section 2.3 dedicated to extended elastic impedance method (EEI) and present basic concepts involved in this approach which is the focus of the thesis. Section 2.4 is a brief overview of the study area which is adapted from Norwegian Petroleum Directorate (npd.no).

2.1 Inversion Algorithm

In this section a brief summary of inversion algorithm is presented. It is necessary to clarify exactly what is meant by inversion algorithm. Mathematically the main goal of an inversion algorithm is to "minimize or maximize an objective function". A quantitative measure of the misfit between the observed data and the data predicted using the inverted model will always include in objective function (Technical Note, Earthworks-reservoir.com).

In the field of seismic exploration, inversion algorithm is generally divided into two main categories, deterministic and stochastic. The term deterministic has come to be used to refer to a "model from which predictions are selected and determined directly through a functional relationship" (Technical Note, Earthworks-reservoir.com). The deterministic inversion gives one optimum result (best single answer) and is completely repeatable (Kemper, 2010). "The output of deterministic inversion algorithm is relatively smooth estimate of the impedance" (Francis, 2006). Although it is a useful approach; major limitations, however, are still present in deterministic algorithm. Firstly, this could lead to potentially misleading and costly error in interpretation, since the model is embedded in the result and may potentially cause artifacts (Francis, 2002). The second restriction we probably face is, since this approach produce only optimal solutions, hence "unable to reproduce the full range of impedance observed in the well" (Francis, 2002).

To solve the deterministic challenges, stochastic inversion rise more demand and has evolved over the past several years. Stochastic inversion can provide a set of possible answers, in other words it gives various equi-probable realization of impedance. These multiple realizations potentially contain the correct impedance that agrees with the 3D seismic volume (Kemper, 2010). By analyzing of the multiple impedance realizations we are able to explore uncertainty in lithology and fluid classification. It is important to notice that one cannot claim that a particular realization is the perfect and one hundred percent correct answer.

It is not possible to repeat stochastic inversion since it uses random number generator to span the solution space. Therefore if we rerun stochastic inversion we could get slightly different realization from primary attempt (Francis, 2003).

Stochastic inversion is divided into two sub-groups, elastic and petro-elastic. In elastic approach data is invert to impedances (for instance, “acoustic impedance if invert only a full stack or acoustic impedance and shear impedance if we invert two or more partial stacks”). In petro-elastic approach we use rock physical models and invert them directly to petrophysical properties such as volume of shale, water saturation and porosity, etc. (Kemper, 2010).

A common and often-described inversion techniques which is widely used in seismic exploration industry are coloured inversion (deterministic), sparse spike inversion (deterministic), model based simultaneous inversion (deterministic), geostatistical inversion (stochastic-elastic) and bayesian inversion (stochastic-petroelastic). Since the understanding of existing implementations of seismic inversion algorithm is out of the scope of this study, we will not drill into subject any further.

Figure 2.1 shows a flowchart on general approach to seismic inversion. We start with some type of seismic volume and build a geological model, and then we pass them into some inversion algorithms and come up with inverted seismic volume which attains the same physical property as geological model.

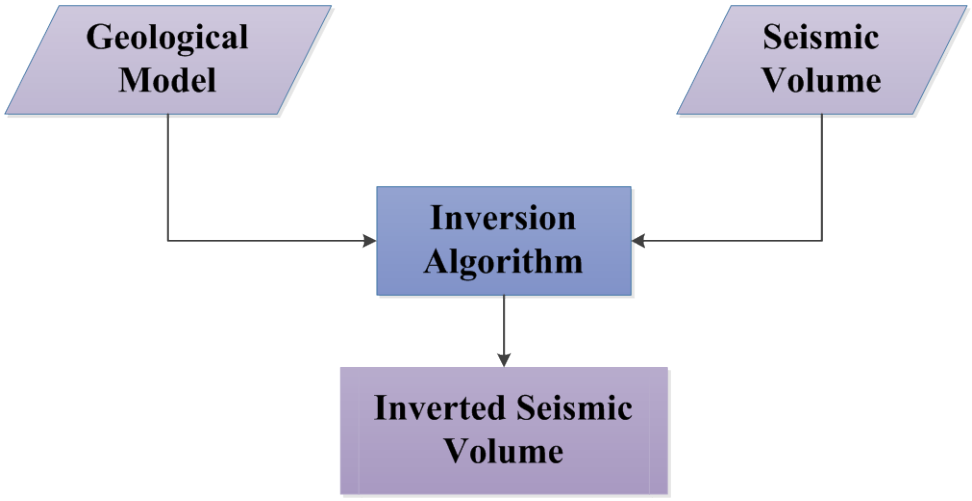

Figure 2.1: General approch in seismic inversion (adopted from Hampson-Russell knowledgebase).

Figure 2.2 illustrates more recent inversion approach to build acoustic impedance (ρV_P), shear impedance (ρV_S) and density (ρ) models and invert the seismic angle gathers simultaneously. In brief, simultaneous inversion is the process of inverting pre-stack data for acoustic impedance, S-impedance and density at the same time. We use the relationship between the background trends of these logs to guide the inversion process.

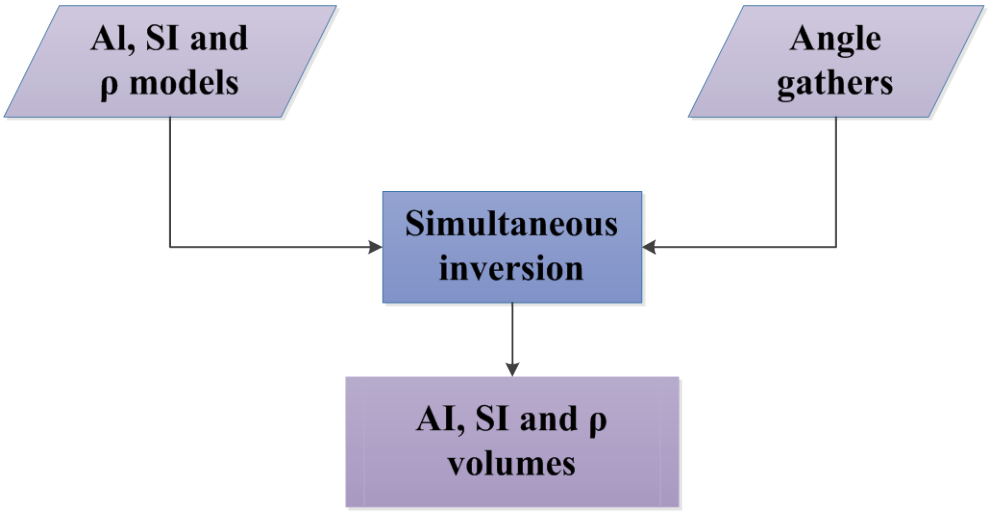

Figure 2.2: Recent inversion approach to build impedance models by using simultaneous inversion (adopted from Hampson-Russell knowledgebase).

2.2 Elastic Impedance

The basic idea behind conventional acoustic impedance (AI) inversion method is an assumption of a P-wave from subsurface interface at normal incidence angle (Latimer, Rebecca., Davison, Rick., Van Riel, Paul, 2000). Although in some circumstances like small offset range in a CDP gather, this assumption is almost fulfilled and the inversion produces reliable results; however, in many hydrocarbon reservoirs similar acoustic impedance value has been observed between hydrocarbon saturated reservoir and the surrounding shale which makes it difficult, or in some cases even impossible, to analyze and discriminate between reservoir sand and surrounding area on zero offset seismic data (Connolly, 1999). With recent progress on AVO technique which make easier differentiate hydrocarbon reservoir from the surrounding shale and cap rock, therefore , there is a rise in demand on analyze non-zero offset seismic data. Elastic parameters from non-zero offset data achieved by elastic impedance technique were represented by Patrick Connolly in 1999. Connolly`s method is suitable for fluid discrimination and lithology prediction for various reservoirs, since it includes more information of lithology and fluid than acoustic impedance.

In total, “elastic impedance (EI) is a generalization of acoustic impedance for variable incidence angle. It provides a consistent and absolute framework to calibrate and invert non-zero offset seismic data” (Connolly, 1999). Preliminary work on elastic impedance undertaken by Connolly demonstrated that the elastic impedance approach provides better inversion results compared to traditionally quantitative use of AVO information (e.g. intercept and gradient method). The EI approximation is derived from linearization of Zoeppritz equations, usually Aki and Richards two term approximation, where θ is the angle of incidence at reflector. The most popular definition of elastic impedance is illustrated by equation 2.1.

$$EI(\theta) = V_p^a * V_s^b * \rho^c \qquad (2.1)$$

$$a = 1 + sin^2\theta$$

$$b = -8Ksin^2\theta$$

$$c = 1 - 4K\ sin^2\theta$$

$$K = (\frac{V_S}{V_P})^2$$

As shown in equation 2.1 the elastic impedance is a function of P-wave velocity (V_P), S-wave velocity (V_S), density (ρ) and incident angel (θ). The factor K is assumed constant and is usually set to the average of V_P and V_S velocity across the interface or over the zone of interest (ZOI).

Connolly (1999) showed that EI decrease with increasing incident angle compared to AI at normal incidence(θ). While Connolly`s work provides good results and useful guides for enhanced reservoir characterization, restriction of incident angle of equation 2.1 was serious challenge. The key problem is that EI has strange unit and dimensions and the values do not scale correctly for different angles (Whitcombe, 2002).

The EI limitation was overcome by Whitcombe (2002). He modified equation 2.1 by introducing reference or normalizing constant $\alpha_\circ, \beta_\circ, \rho_\circ$ which represent average values of velocities and densities over the zone of interest or values at the top of the target zone (equation 2.2) (Whitcombe, 2002). By applying the normalizing constant consequently, we remove the variable dimensionality and provide the elastic impedance with the same dimensionality and correct the scale of acoustic impedance. Whitcombe further introduced extended elastic impedance approach or EEI.

$$EI(\theta) = \alpha_\circ\rho_\circ\left[\left(\frac{\alpha}{\alpha_\circ}\right)^a * \left(\frac{\beta}{\beta_\circ}\right)^b * \left(\frac{\rho}{\rho_\circ}\right)^c\right] \qquad (2.2)$$

$$\alpha = P - wave\ velocity$$

$$\beta = S - wave\ velocity$$

$$\rho = Density$$

$$\alpha_\circ, \beta_\circ, \rho_\circ : The\ average\ of\ P - wave\ velocity, S - wave\ velocity\ and\ density$$

2.3 Extend Elastic Impedance

As mentioned before, impedance inversion is usually applied to zero offset data. In 2002, Whitcombe refined the definition of elastic impedance. He broadened the definition of elastic impedance to remove the dependence of its dimensionality on the angle θ. He recognized some properties of rock cannot be predicted from existing seismic gathering due to limitation on incidence angle range (0-30°) in the elastic impedance (Whitcombe, D. N., Connolly, P. A., Reagan, R. L., Redshaw, T. C, 2002). That is to say, $\sin^2\theta$ needs to exceed unity to estimate some petrophysical properties; however, it is impossible that the reflectivity values exceed unity without negative (and therefore unrealizable) impedance contrast (Hicks, G. J., Francis, A, 2006).

Therefore, Whitcombe et al. (2002) introduced the extended elastic impedance (EEI) concept to solve the elastic impedance limitation. He extended the angle range from 0-30° degrees (which is defined mathematically over a 0-90° angle (0-0.25) range which corresponds to $\sin^2\theta$) by substituting $\sin^2\theta$ with $\tan\chi$ (Whitcombe et al. 2002). The variable θ is now a new function called χ (chi angle or project angle) which varies between -90° and +90° (Figure 2.3 and Figure 2.4). The EEI equation is expressed as:

$$EEI(\chi) = \alpha_{\circ}\rho_{\circ}\left[\left(\frac{\alpha}{\alpha_{\circ}}\right)^{p} * \left(\frac{\beta}{\beta_{\circ}}\right)^{q} * \left(\frac{\rho}{\rho_{\circ}}\right)^{r}\right] \qquad (2.3)$$

Where

$$p = (cos\,\chi + sin\,\chi)$$

$$q = -8K\,sin\,\chi$$

$$r = (cos\,\chi - 4K\ sin\,\chi)$$

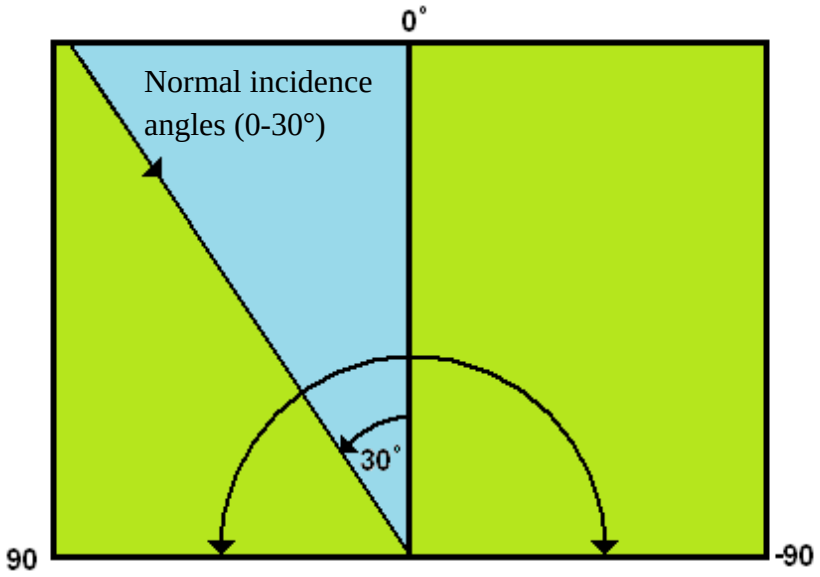

Figure 2.3: Extended elastic impedance angles can range from -90° to +90°, at which values $\sin^2 \theta$ is physically impossible (adopted from Hampson-Russell help system).

The distinct difference between the extended elastic impedance and normalized version of elastic impedance is the change of variable. EEI is a function of χ (an angle in an abstract construction) and EI is a function of θ (an angel in a physical experiment) (Francis, A., Hicks, G. J, 2006). This can lead to EEI much more efficient than EI method and supposed to give different outcomes than standard EI inversion method. It is important to notice that new variable (χ) allows calculation of impedance value beyond physically observable range of angle θ (including imaginary angles not necessarily recorded in the gathers). A clear example of this situation happens when shear impedance corresponds to $\sin^2\theta$ = -1.25. It is obvious, negative angle is not physically recordable but can be projected from angle gathers by linear extrapolation (Hicks, G. J., Francis, A, 2006).

It is easy to show that the EEI log at $\chi = 0$ is similar to EI log at $\theta = 0$, which is simply the acoustic impedance (AI). Whitcombe et al. (2002) provides a simple robust application for deriving lithological and fluid sensitive seismic impedance volumes. According to his perspective under certain approximation, the EEI log at various chi angles proportional to different rock elastic parameters (Figure 2.5).

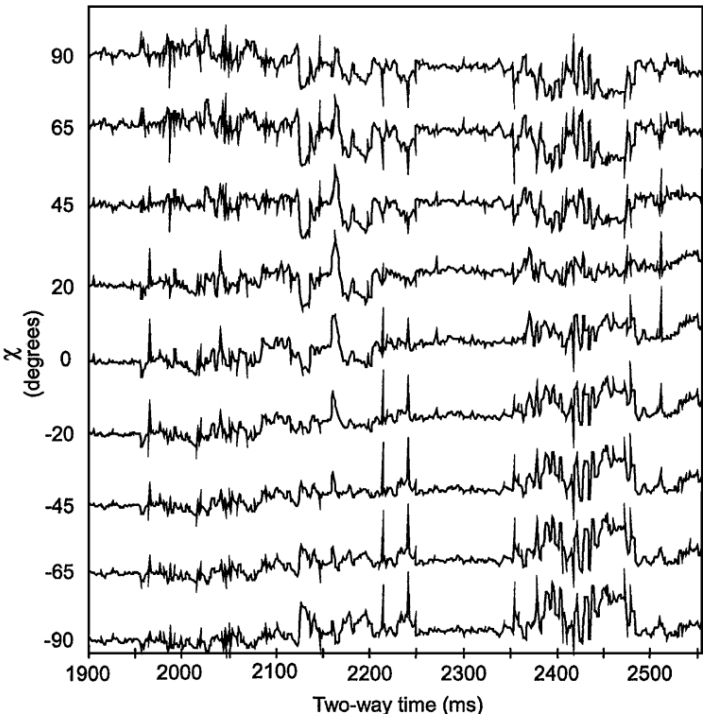

Figure 2.4: The EEI functions for various χ values for particular well. Note the inverse correlation between EEI ($\chi = 90°$) and EEI ($\chi = -90°$). (Whitcombe et al. 2002)

In other words the chi angle can be selected to optimize the correlation of the EEI curves with petrophysical reservoir parameters, such as V_{Shale} , S_w and porosity or with an elastic parameters such as bulk module, shear module and lamé constant and so on (Whitcombe et al. 2002). Therefore, EEI logs for specified angles from these parameters can be produced by using EEI equation which is suited for tie well data directly to seismic data (Figure 2.5). Directness of EEI method is the main advantages which provide an EEI volume attributes that correspond to petrophysical parameters of interest.

Equation 2.4 is two term linearization of Zoeppritz equation for reflectivity (Aki & Richards, 1980)

$$R_p(\theta) = A + Bsin^2\theta \qquad (2.4)$$

Regarding to Whitcombe method when $\sin^2\theta$ replaced by $\tan\chi$, so equation 2.4 represented as equation 2.5 which allows angle to vary from $-90°$ to $+90°$ (A=intercept, B=gradiant).

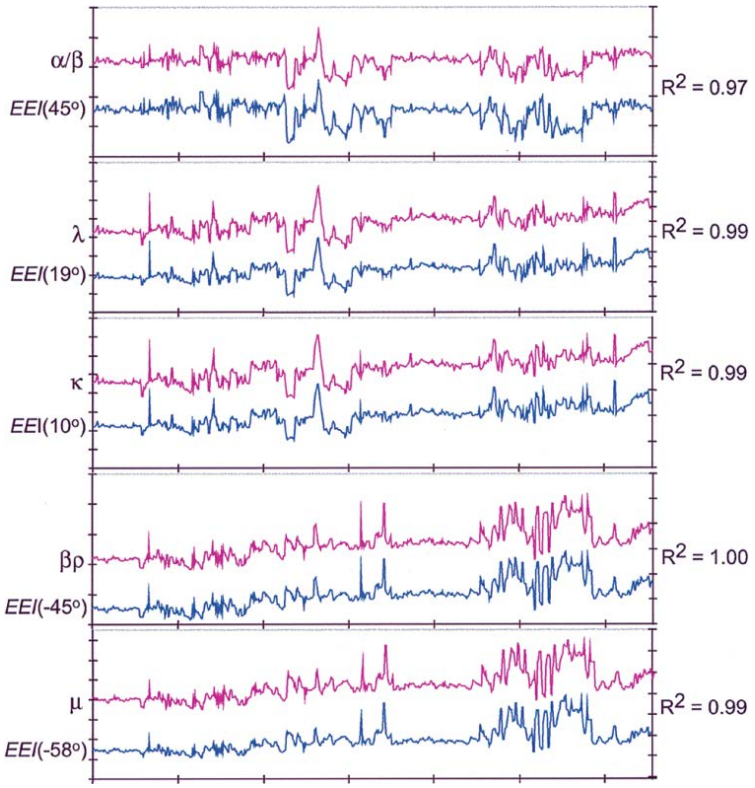

Figure 2.5: Comparisons between elastic parameters and equivalent EEI curves for particular well, representing the high degree of correlation. The EEI function is defined as a function of the angle χ, not the reflection angle θ. (Whitcombe et al. 2002)

$$R_p(\theta) = A + Bsin^2\theta \Rightarrow R(\mathcal{X}) = A + B\,tan\,\mathcal{X} \qquad (2.5)$$

In this study we focus on the extended elastic impedance inversion, EEI method which is carried out to generate several seismic attributes (V_P/V_S, LMR, Poisson`s ratio, bulk module, water saturation, etc.). Comparisons of these, help to determine the sensitivity of elastic parameters to seismic anomaly, improve reservoir characterization and enhance fluid and lithology imaging.

Figure 2.6 shows the general concept on EEI inversion approach. We can see from the flowchart EEI inversion method involves building an EEI (χ) model and inverting EEI (χ) volume using an inversion algorithm to create an EEI output.

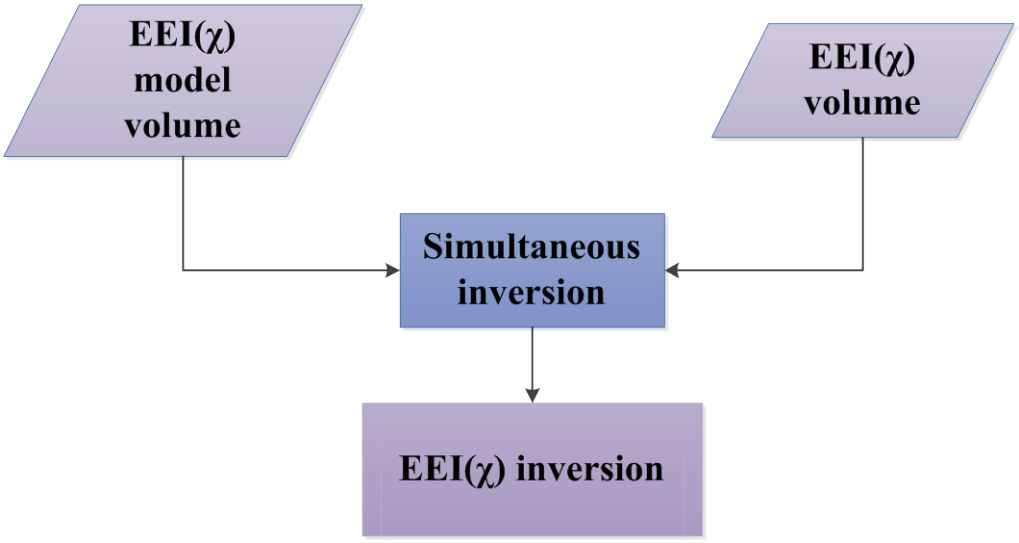

Figure 2.6: General concept on extended elastic impedance (EEI) inversion approach (adopted from Hampson-Russell knowledgebase).

2-4 Study area

The study area is Yttergryta field located in Norwegian Sea, Yttergryta is a subsea gas and condensate field located approximately 5 km north of the Midgard deposit (33 km east of Åsgard B). The average water depth in the area is about 300 meters. The field was discovered by the exploration well 6507/11, that was drilled by the Stena Don semi-submersible rig in July 2007. The reservoir contains gas in Middle Jurassic sandstone of the Fangst Group and lie at depth of 2390 up to 2490 meters (npd.no).

According to Norwegian Petroleum Directorate's report, the field came on stream in January 2009, and was shut down in late 2011 because of water production in the gas production well. Figure 2.7 shows the location of study area in the Norwegian Sea.

In this study, two wells have been considered for detail studies. The well 6507/11-8 and well 6507/11-9 which both overlay available seismic section.

Well 6507/11-8 (429994.97 EW UTM , 7221898.70 NS UTM) was drilled as sixth exploration well on Yttergryta prospect (total vertical depth of 2749 m below the sea surface) which is located on the eastern part of the Halten Terrace, approximately 1 km of the north of the Midgard discovery. The main purpose of the well was to identify gas in reservoir rock from the early to middle Jurassic. The secondary objective of well was to acquire data and test for possible hydrocarbons in the Tilje and Åre formations (npd.no).

Generally, the available well report indicates that the lithology down to top Garn formation where the sand reservoir occurs (at 2416 m) was mainly claystone with no reservoir quality. The petrophysical evaluation showed high hydrocarbon saturation in the Garn formation, and excellent reservoir quality with 28% porosity and up to 6 Darcy permeability. Available MDT pressure data illustrated that the reservoir was in a dynamic stage of depletion due to production from the Åsgard Field (Midgard discovery). The preliminary estimate of the discovery is between 1 and 3 billion standard cubic meters of recoverable gas (npd.no).

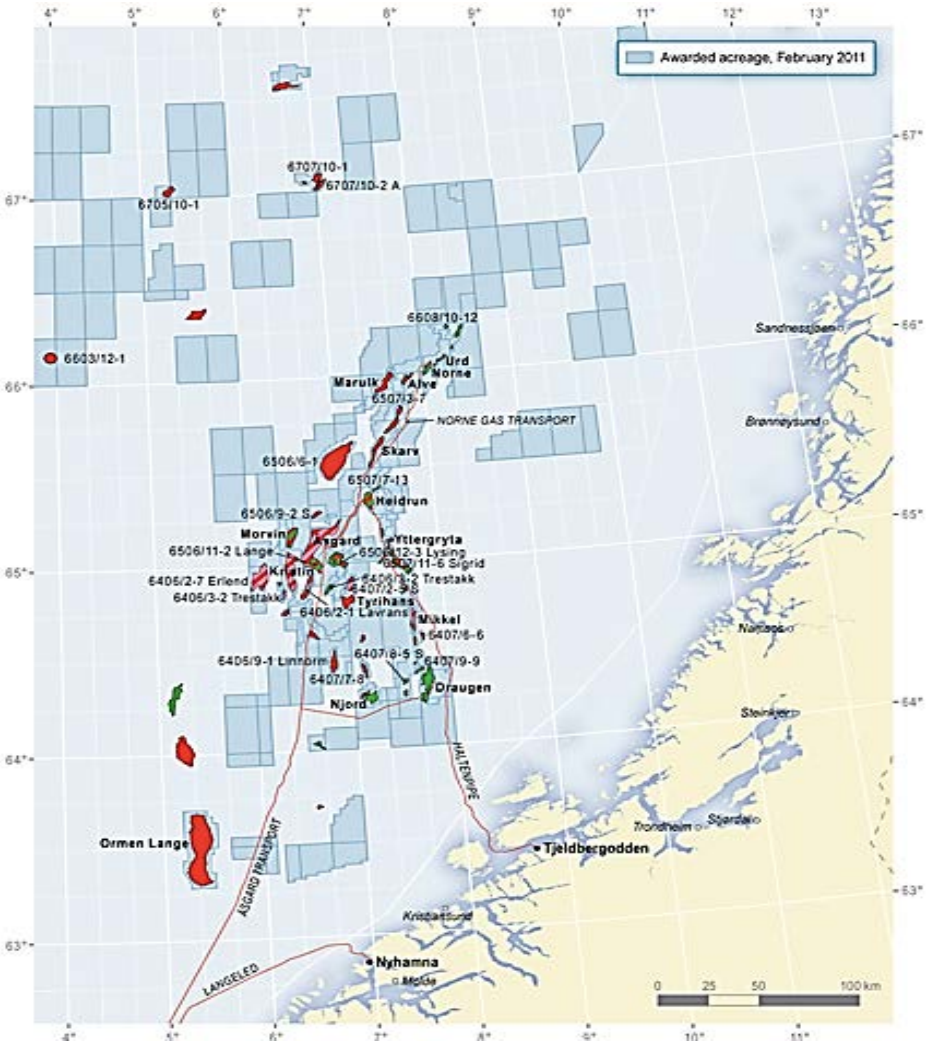

Figure 2.7: Location of study area in the Norwegian Sea (from www.npd.no)

Well 6507/11-9 (425900.64 EW UTM ,7226521.88 NS UTM) was drilled as third exploration well on the Natalia prospect (total vertical depth of 3040 m below the sea surface) which is located on the eastern part of the Halten Terrace in the Grinda Graben, approximately 5 km north of the Midgard Field in the Norwegian Sea. The subsurface structure is interpreted a rotated fault block and comprise of Jurassic reservoir sandstones. The primary target of the well was to prove presence of hydrocarbons in Jurassic sandstones. Also the hydrocarbon migration route in the prospect area was examined as secondary objective (npd.no).

Operation report indicates that the well penetrated rocks of Quaternary, Tertiary, Cretaceous and Jurassic age. Similar to well 6507/11-8, the lithology down to top Garn formation is claystone with no reservoir quality. The well penetrated the reservoir section at about 2597 m. The well

analysis proved that there is approximately 40 m of gas sand in the Garn formation which is estimated at about 1.5 billion standard cubic meters of recoverable gas. The reservoir properties and sedimentary facies observed in the well (porosity 26% and permeability is estimated 4 Darcy) are comparable to the excellent reservoir properties observed on the Midgard Field (npd.no).

Figure 2.8 shows the location of well 6507/11-8 and well 6507/11.9 in the Norwegian Sea.

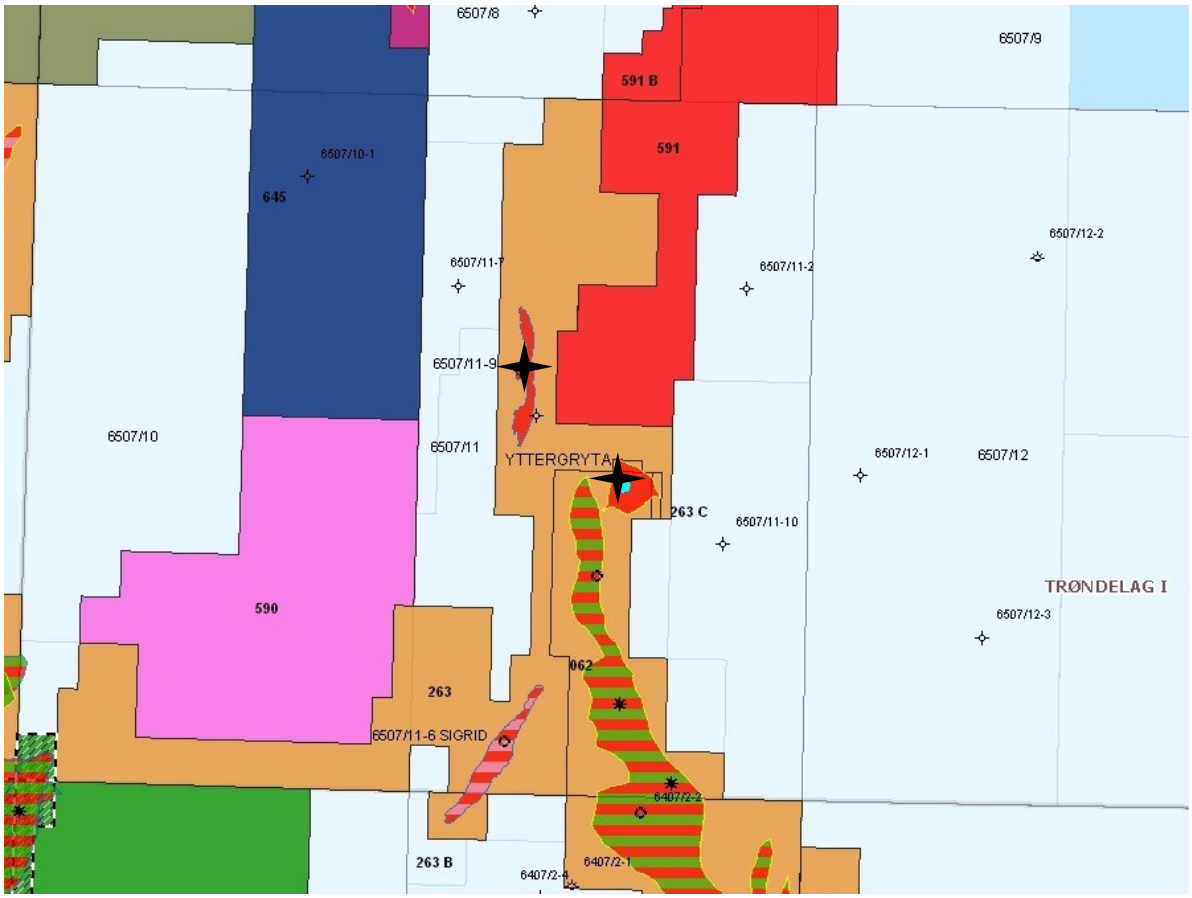

Figure 2.8: Location map of Well 6507/11-8 and Well 6507/11.9 (Adopted from www.npd.no)

3. Well Log Analysis

Well log data can provide vital and valuable information which is very helpful in defining a reservoir and other important interval in the well. In this study, three wells were considered but only two have sufficient logs with good quality located in seismic area. In this work well 6057/11-8 and well 6057/11-9 have been considered for detail studies. However, well 6507/11-6 has been also analyzed in some aspects for extended elastic impedance and determining optimum chi angle and was compared with the main wells to improve correlation study results.

In this chapter, analysis of well log data is provided for well 11-8 and 11-9 to evaluate the relationship between elastic parameters along with their potential for predicting lithology and fluid contents. Both wells have good quality P-wave and S-wave velocity and density log which were used as main input to obtain petrophysical parameters and other attribute pairs required for rock physics study. All of these were derived algebraically from key seismic parameters V_P,V_S, ρ.

In addition, good quality gamma ray (GR) log and resistivity log provide sufficient knowledge about location of reservoir sand and improve log interpretation. The results of interpreted well logs revealed that two hydrocarbon zones in the well 11-8, the gas saturated reservoir occurs at 2425 – 2447 m and also between 2460 – 2510 m (MD from KB). Also one hydrocarbon zone accrues between the depth range of 2608 - 2636 m (MD from KB) for well 11-9. Figure 3.1 and Figure 3.2 show the available logs and location of interpreted hydrocarbon zones for well 11-8 and 11-9 respectively. At each well, the target area is the sandstone (highlighted by red color) with lower P-wave velocity and density than top and bottom of surrounding area. All depth in this study refer to KB (Kelly bushing) unless otherwise stated.

The well based cross plot analysis of acoustic and elastic impedance parameters used as a tool to establish quantitative relationship between reservoir properties, distinguish different lithologies and fluid contents. In this section, the most useful rock physic cross plots will be summarized to delineate the gas sand reservoir and provide better comprehension of the relationship between rock physic parameters and lithology-pore fluid in the zone of interest (ZOI).

This step is the fundamental stage for reservoir characterization. The main objective of this section is to evaluate and gain knowledge about sandstone reservoir quality, sand distribution and fluid content in zone of interest. This will improves our understanding of the expected seismic signature in inversion step.

Hampson-Russell software package (HRS-9) and MATLAB have been used for log editing and calculation, application of fluid substitution, check shot calibration and plot the data.

3.1 Well log interpretation

3.1.1 Density

A density log measures the space between electrons in a rock. “The bulk density is the density of formation and all it is components and will be function of volume of porosity, matrix and fluid” (Schlumberger, 1972). Density log helps identify evaporate minerals, detect gas bearing zone and complex lithology. Normally the density will decrease from shale unit to sand unit.

As shown in Figure 3.1 well 11-8 records a low density of about ~ 1.95 - 2 g/cc in the sand reservoirs at 2425 – 2447 m and also between 2460 – 2510 m. Likewise well 11-9 (Figure 3.2) shows similar behavior and record low density value of about ~ 2.05 g/cc in target area (~2608 - 2636 m). Although all sand units show low densities; however, as we can see from both figures, density log strongly affected by the presence of gas and record the lowest density values. These figures show that there have been marked fall in the target area which suggest presence of hydrocarbon.

3.1.2 P-wave velocity

A P-wave sonic log (compressional velocity) measures “the transit time (Δt in m/s) of an acoustic waveform between a transmitter and a receiver” (Schlumberger, 1972). Figure 3.1 and Figure 3.2 show P-wave velocity logs.

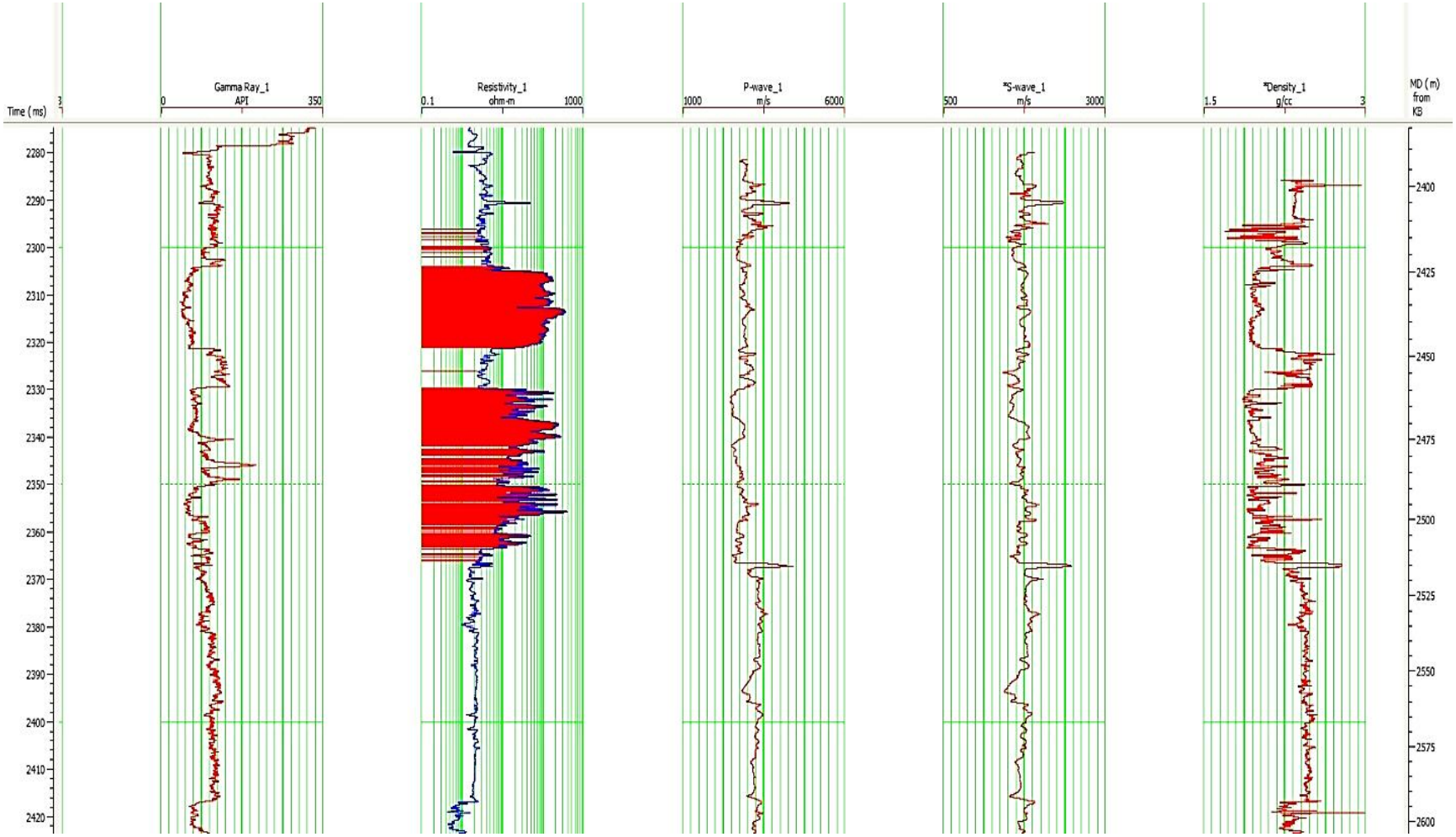

Figure 3.1: Available logs for well 11-8 (from left to right: GR, resistivity, P-wave velocity, S-wave velocity and density log). The read area represents the hydrocarbon zones

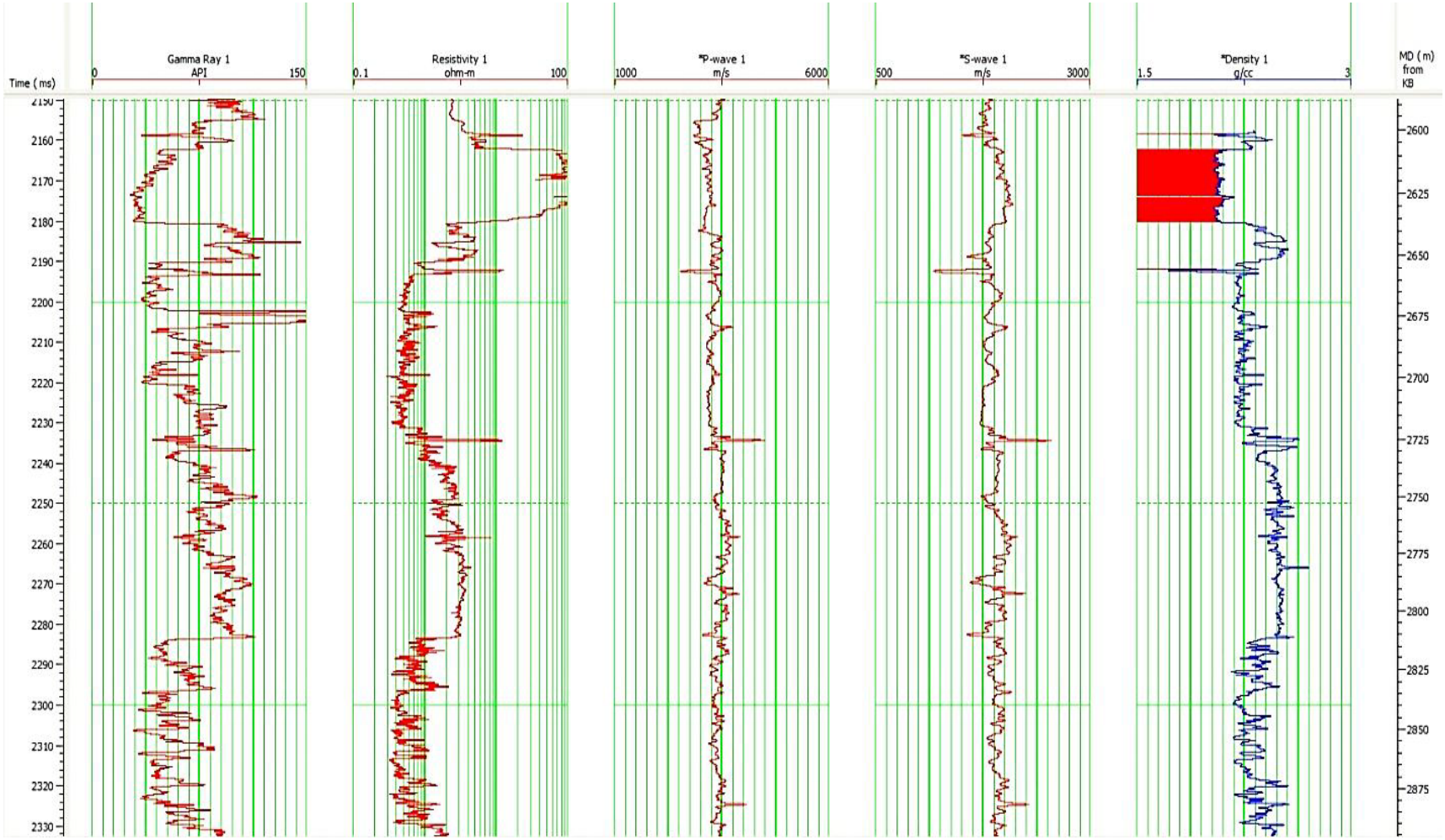

Figure 3.2: Available logs for well 11-9 (from left to right: GR, resistivity, P-wave velocity, S-wave velocity and density log). The read area represents the hydrocarbon zones

It can be seen from the figures that P-wave velocities clearly decrease in reservoir for both wells. The P-wave logs show there is about 20 percent velocity reduction (well 11-8) and about 15 percent velocity reduction (well 11-9) occur when logs moving into the reservoir sandstone.

3.1.3 S-wave velocity

Shear waves or secondary wave, have a slower velocity when compared to the P-waves for given geological information. Both wells in this study have had good quality and long enough shear waves logs within target intervals. Under the situation of lack of share wave data, one method would be to predict a pseudo shear wave log from a measured compressional velocity by equation 3.1 called Greenberg-Castagna equation (1992).

$$V_P = 1.16\,V_S + 1.36 \qquad (3.1)$$

We should consider the fact that this simplified equation (Castagna`s relationship) will only yield the background trends which may be different from real shear wave measured in the field.

Figure 3.3 shows a cross plot of V_P and V_S in well 11-8. The black arrows represent fluid effects and porosity effects which are superimposed onto cross plot. This figure is quite revealing that porosity controls the change in velocity, higher porosity values falling at lower left and lower porosity values falling at the upper right. This trend is general behavior in clastic reservoir.

The red polygon represents gas sand reservoir. The gas saturated area and non-reservoir area (brine sand and shaly sand) fall along two well separated trends, trend of gas bearing sandstone and trend of water bearing sandstone and shale. This notable trend is a cornerstone for all direct hydrocarbon detection method and also proves the importance of shear information function for discriminating lithology and pore fluid content. “Variation in porosity, shaliness and pore pressure move data up and down along the trends, while changes in fluid saturation move data from one trend to another” (Avseth, P., Mukerji, T., Mavko, G., 2005).

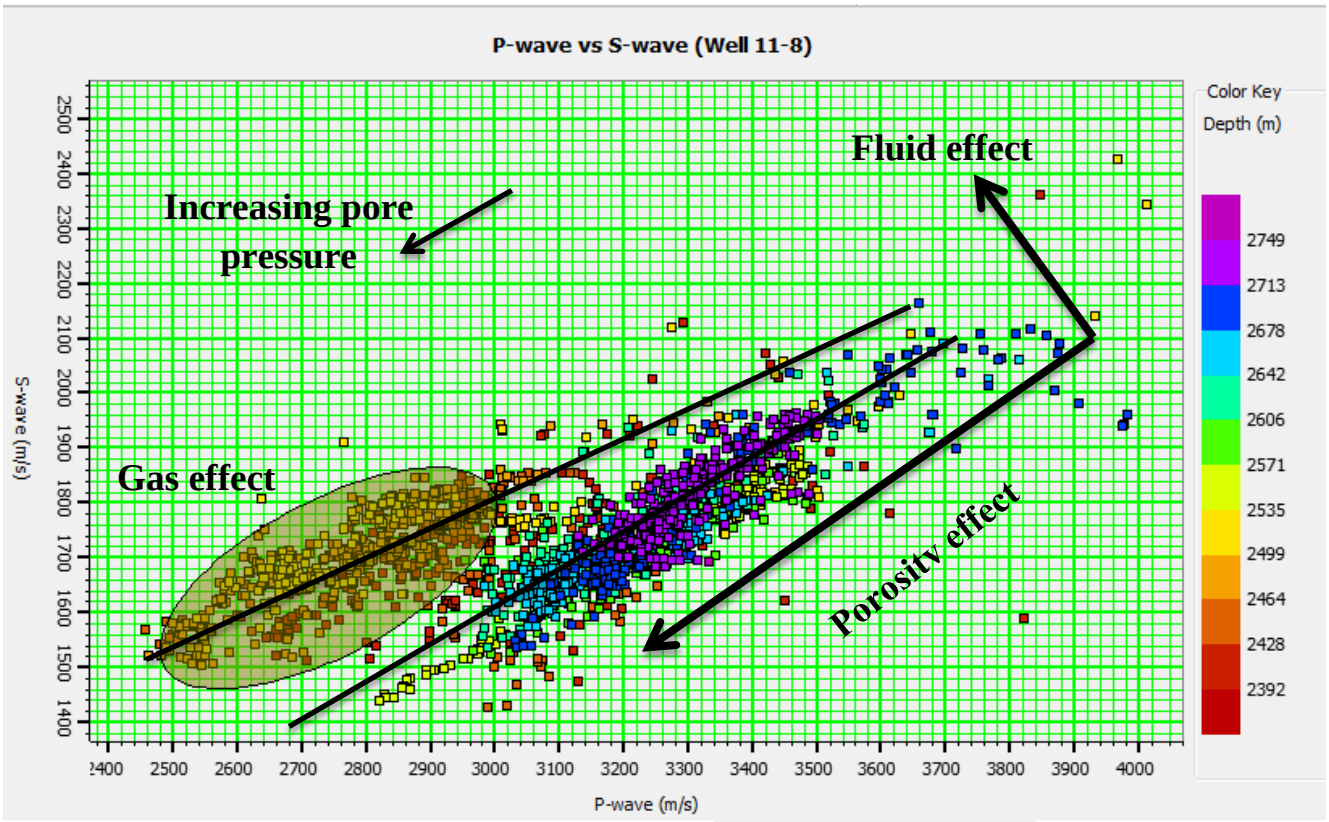

Figure 3.3: Crossplot of V_P vs V_S for well 11-8, The black arrows represent direction of increasing porosity and pore pressure .The saturation trend is perpendicular to that for porosity, caly and pore pressure.

It is important to notice that all the selected ellipses/polygons in this research are based on simultaneously comparison study with well log observation.

3.1.4 Gamma ray log

Gamma ray logs measure the radioactivity of formations in the well (naturally accruing or put there in mud system) which connected to clay mineral, oil source rock, organic matter and shale in reservoir rock (Schlumberger, 1972). Gamma ray log is known to aid in lithology identification and recognize layers of different petrophysical property in the formation. In addition, we will consider gamma ray log often as a good shale indicator (providing sand/shale cutoff). Shale free sandstones and carbonates normally have low radioactive concentrations hence represent low gamma ray reading (less than 70-75 API units).

From Figure 3.1 and Figure 3.2 we can clearly observe the transition between shale unit and sand formation around 2425 m for well 11-8 and 2608 m for well 11-9 (reservoir sand shows deflection to the left in both wells).

Low value of gamma ray log in clastic sediments typically shows that log has moved into clean formation (sand units). The reservoir interval for well 11-8 and well 11-9 record low values of gamma ray, $\sim 55 - 65$ and $\sim 50 - 55$ respectively. Gradual decrease in gamma ray log as shown in Figure 3.2 is likely to represent small amount of clay in top of the reservoir. Likewise from Figure 3.1 we can interpret that first hydrocarbon zone is almost clean sandstone, however gamma ray log indicates that second hydrocarbon zone is slightly shaly at the bottom (a shale layer at ~ 2450 separates first gas zone from second gas zone). Regarding the gamma ray log, below the reservoir sand is interpreted as combination of wet sand and clay layers for both wells.

3.1.5 Resistivity log

Resistivity is “the property of a material or substance to obstruct or resists the flow of an electric current” (Schlumberger, 1972). Salt water is conductive while hydrocarbon acts as insulator (non-conductive) therefore we expected a low resistivity values in brine saturated rock and high resistivity values in hydrocarbon saturated rock. In other words, when the hydrocarbon saturation of pores increases, rock resistance to transmit the current will increase too. The combination of the gamma ray log and resistivity log are normally used to differentiate between hydrocarbon and non-hydrocarbon bearing zones.

A clear example of gamma ray and resistivity log combination are shown on Figure 3.1 and Figure 3.2 for well 8-11 and 9-11 respectively. It is apparent from the figures that available resistivity logs increases significantly due to presence of non-conducting hydrocarbon in target area (low GR value) as compared to lower values in the surrounding formation (high GR value). The marked area represents hydrocarbon saturated reservoir.

3.2 Generate other logs and interpretations

Once the basic rock physics parameters are determined and analyzed, it is possible to generate other parameters that enhance lithology and fluid discrimination.

3.2.1 V_P/V_S ratio

Castagna et al. (1985) indicated that the use of V_P/V_S ratio (the ratio of compressional velocity to shear velocity) is "key issue for determination of lithology from seismic or sonic log data, as well as for direct seismic identification of pore fluid" (Avseth et al. 2005). Several studies have stated that the use of V_P, V_S and V_P/V_S ratio in seismic exploration as reliable fluid discriminator in siliciclastic environments. The P-wave velocity is more sensitive to fluid changes than the S-wave velocity. Compressional velocities travel through both rock and fluid and are slower in gas area, as compared to water area. In contrast S-wave velocity is mostly insensitive to fluids and only moves through the rock. This means that the differences in the V_P/V_S ratio inside a reservoir would indicate different fluid saturation.

Figure 3.8 and Figure 3.9 show V_P/V_S ratio logs for well 8-11 and 9-11 respectively. Here a significant drop in the V_P/V_S ratio shows the presence of hydrocarbons (gas sand reservoir). For instance we can see that, the value of V_P/V_S in the gas saturated reservoir are approximately 1.62 while brine saturated sand below the target area has a V_P/V_S ratio value about 1.83. (Figures with higher quality are included in appendix B).

Several case studies and rock physic reports confirm that, high values of V_P/V_S ratio are normally correlated with low quality reservoir rock while low value of V_P/V_S correlates with good quality reservoir rock. We should note that, although the V_P/V_S ratio may show a good degree of fluid discrimination and reservoir quality, is not, however, sufficient for final decision making.

Figure 3.4 shows a cross plot between P-wave velocity and V_P/V_S ratio for well 11-8. The gas sand reservoir is highlighted within the red polygon in the cross plot. As shown in Figure 3.4 presence of gas causes significant drop in P-wave velocity and V_P/V_S ratio; however, there is poor fluid discrimination in higher velocities (stiffer rock).

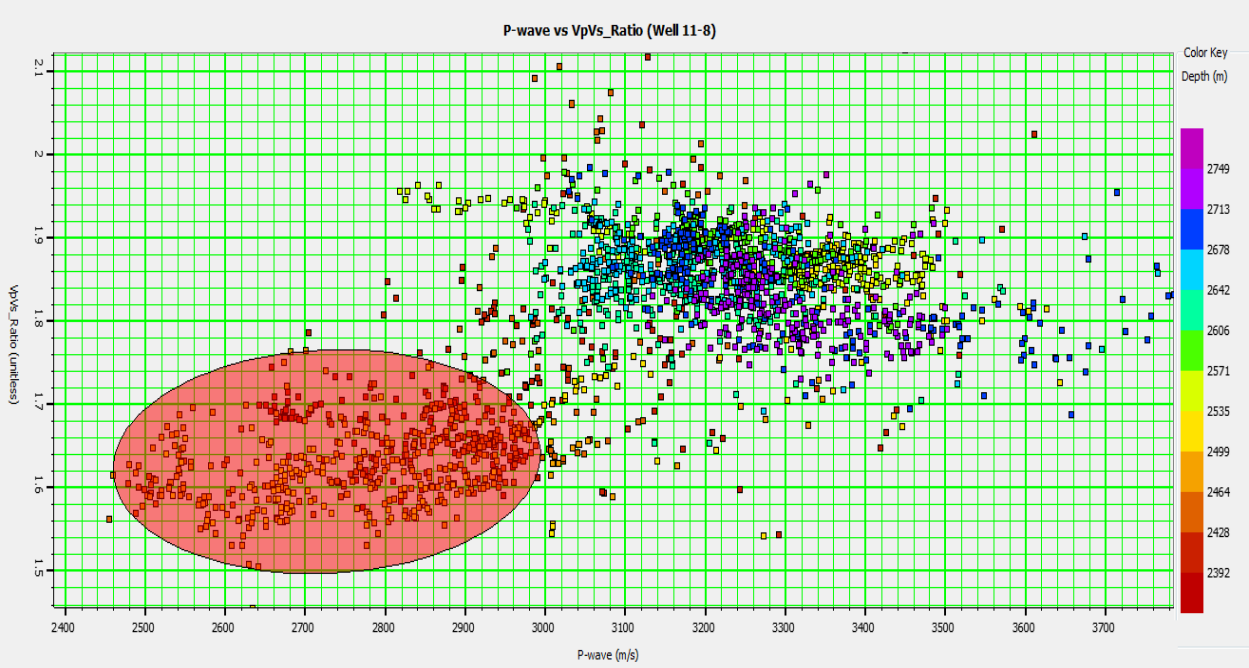

Figure 3.4: The reservoir sand can be clearly interpreted on V_P/V_S versus P-wave velocity cross plot (well 11-8).

Figure 3.5 shows acoustic impedance log (AI) - also called P-impedance versus S-impedance log for well 11-9. Acoustic impedance is the product of P-wave velocity and density and traditionally is a popular technique for lithology and pore fluid prediction. (S-impedance is the product of S-wave velocity and density). It is clear from Figure 3.5 that in study area, presence of gas cause decrease in P-wave velocity and density. As a consequence, reduction in acoustic impedance (AI) observed in gas saturated sand compared to surrounding non-reservoir area (shale and shaly sand). From Figure 3.8, it is apparent that the S-impedance decrease in gas reservoir for well 11-8, is mostly because the additional parameter, density which is significantly drop in target area.

The cross plot between P-impedance versus S-impedance for well 11-9 is shown in Figure 3.5, the cross plot is color coded by depth (m). It is apparent from this figure that combination of P-impedance with S-impedance in this study area is quite effective to distinguish reservoir sand facies from non-reservoir facies.

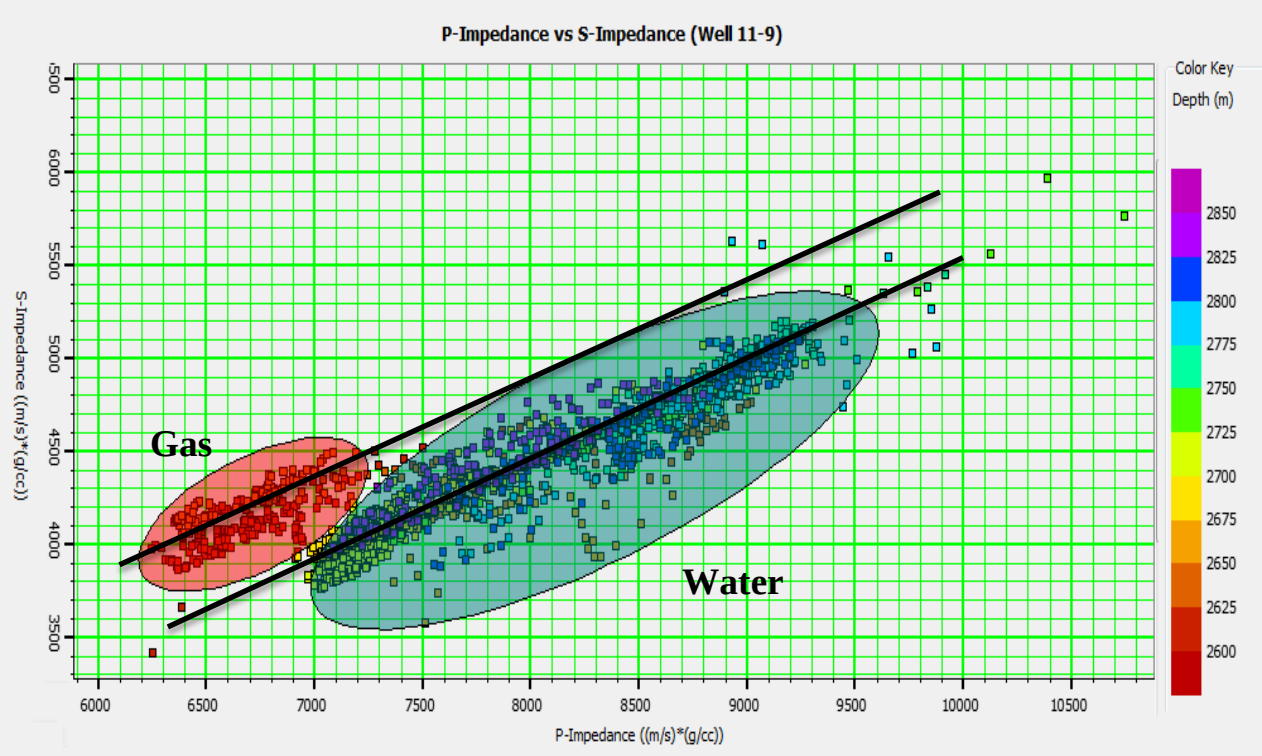

Figure 3.5: Acoustic impedance (P-impedance) versus S-impedance cross plot for well 11-9. Good separation between gas sand zone and other lithologies was confirmed.

Figure 3.6 shows a cross plot between acoustic impedance (AI) and V_P/V_S ratio for well 11-9. Generally the cross plot of acoustic impedance versus V_P/V_S identify geologic trend and facilitated the discrimination of gas sand from brine sand as well as the separation between sand and shale; however, one should be aware that this finding is not general and is not repeated in all cases (Avseth et al. 2005). In some area shale and sand formation have similar Al values which make lithology and fluid prediction difficult or indistinguishable. High risk targets due to lack of contrast between acoustic impedance and adjacent shale causes an increase in demand for other techniques for lithology-pore fluid prediction to reduce uncertainty.

Figure 3.7 represents the corresponding log sections for P-impedance vs. S-impedance and V_P/V_S vs. P-wave velocity , where the captured polygons are shown in log sections.

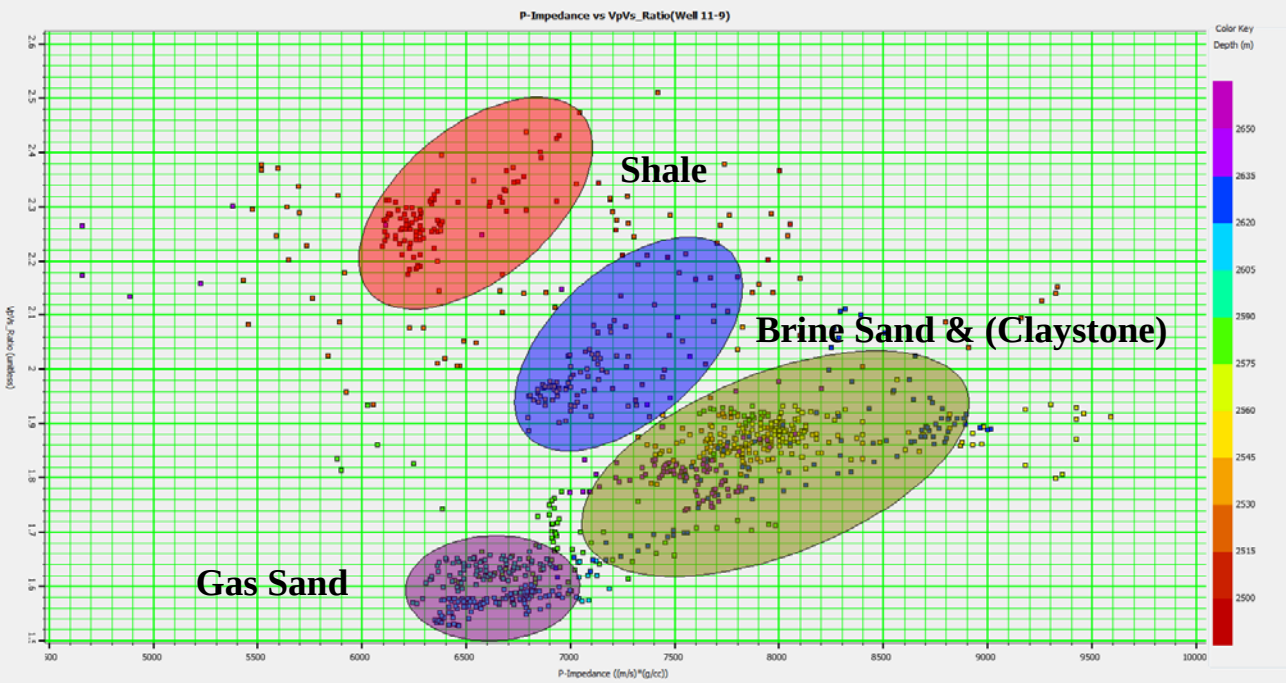

Figure 3.6: Acoustic impedance versus V_P/V_S ratio cross plot (well 11-9).

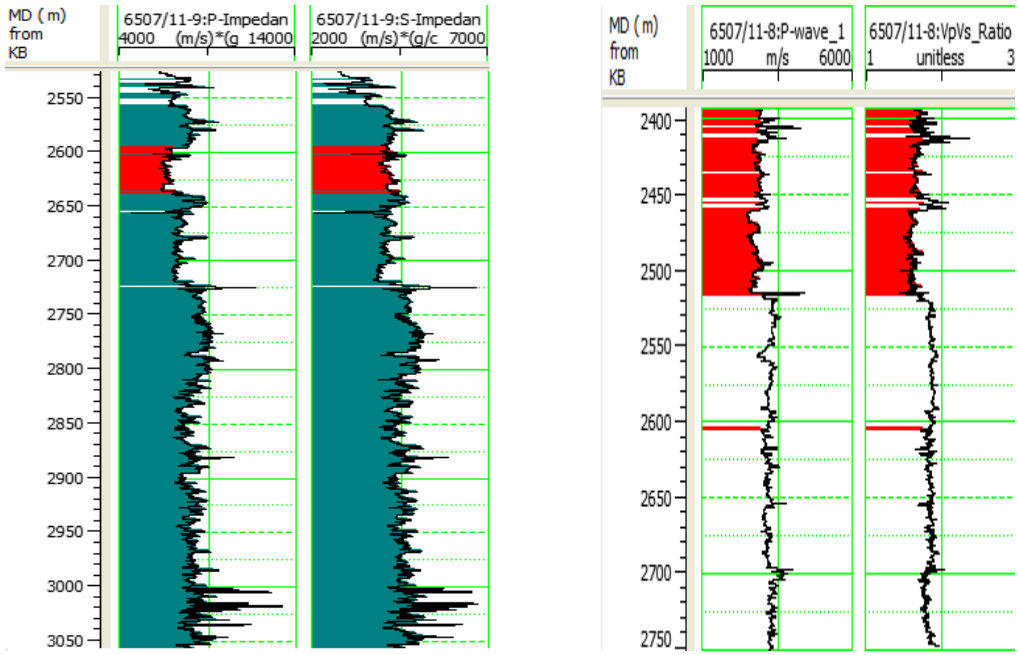

Figure 3.7: Log sections for P-impedance vs. S-impedance and V_P/V_S vs. P-wave velocity.

According to Figure 3.6 we can define four clusters in the cross plot domain and separate lithology and pour fluid. Purple polygon represents gas sand area which has low value of V_P/V_S and acoustic impedance. Shale represents by red polygon with high value of V_P/V_S and low value of acoustic impedance. Brine sand and shaly sand are also shown by gray and blue polygon respectively. As we expected brine sand has higher acoustic impedance and V_P/V_S valuesthen gas sand.

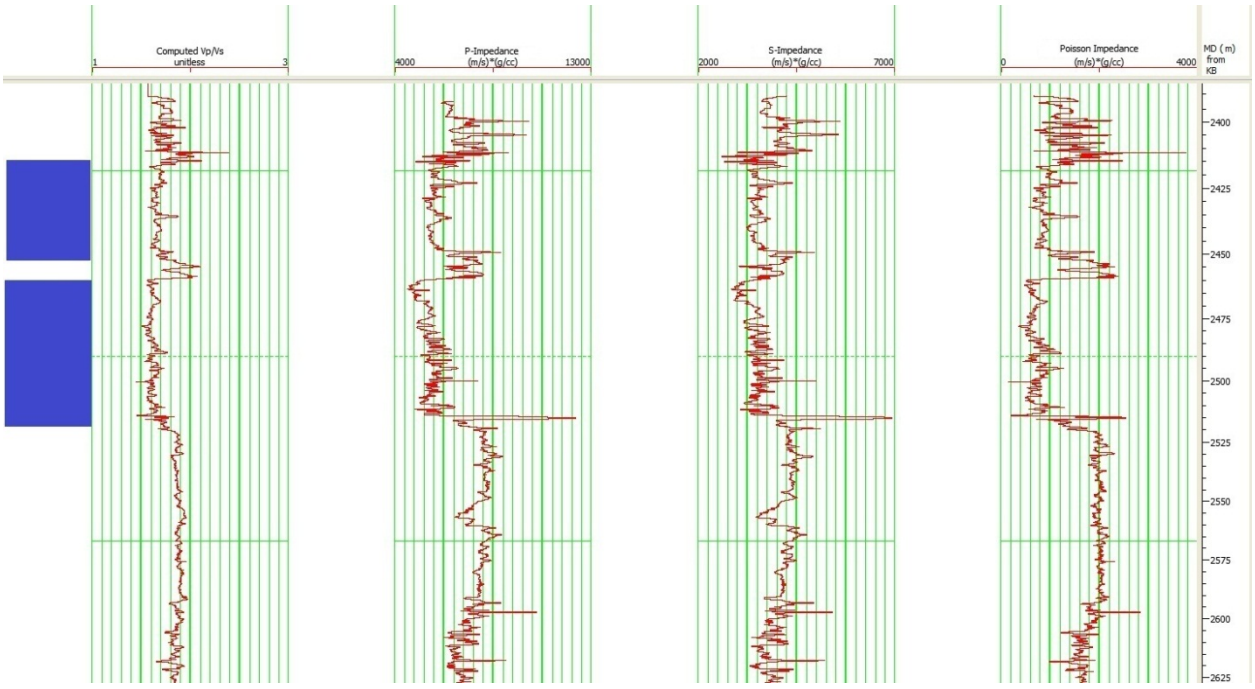

Figure 3.8: From left to right:V_P/V_S, P-Impedance ,S-Impedance and Poisson Impedance log for well 11-8, blue rectangle parts represent the hydrocarbon (gas) zones. The acoustic impedance logs differentiate the gas saturated reservoir from surrounding area. Note predicted drop in V_P/V_S ratio at the zone of interest.

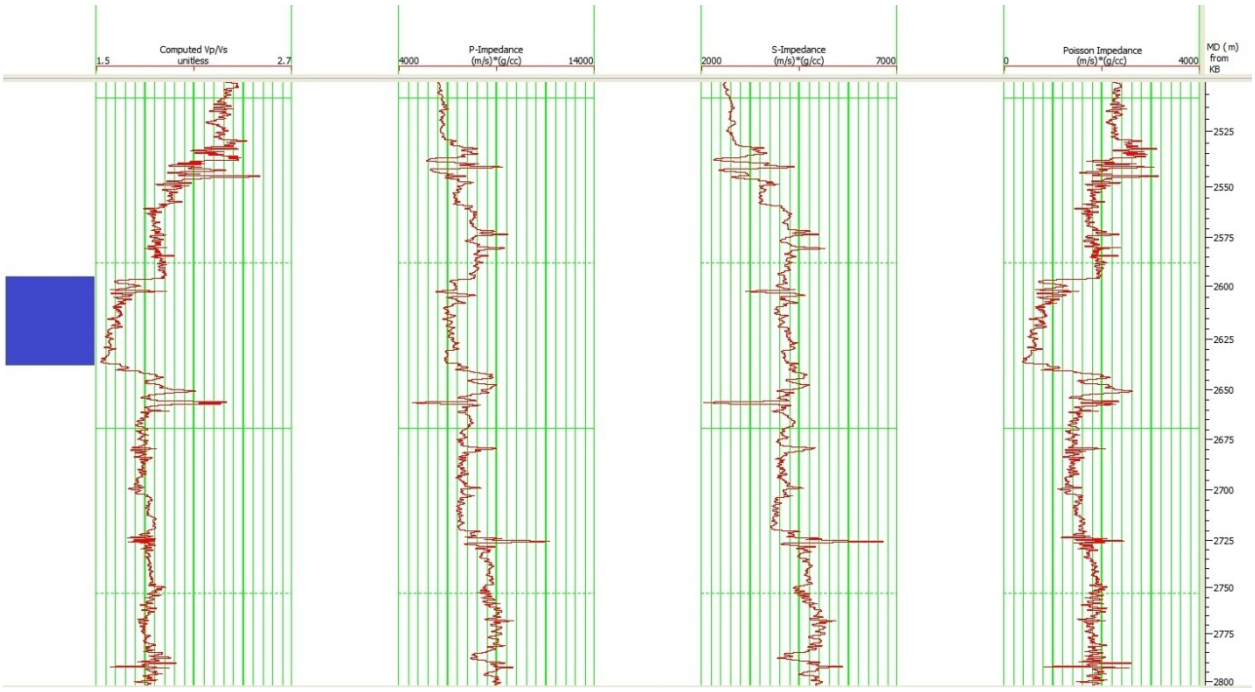

Figure 3.9: From left to right:V_P/V_S, P-Impedance ,S-Impedance and Poisson Impedance log for well 11-9, blue rectangle represent the hydrocarbon (gas) zones. The acoustic impedance logs differentiate the gas saturated reservoir from surrounding area. Note predicted drop in V_P/V_S ratio.

3.2.2 Poisson impedance

In 2006, Quakenbush introduced Poisson impedance method as new hydrocarbon indicator tool. "The Poisson Impedance (PI) is an attribute value by performing the rotation to the cross plot of P-impedance (acoustic impedance) versus S-impedance (shear impedance)" (Quakenbush, M., Shang, B., Tuttle, C, 2006).

In his major study, Quakenbush et al. (2006) showed that in some area it is difficult to distinguish the lithology-fluid distribution on acoustic impedance and share impedance cross plot and highlights the need for new approach. He proposed axis rotation of P-impedance and S-impedance cross plot to make the axis parallel with the trends, this may result in distinct discrimination of lithology – fluid distribution. Mathematically, this relation is called Poisson impedance and can be shown as equation (3.2).

$$PI = AI - \mathcal{C}\, SI \qquad (3.2)$$

Where $\mathcal{C}$ is the term that optimizes the rotation (rotation of the axis) to improve fluid and lithology discrimination. Figure 3.10 illustrates the idea of Poisson impedance and axis rotation introduced by Quakenbush et al. (2006).

The biggest advantage of Poisson impedance is that "it can excellently characterize lateral variations of sandstone – mudstone layers and oil-gas-water layers in some area". Moreover it has the capability to remove mudstone background of P and S impedance, hence can be feasible in regions with larger structural amplitude (Tian, Lixin., Zhou, Donghong., Lin, Gulkang., Jiang, Longcong, 2010). Cross plotting PI and other elastic parameters with varied lithological and fluid sensitivity could provide new and favorable method to predict the sandstone reservoir distribution, reservoir quality, and fluid content potential.

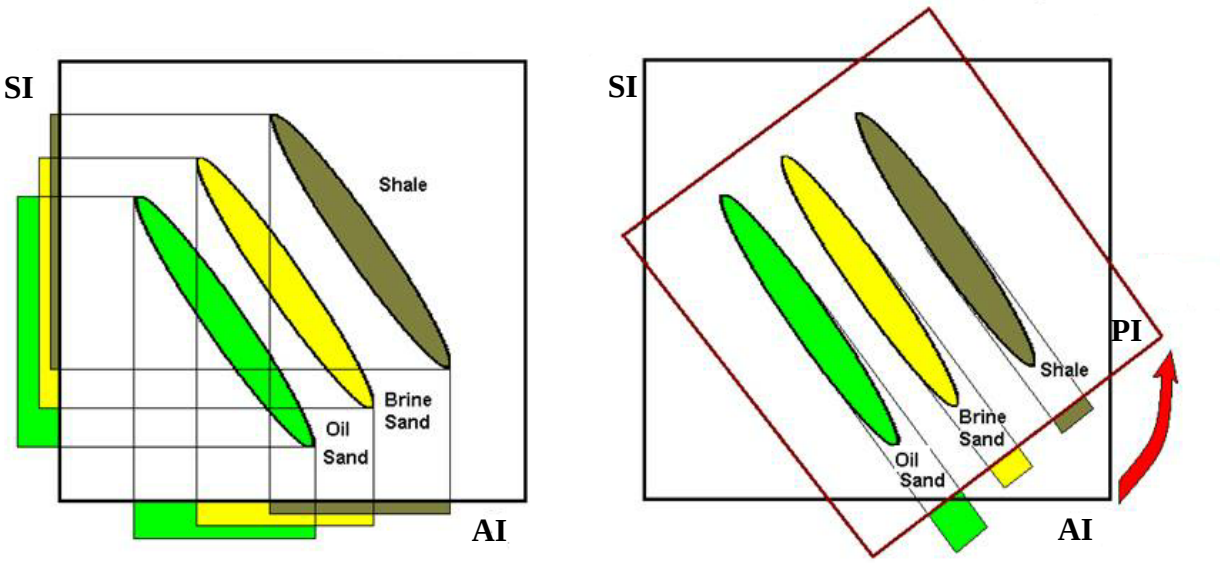

Figure 3.10: schematic view of AI-SI cross plot with shale, brine sand and oil sand. Note that define clusters are not discriminated along the AI or SI cross plot alone , but with a rotation of the axes, clusters in this case can be perfectly discriminated (Adopted from Hampson-Russell help system)

A serious weakness of this method, however, is that sometimes it is difficult to get the exact value of constant $\mathcal{C}$ in equation (3.2) in practical application. For more accurate $\mathcal{C}$ calculation, Target Correlation Coefficient Analysis (TCCA) method has been used in this work which has been introduced by Tian et al. (2010). This method carries out the calculation of the correlation coefficient between Poisson impedance versus target parameters (here water Saturation (S_w)) for different $\mathcal{C}$ values. The maximum correlation coefficient is reached in $\mathcal{C}$ = 1.761 for S_w (correlation coefficient = 0.731) (well 11-8). Then the Poisson impedance attribute was derived from equation (3.2) by inserting 1.761 for $\mathcal{C}$ value (Figure 3.8).

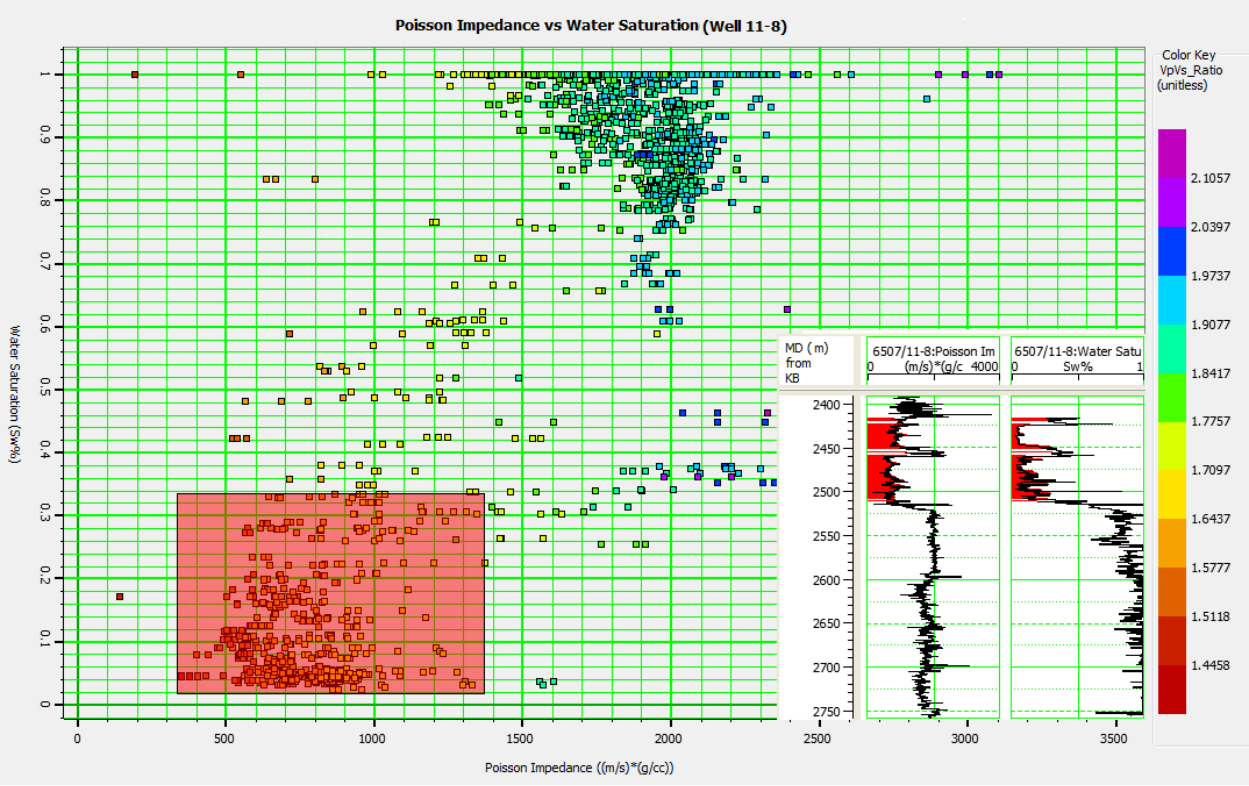

Figure 3.11: Poisson impedance versus S_w cross plot for well 11-8

Although P-impedance and S-impedance cross plot in this study area show reasonable separation between wet sand and gas sand, Poisson impedance result is encouraging too. Figure 3.11 presents the cross plot of Poisson impedance versus S_w content and shows the advantage of Poisson impedance for distinguishing gas sand reservoir from water sand. As can be seen from the Figure 3.11 the interpreted hydrocarbon zone has been highlighted by the application of

Poisson impedance. Cross section of red polygon with logs indicates good fit with field observation.

3.2.3 Shale Volume

Shale is usually more radioactive than sand or carbonate. Volume of shale can be calculated from the gamma ray log and can indicate the presence or absence of clay. The volume of shale (V_{Shale}) is expressed as a fraction or percentage.

Several relationships exist for V_{Shale} calculation from gamma ray log (non-linear empirical responses as well as a linear response). The none-liner responses include Larinov equation (1969) for tertiary and older rocks, also the Steiber (1970) and the Clavier (1971) equations (Appendix A). All non-linear responses are based on geographic area or formation age. They are also more optimistic and produce lower shale volume values than the linear responses (Krygowski, 2004).

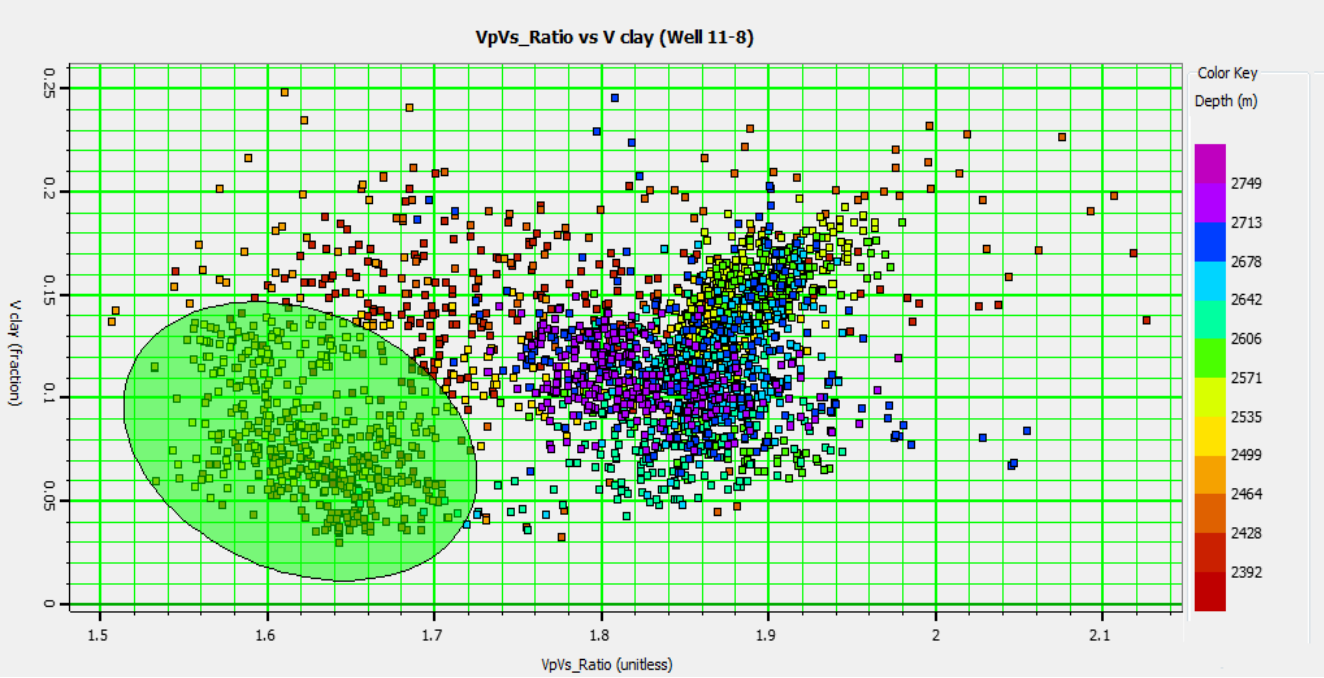

Figure 3.12: Volume of shale and V_P/V_S ratio cross plot for well 11-8. The gas sand zone spreads out from non-reservoir area.

In normal circumstances when the V_{Shale} log shows very low value, it is interpreted to be clean facies like sand while a high V_{Shale} value is interpreted as clay rich facies such as shale. For more accuracy and to reduce uncertainty in interpretation, it is important to take into account our knowledge about the geology of the subsurface to avoid some pitfalls in interpretation.

Figure 3.12 shows cross plot between volume of shale and V_P/V_S ratio for well 11-8. As can be seen from the plots, the V_P/V_S ratio is less for gas sand which is captured by polygon (almost clean facies).

3.2.4 LMR

In 1997, Goodway proposed a method to extract rock properties. He promoted the usage of relationship between lamé parameters λ (Incompressibility), μ (rigidity) and ρ (density) and their ability to perform inversion. λ and μ are obtained from equation (3.3) and (3.4). Goodway (1997) demonstrated that, how LMR (**L**ambda-**M**u-**R**ho) approach can be used to separate lithologies and identify gas sands.

$$Z_s^2 = (\rho V_s)^2 = \mu\rho \qquad (3.3)$$

$$Z_p^2 = (\rho V_p)^2 = (\lambda + 2\mu)\rho \quad \Rightarrow \lambda\rho = Z_p^2 - 2Z_s^2 \qquad (3.4)$$

Mu-Rho or rigidity is defined as the “resistance to strain resulting in shape change with no volume change” (Goodway, B., Chen, T., Downton, J., 1997). This parameter is very useful for lithology discrimination and is related to the rock matrix. Quartz is the dominant mineral in the sand matrix, therefore sandstone usually associated with high rigidity than shale and coal (Goodway et al. 1997). The most interesting result from this principle is that sand matrix has higher value of Mu-Rho (MR) than the overlying shale.

Lambda-Rho or incompressibility is a very useful parameter to distinguish fluid content which is subjected to pore fluid. A number of studies have found that sandstone containing hydrocarbon is less dense than sandstone containing water and also are more compressive than wet sandstone. As a result, in sand reservoir containing hydrocarbon the Lambda-Rho (LR) log shows low incompressibility values.

Figure 3.13 and Figure 3.14 show lambda-Mu-Rho, lamé constant and shear module log which generate from input logs for well 11-8 and 11-9 respectively. Blue rectangular parts represent hydrocarbon (gas) zones. (High quality figures are included in appendix B).

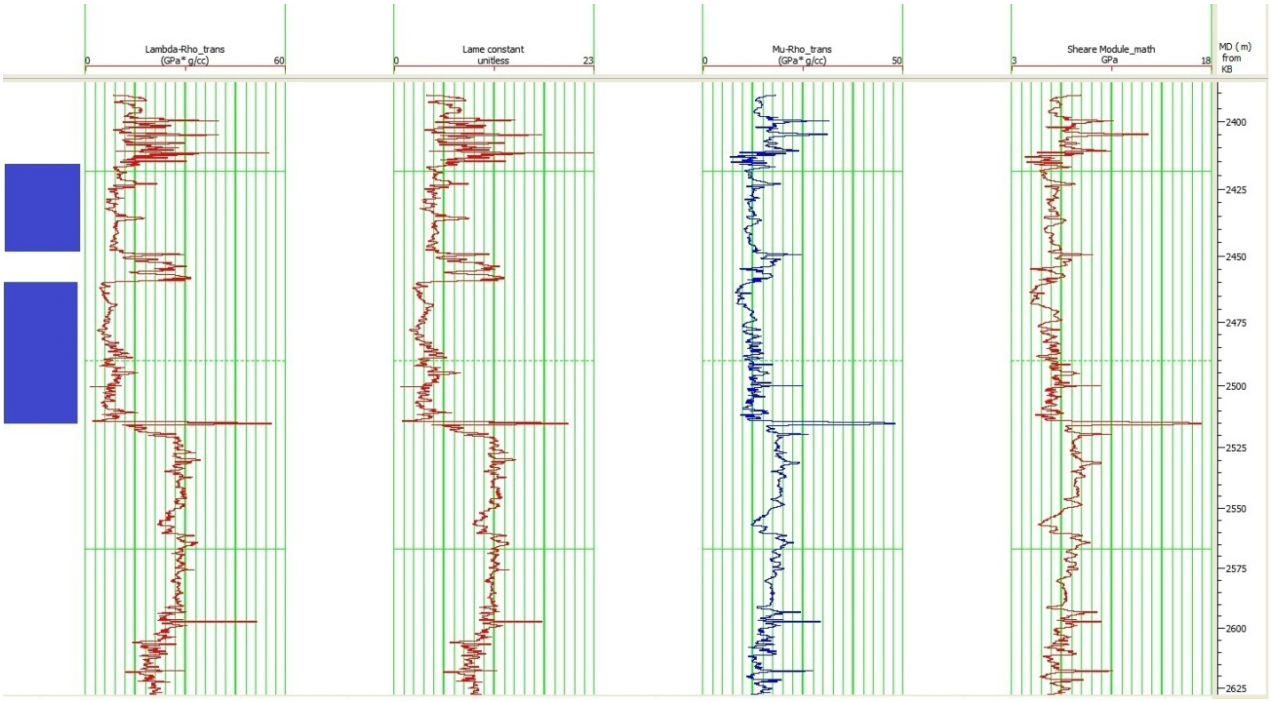

Figure 3.13: From left to right: Lambda– Rho, lamé constant, Mu-Rho and shear module log for well 11-8.

We expected share modulus to be consistent or no significant change in gas sand reservoir; however, Figure 3.13 indicates that the shear modulus decrease significantly and read low values in the zone of interest. The possible explanation for this event, as is clearly seen from Figure 3.1, is that the density log read low value in a gas zone compared to water zone, so this will cause the shear modulus to drop.

If the filtrate invasion is very shallow (which we sometimes see in gas zones) the density log will almost reflect the true formation density, so the density log, and the computed shear modulus, will read particularly low compared to water/oil, and even other gas zones where the invasion is much deeper. It is important to note that we will not get consistent shear modulus in a gas zone if the invasion depth is changing, so causing the density log to change as it sees more or less gas.

Normally some fluid substitution corrections are required for the invasion effects on input data. Also it is crucial to be sure about the quality of the input shear sonic and density data to determine if either of these read unusually low value. For example the density could read a washout instead of formation, or the shear sonic could be incorrectly measured from the waveforms.

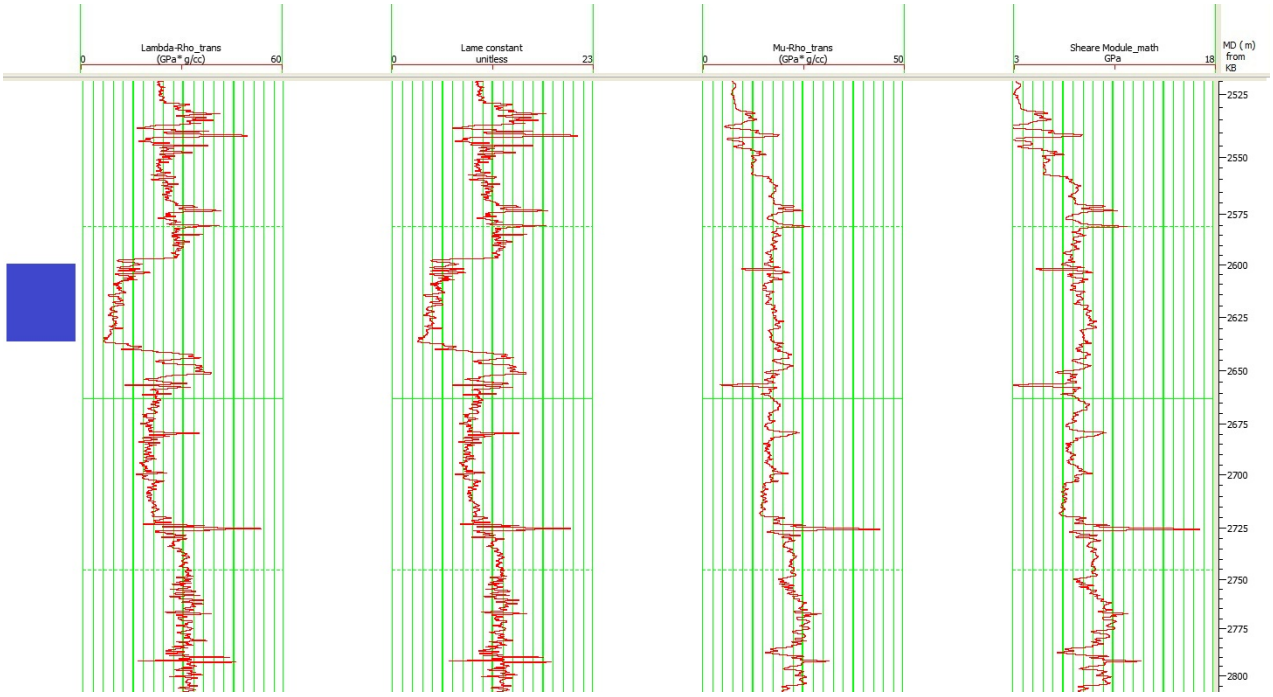

Figure 3.14: From left to right: Lambda– Rho, lamé constant, Mu-Rho and shear module log for well 11-9.

Different lithology has different rock properties behavior which is related to fluid content and mineral properties. In order to identify lithology and fluid separation, the LMR cross plotting was performed ($\mu\rho$ in y axis and $\lambda\rho$ in x axis).

Regarding the rigidity and incompressibility, gas sand reservoir should correspond to the low λ incompressibility (<20 GPa) combined with high rigidity μ (>15 GPa) of sand grain. We should consider the fact that neither λ nor μ are powerful and accurate indicator individually, however the combination of λ and μ exerts a direct indicator for both lithology and fluid content (Hazim, H., Al-Dabagh., Alkhafaf, Shireen, 2011).

Figure 3.15 shows the guideline plot for interpretation of $\lambda\rho$ versus $\mu\rho$ cross plot, presented by Goodway et al. (1997). The threshold cut off, separate porous gas sand from shaly gas sand and also separate clastic rocks from carbonates.

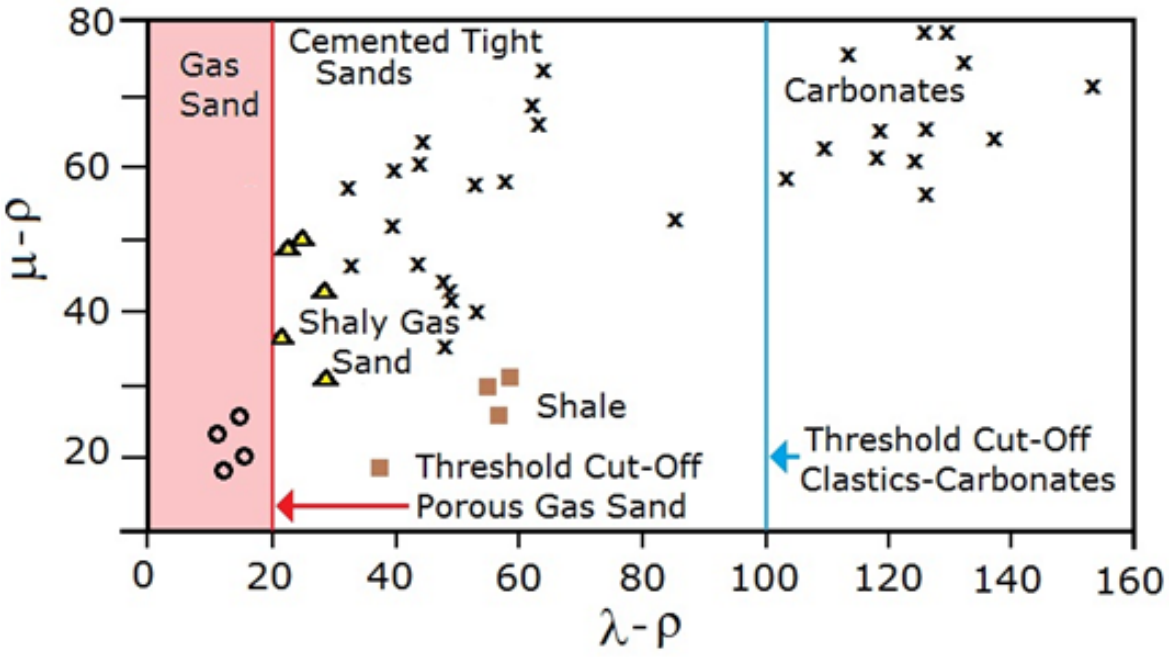

Figure 3.15: Guideline plot for LMR interpretation (adopted from Goodway et al. (1997))

Figure 3.16 shows the LMR cross plot for well 11-8 and 11-9 respectively. The plots show different clusters that are associated with varied lithologies and fluid. The gas sand reservoirs are captured with polygons in both cross plots.

The sand reservoir is corresponded to low λ value and high μ value. The results confirm that we can use this method with confidence to determine reservoir characteristics and separating gas sands from brine sands and shale.

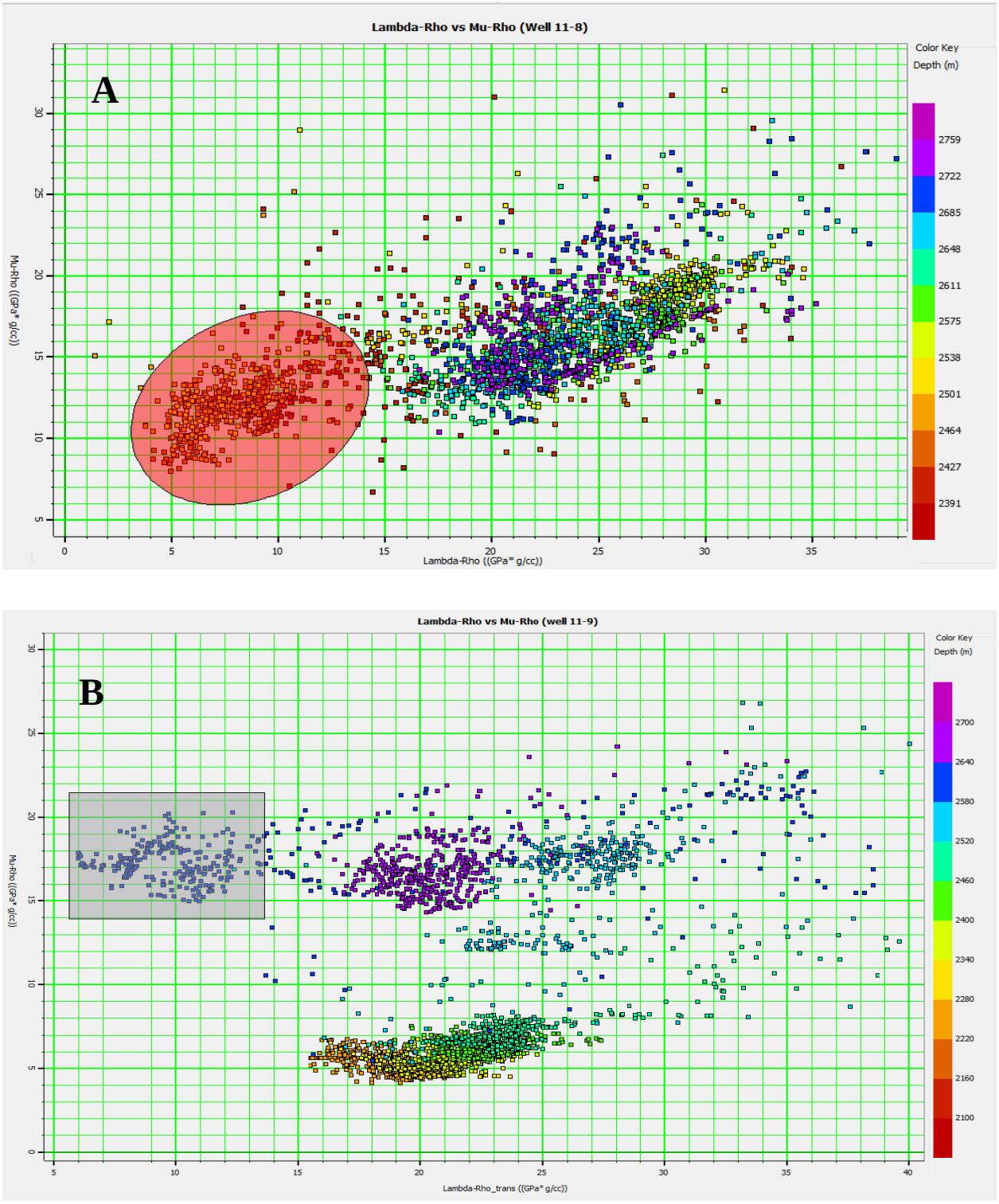

Figure 3.16: The cross plot shows how the LMR volume discriminate reservoir, typically the reservoir zone is interpreted along the edge with low λρ value which represents area with relatively low incompressibility. A) Well 11-8, B) Well 11-9

Figure 3.17 shows cross plot between λ/μ and density (ρ) for well 11-9. What is interesting in this cross plot is that the gas sand reservoir spreads out from non-reservoir area.

Figure 3.18 shows cross plot between λ/μ and acoustic impedance for both wells (11-8 and 11-9). It is clear that one is able to define different clusters regarding to λ/μ values. Yellow polygon represents gas saturated sand areas which are easily distinguished from the other lithologies.

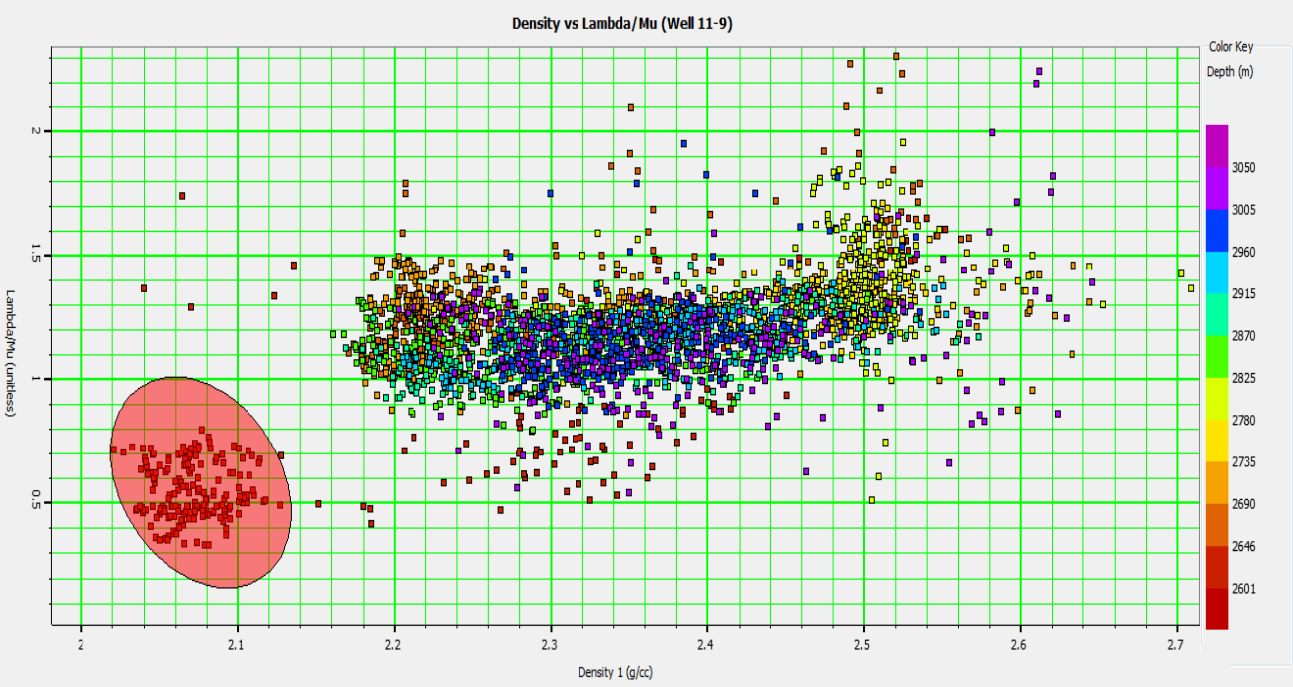

Figure 3.17: Cross plot between λ/μ and density (ρ) for well 11-9.

Figure 3.19 represents the corresponding log sections for cross plot between λ/μ and acoustic impedance for well 11-8 and 11-9 where the captured polygon is shown in log sections.

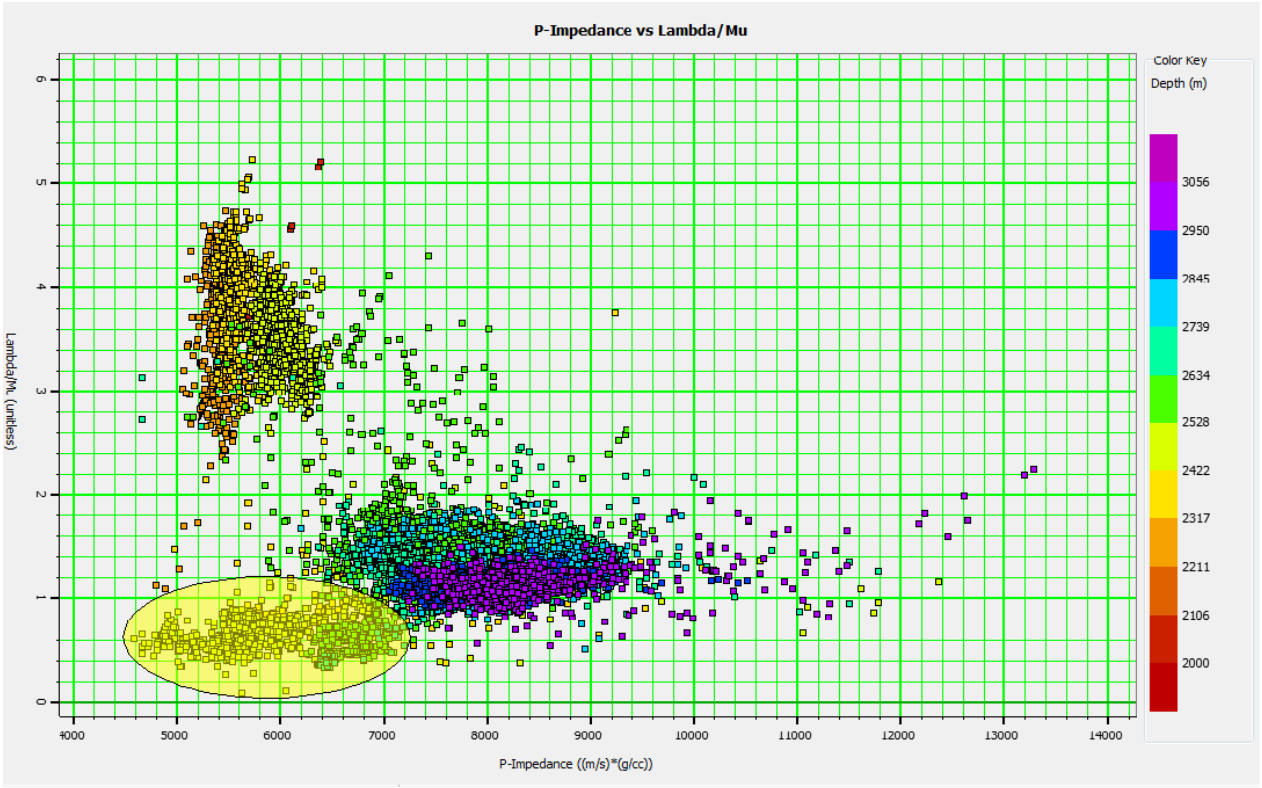

Figure 3.18: Cross plot between λ/μ and acoustic impedance for well 11-8 and 11-9.

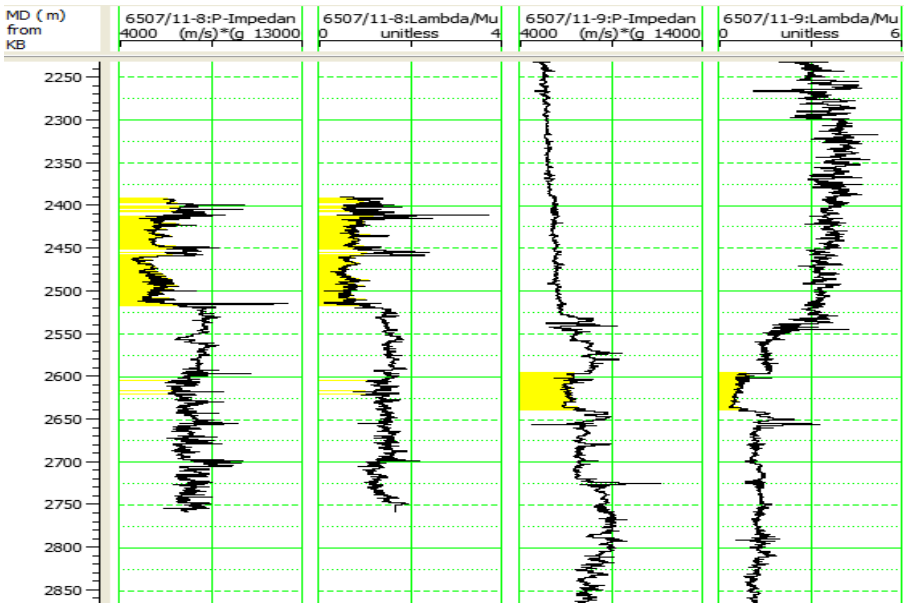

Figure 3.19: Corresponding log sections for P-impedance vs. λ/μ cross plot.

3.2.5 Bulk Modulus

Bulk modulus is a measure of a material's resistance to change in volume. "The presence of porosity in a rock decreases the rock's resistance to change in volume and hence decreases bulk modulus" (David, C., Ravalec-Dupin, M., 2007). Regarding the hydrocarbon exploration, bulk modulus is one of the practical porosity indicators especially in the presence of stiff rocks (equation 3.5).

$$K = \rho \left({V_P}^2 - \left(4 \times \left({V_S}^2 / 3 \right) \right) \right) \qquad (3.5)$$

Figure 3.20 and Figure 3.21 show the behavior of bulk modulus log in reservoir sand and surrounding shale. By increasing porosity of the rock in sand reservoir, stiffness of the rock will be decreased as we expected, therefore we observed low values of bulk modulus in target area for both wells.

There is a large volume of published studies describing the role of the bulk modulus in exploration industry. These studies have revealed that the bulk modulus is much more strong as young`s modulus specially in stiff rocks (e.g. carbonate).

3.2.6 Poisson's ratio

Another important parameter is the Poisson's ratio (σ). It measures "how compression or tension can change a body of material" (David et al. 2007). The importance of Poisson's ratio was discovered when Ostrander (1984) published his famous paper and stated that "presence of the gas in the reservoirs lead to Poisson's ratio possess low values". Ostrander defined Poisson's ratio as the ratio of the relative change in radius to the relative change in length (Ostrander, 1984). A change in the ratio could potentially indicate a change in pore fluid and pronounced on AVO characteristic.

Poisson's ratio can be derived in several ways such as velocity method or LMR (equation 3.6 and 3.7, respectively). In this work Poisson's ratio log was achieved by using velocity method calculation.

$$\sigma = \frac{\left(\frac{V_p}{V_s}\right)^2 - 2}{2\left(\frac{V_P}{V_s} - 1\right)} \qquad 3.6$$

$$\sigma = \frac{\lambda\rho}{2(\lambda\rho + \mu\rho)} \qquad 3.7$$

Figure 3.20 and Figure 3.21 show the computed Poisson's ratio logs. Blue rectangular parts represent hydrocarbon (gas) zones. We observe that the gas saturated formation possess very low Poisson's ratio (~0.15 – 0.2 for well 11-8 and well 11-9) compared to the surrounding formations in both wells. For different lithologies of the same fluid, normally the shalier lithology will plot at relatively higher Poisson`s ratio than the sand lithology.

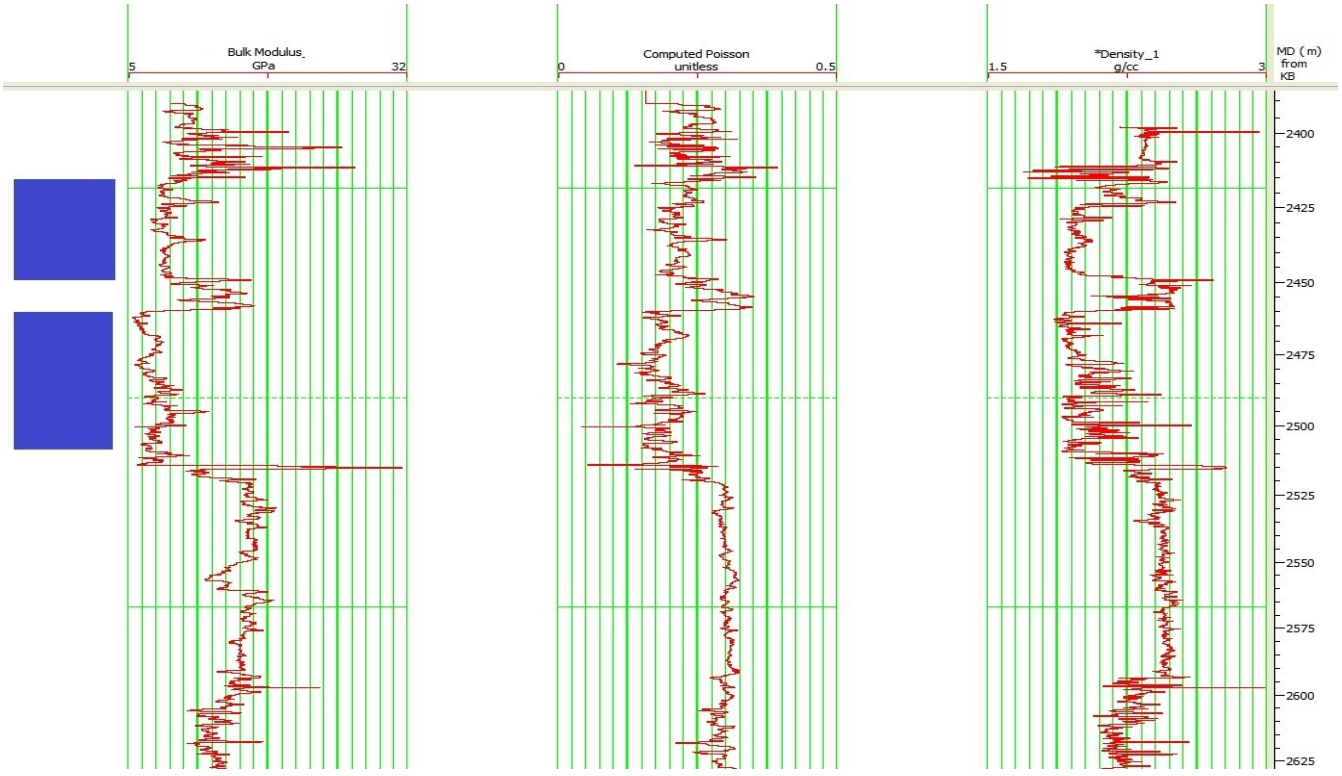

Figure 3.20: From left to right: bulk modulus, Poisson`s ratio and density log for well 11-8.The reservoir sands are characterized by low density, bulk modulus and Poisson`s ratio value.

It is possible to identify hydrocarbon zones by investigating the relationship of Poisson`s and V_P/V_S ratios. Figure 3.22 shows the guideline plot for interpretation of Poisson's ratio versus V_P/V_S ratio for hydrocarbon detection.

According to the guideline plot and based on additional log information, we can classify gas, water and shale zone in the area. Figure 3.23 shows a cross plot of Poisson's ratio versus V_P/V_S ratio in log domain for well 11-9. Cross section of selected area on the cross plot domain completely good fit with our pervious observation about gas reservoir location.

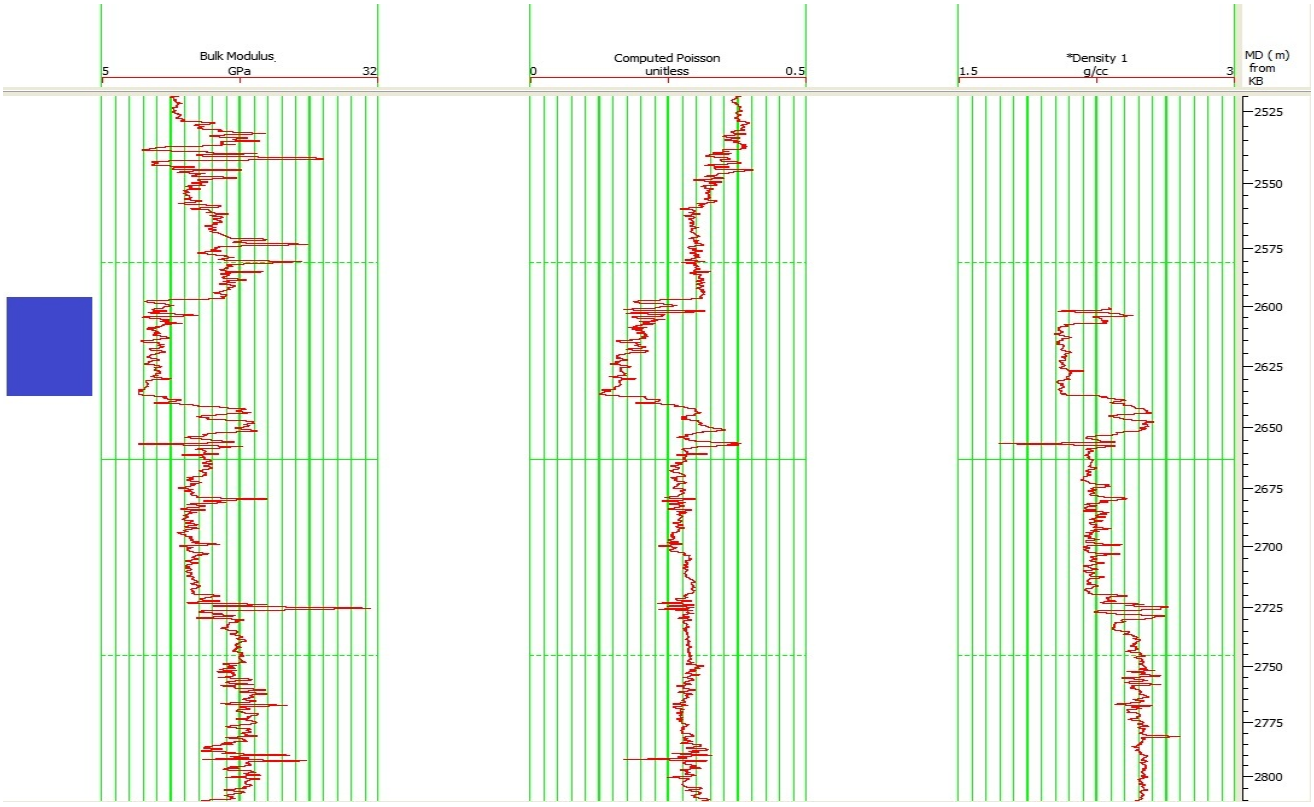

Figure 3.21: From left to right: bulk modulus, Poisson`s ratio and density log for well 11-9. The reservoir sand are characterized by low density, bulk modulus and Poisson`s ratio value.

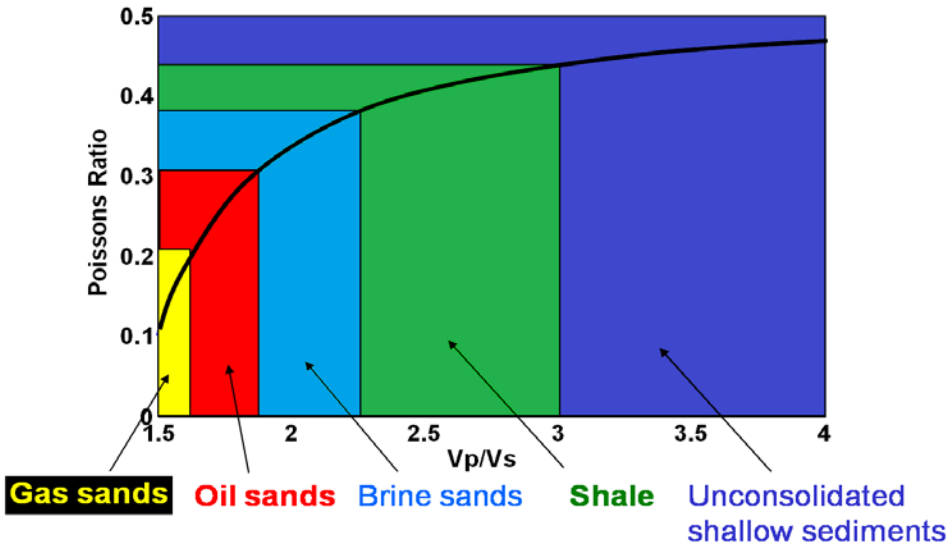

Figure 3.22: Guideline plot for Poisson`s ratio versus V_P/V_S (adopted from Per Avseth lecture note).

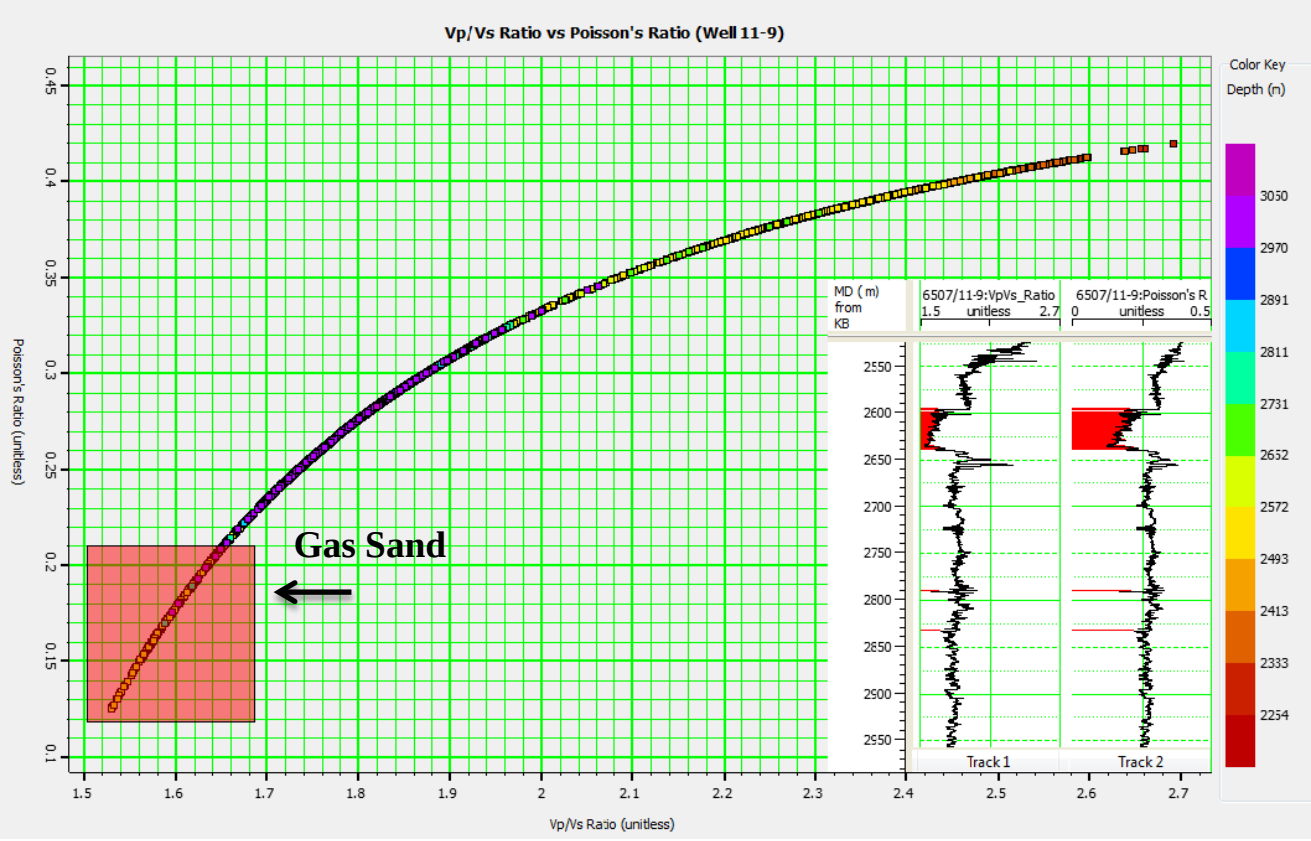

Figure 3.23: Poisson`s ratio versus V_P/V_S cross plot. The gas sand reservoir captured by read polygon.

3.3 Rock Physic Template

Rock physics templates (RPTs) are efficient tools which allow us to overly petrophysical interpretive templates over a cross plot and is associated to enhance lithology and pore fluid prediction (Avseth et al. 2005). The ultimate goal of rock physics template is to interpret and categorize well log and seismic data in order to reduce hydrocarbon exploration risk. Rock physics templates were introduced by Ødegaard and Avseth (2003) and were further developed by Avseth (2005) as an advantageous toolbox to evaluate the relationship between local geologic parameters, rock physics properties and prediction of lithology and pore fluid.

Avseth (2005) pointed out that the rock physics templates enable geoscientists to "determine variation in inverted seismic signature as function of well log attributes such as V_P, V_s and density in relation to pore fluid saturation, porosity, etc."(Avseth et al. 2005). In his major study he also demonstrated that RPT provides a guidance about how seismic response from subsurface structure could be potentially altered by a change in pressure, temperature, burial depth and digenetic effects.

Figure 3.24 represents an example of RPT superimposed onto V_P/V_S versus acoustic impedance cross plot. It contains porosity trends for different lithologies, and increased gas saturation for sand formation. The black arrows indicate different geologic trends: 1) increasing shaliness, 2) increasing cementation, 3) increasing porosity, 4) decreasing effective pressure, and 5) increasing gas saturation (Avseth et al. 2005).

It is clear from Figure 3.24 that RPT shows porosity increasing from right to left and gas saturation increasing from top to bottom. However, it is important to notice that, due to some reasons the rock physics templates are not unique and absolutely true, while they mostly will be handy in our interpretation and delineation of promising zones.

Figure 3.25 provides the calculated rock physics template superimposed onto cross plot of V_P/V_S versus acoustic impedance for in-situ data of well 11-8 and 11-9. The cross plot points are color coded as a function of V_P/V_S ratio shown on the color bar. The rock physics template is calibrated by well 11-8; however, almost similar geological environment makes it applicable for well 11-9 as well.

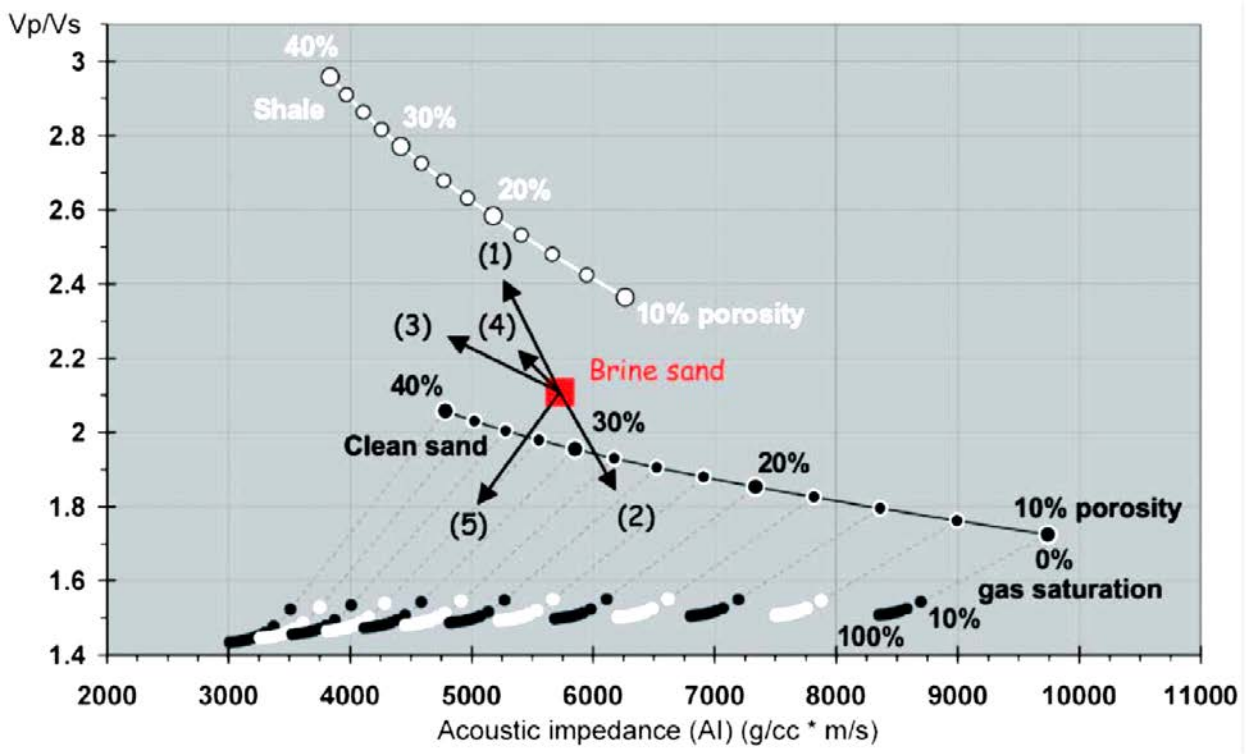

Figure 3.24: Typical example of rock physic template (RPT) superimposed onto V_P/V_S versus acoustic impedance cross plot (Avseth et al. 2005).

Three clusters can be identified in the data. Based on log information we can easily separate lithology and pore fluid (shale, gas sand, brine sand and clystone). From the figure we can see that, shale has higher V_P/V_S ratio and low acoustic impedance while the hydrocarbon (gas) sand has very low V_P/V_S ratio and low acoustic impedance values. As expected brine sand has higher acoustic impedance and V_P/V_S value than the gas sand area. RPT indicates that our reservoir sands fall within a porosity range of about 22% - 30%. Another useful information we can obtain from combination of rock physics template with cross plot data is that at least the sand reservoir not for well 11-8 nor 11-9, is 100% gas saturated (dotted lines indicate the gas saturation) and from this we can interpret that sand reservoirs probably contain about 10% - 15% water (Figure 3.25).

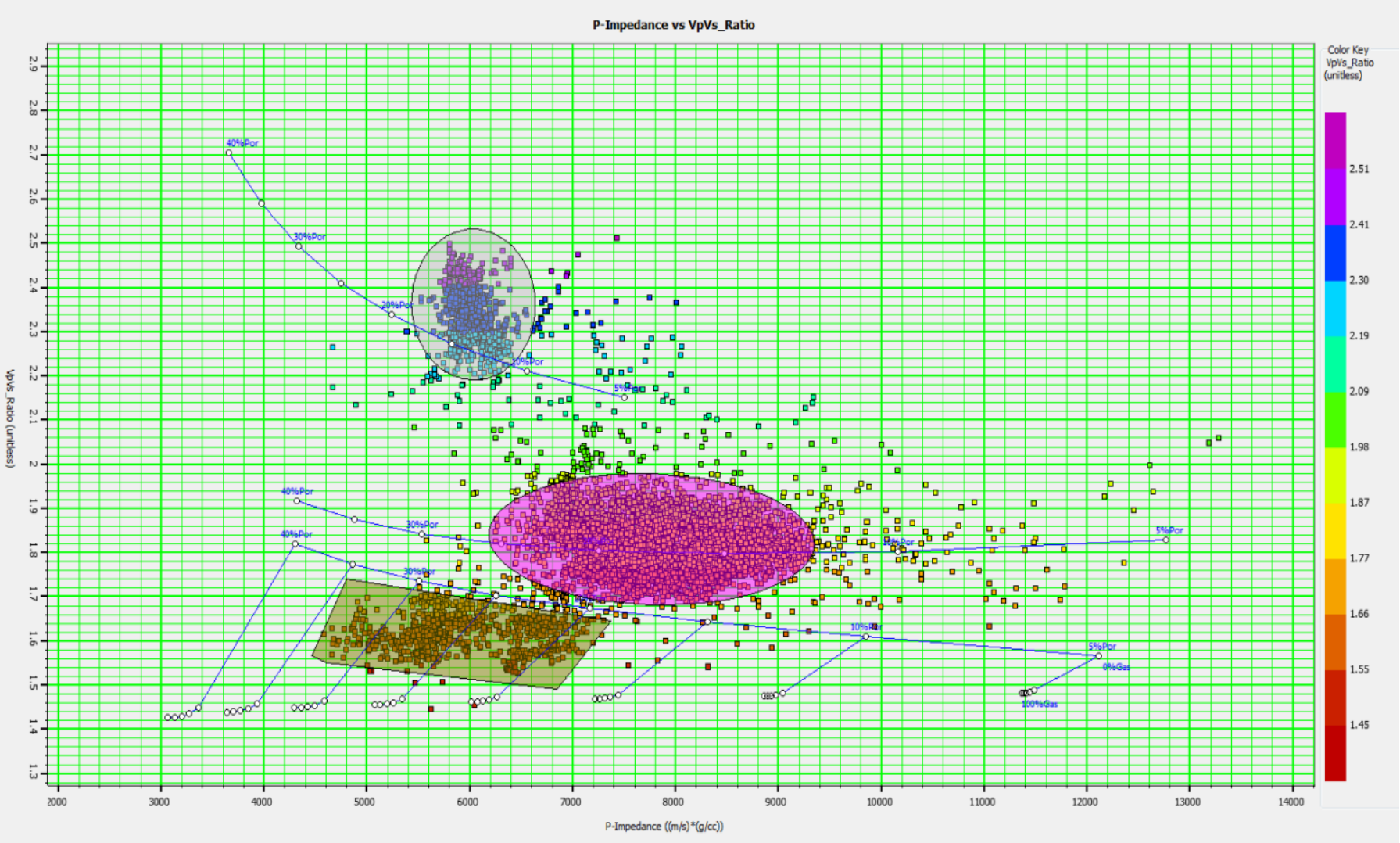

Figure 3.25: V_P/V_S vs Al cross plot for well 11-8 and 11-9 superimposed with the calculated rock physic template

3.4 FRM well modeling

The fluid replacement modeling (FRM) allows us to see what logs would look like or behave with different quantities not encountered in any well (Avseth, P., Dvorkin, J., Mavko, G., and Rykkje, J., 2000). Fluid substitution also shows how the presence of different fluid changes the reservoir properties and quantifying the various scenarios away from well control. In lack of well log observation, we employ rock physics in fluid substitution for understanding and predicting how seismic velocity depends on pore fluid.

The famous Gassman`s relation (1951) is main core of fluid substitution which estimates any pore fluid saturation. With same porosity, softer rock is more sensitive to fluid replacement than a stiffer rock. We model different fluid saturation scenarios in order to test rock property estimation by seeing which properties generate model that matches with the real logs (Avseth et al. 2000).

In fluid replacement approach we deal with three fundamental elements: P-wave velocity, S-wave velocity and density which are applied over the zone of interest. Adding shear wave velocity information often allows us to better understand the pore fluid type and fluid signature. It is important to note that fluid substitution and log modeling must be carefully evaluated and needs accurate and reliable log data (high quality density and porosity) information.

To achieve this purpose, fluid substitution model has been applied for both water and gas in Gassman theory using standard values for quartz sand, water and gas for shear modulus, bulk modulus and density. By doing this, a new set of P-wave, S-wave and density logs (e.g. S-wave.frm) were created for wells to show what the logs would have looked like over the new reservoir condition.

Figure 3.26 indicates the expanded view of in-situ P-wave, S-wave, density and Poisson`s ratio logs (original logs for well 11-9) superimposed on brine saturated logs on the reservoir section (the in-situ fluid is gas in the zone of interest). Comparing in-situ gas saturated logs with the brine saturated logs reveals that V_S (shear velocity) slightly decreases when gas is replaced with brine in well due to the density effect. Replacing gas with brine also causes density and V_P (compressional velocity) logs increase in the zone of interest.

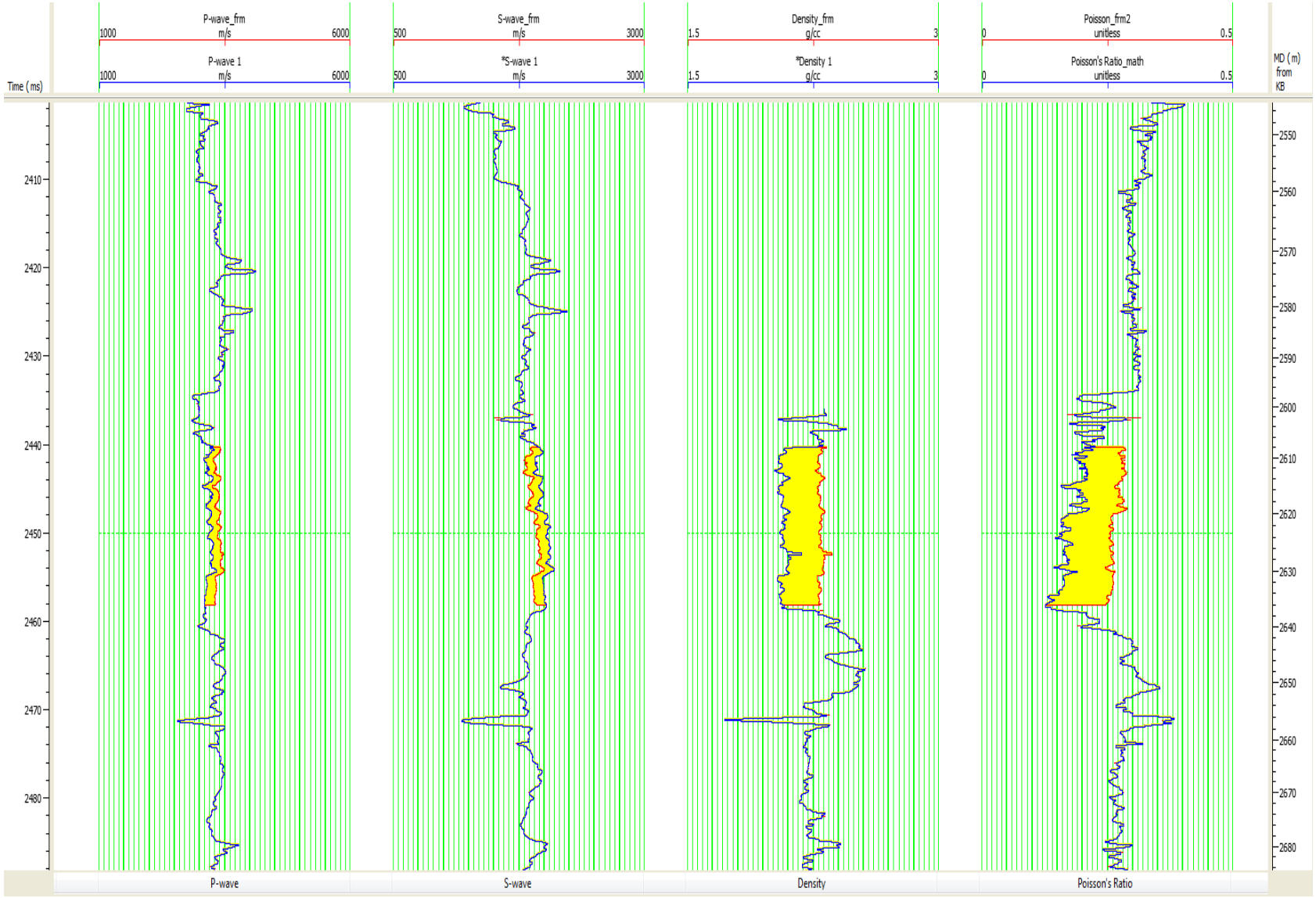

Figure 3.26: Expanded view of in-situ gas interval (blue) is replaced with brine (red) on the reservoir section (Well 11-9). From left to right: P-wave, S-wave, density and Poisson`s ratio log.

4 Extended Elastic Impedance

As we discussed earlier the extended elastic impedance (EEI) is defined as implement rotation in the acoustic impedance and gradient impedance and can be used to obtain elastic parameters and physical properties of reservoir. The basic idea behind EEI inversion method and the key issues which we should view with great care were explained. In this chapter the extended elastic impedance approach is considered to derive several seismic attributes. By applying EEI, the quantitative estimate of reservoir properties are provided which validate the well log and rock physics analysis in third chapter. The main goal of this chapter is to evaluate the sensitivity of EEI approach to seismic anomaly, highlight the difference between reservoir and non-reservoir and identify hydrocarbon zones.

4.1 Extended Elastic Impedance

The initial step in extended elastic impedance method is to determine the best projection angle (χ) (called chi angle) for reservoir target parameters. Practically in any EEI study, determining the optimum angle for a particular target logs is the key to successful application of EEI and should be carefully evaluated. For the purpose of project angle estimation, log attributes which were already estimated in chapter 3 are used, namely, V_P/V_S ratio, bulk modulus(κ), lamé constant (λ, μ), water saturation (S_w), S-Impedance, porosity (ϕ) and so on for cross correlation coefficient study.

The main objective is to cross correlate the petrophysical and elastic parameters from the well log data with extended elastic impedance (EEI) values which are also derived from our reliable P-wave, S-wave and density log (equation 2.3, 11) to find best chi angle (χ) for each target parameters at maximum correlation.

The EEI log spectrum method is used for cross correlation study. In this method, first we generate EEI log spectrum and cross correlate the log reflectivities with the desired reservoir parameters to obtain the optimum angle to use. Figure 4.1 illustrates the procedure for determining the value for χ (called EEI spectrum method).

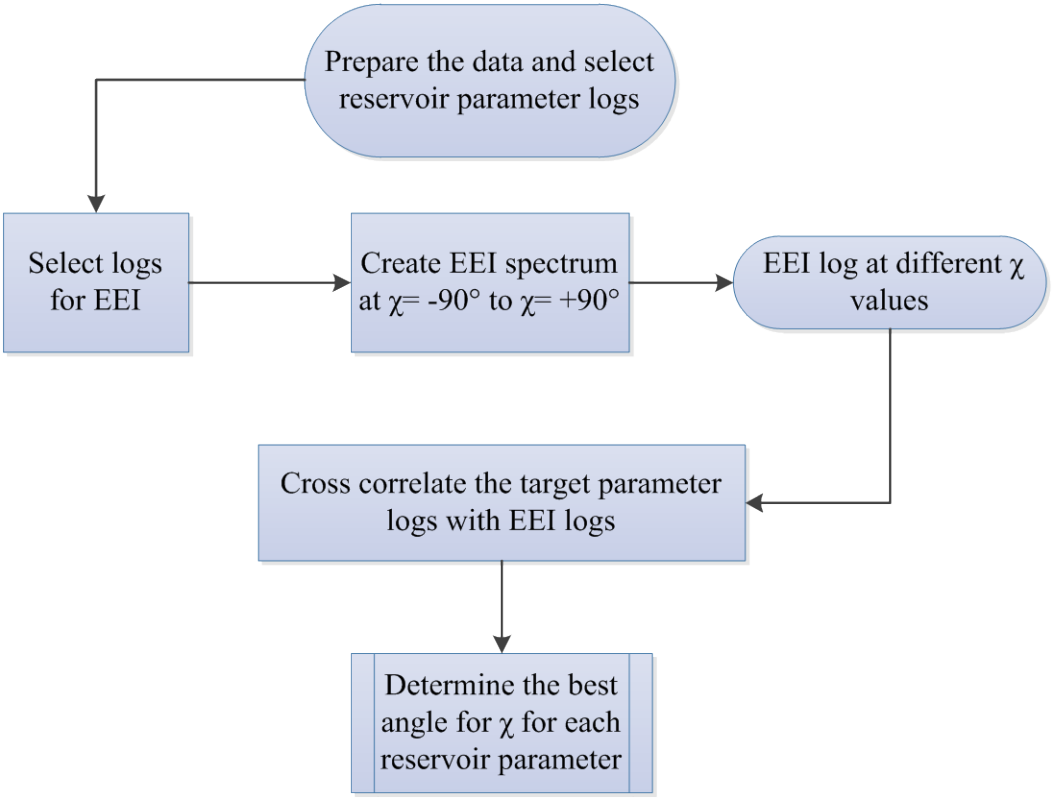

Figure 4.1: EEI spectrum procedure for best chi angle determination

One of the problematic areas in the application of extended elastic impedance is the calculation of project angles. Although extensive research have been carried out on this angle calculation method, angles estimated from petrophysical data will not give precisely the same optimum angles estimated for real seismic data. This is caused both by uncertainties in the seismic velocities and angle calculation. Noise, anisotropy effect and velocity error can cause systematic errors in chi angle calculation (EEI log spectrum method).

Moreover, the optimum chi angle depends on the time window over which correlation coefficient analysis is carried out. Therefore, for more accurate projection angle estimation for different elastic parameters, instead of using the entire log extent (which could potentially include too much geological variation), we should focus on optimum time window that cover only zone of interest (target area) for better geological consistency. The other option to optimize the response is to fulfill the correlation coefficient analysis with desired well logs after removing the low frequency trend from logs data. Since low frequency trend sometimes mask lithology or fluid information (Sharma, 2013).

It is important to note that for different wells with diverse lithology and fluid, the estimation of optimum rotation angle may be different, so it can be hard to find exact optimum chi angle for multiple wells. To tackle this issue, separate chi angles for both wells were calculated as shown in Table 4.1, then some of the angles in the seismic section were reanalyzed and modified to obtain best outcome to improve the lithology and fluid separation.

Whitcombe et al. (2002) demonstrated that "bulk modulus (κ) and lamé`s parameter (λ) tend to lie within an area of EEI space with values of χ from about 10° to 30°". He also stated that shear modulus and V_P/V_S ratio would lies within a range of χ from about -30° to -90° and about 45° repectively. "These areas are therefore likely to be good starting points to look for optimum fluid and lithology impedance functions, respectively" (Whitcombe et al. 2002). Regarding Table 4.1, we can observe that the calculated chi angles are comparable with values stated by Whitcombe.

A	Target Log	χ angle (in degree)	Correlation coefficient (%)
	V_P/V_S	39	0.992
	S_W	43	0.445
	Bulk modulus	18	0.987
	Lambda-Rho	24	0.948
	Mu-Rho	-42	0.99
	Shear Modulus	-53	0.983
	Porosity	42	0.392
	Poisson`s ratio	34	0.797
	GR	17	0.571
	V_{Clay}	13	0.531
	S-impedance	-36	0.996

B	Target Log	χ angle (in degree)	Correlation coefficient (%)
	V_P/V_S	35	0.98
	S_W	25	0.462
	Bulk modulus	15	0.978
	Lambda-Rho	19	0.983
	Mu-Rho	-41	0.99
	Shear Modulus	-56	0.983
	Porosity	-	-
	Poisson`s ratio	29	0.975
	GR	15	0.84
	V_{Clay}	19	0.632
	S-impedance	-39	0.995

Table 4.1: Cross correlation study result represents the maximum correlation of target logs and corresponding chi angle A) well 11-8, B) well 11-9

Figure 4.2 shows the correlation coefficient versus chi angle between EEI curves with V_P/V_S ratio and S_w for well 11-8, respectively. According to this, the maximum correlation coefficient for V_P/V_S and S_w occur at 0.99 ($\chi = 39°$) and 0.445 ($\chi = 43°$), respectively.

Alternatively we could extract the minimum correlations (i.e. zero crossing) for lithology, ($\chi = -18°$) for V_P/V_S . Any anomalies at this angle then should not be related to the lithology. This trick could be a good way to highlight fluid also.

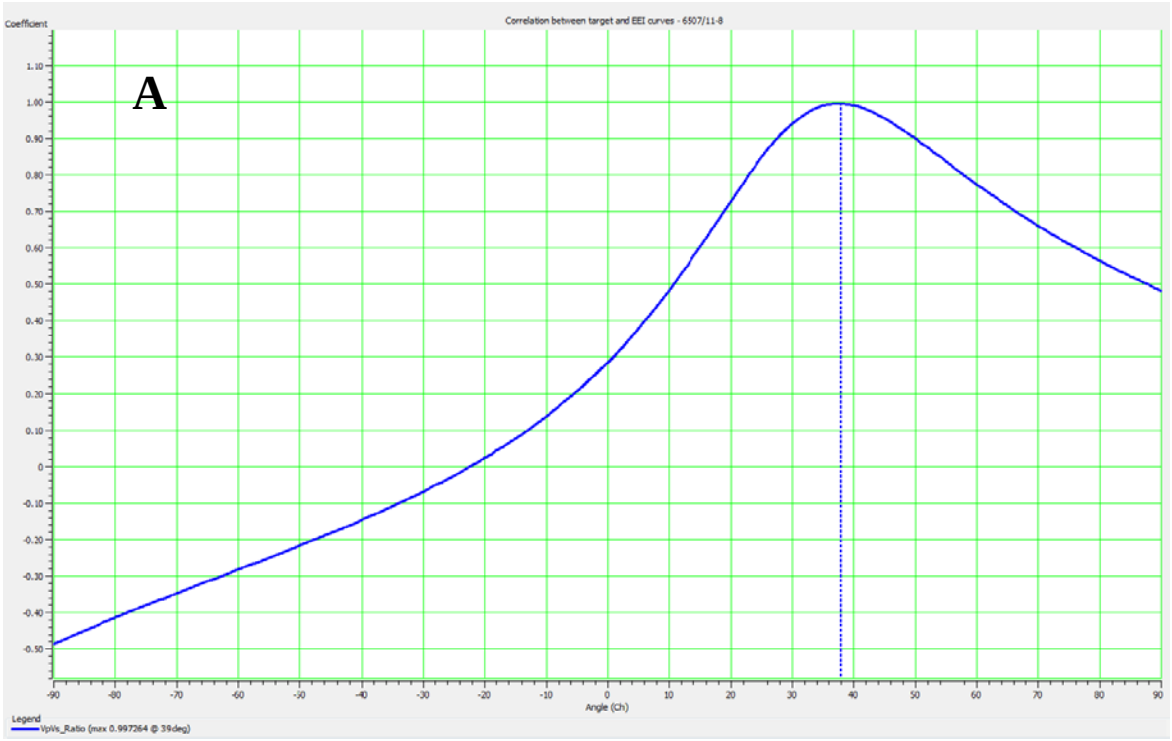

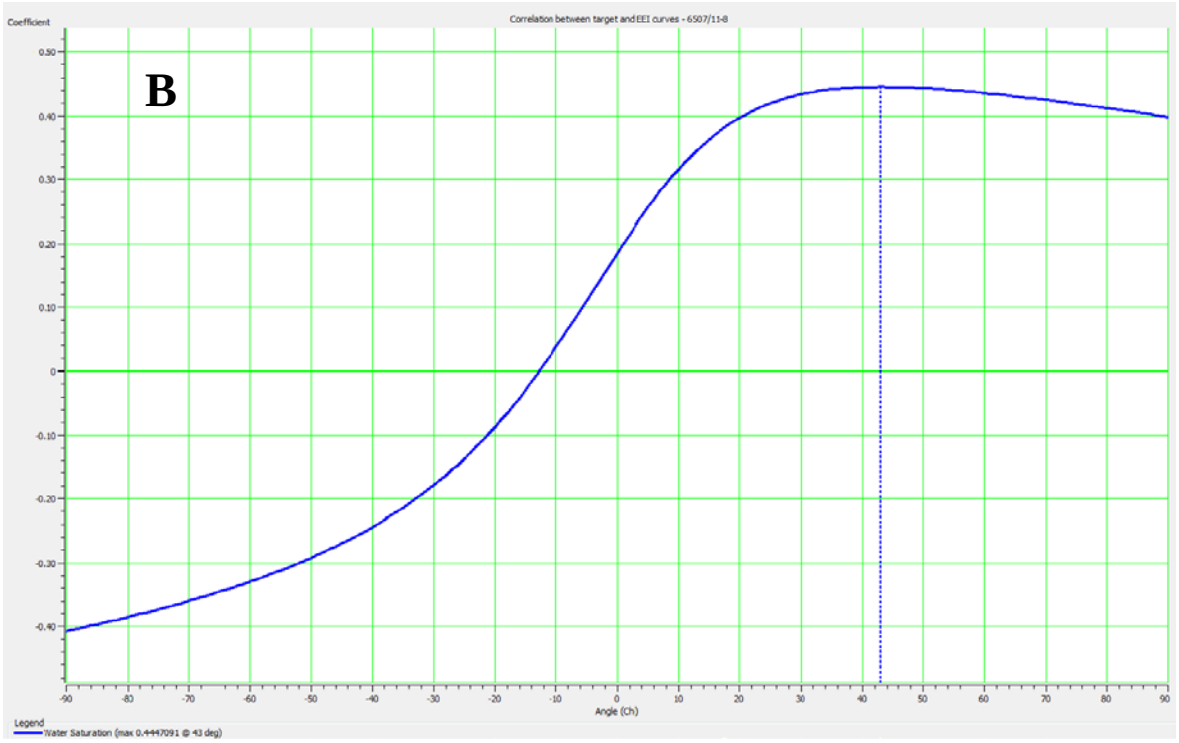

Figure 4.2: The correlation coefficients between EEI and a)V_P/V_S, b) S_w curve for range of values of χ (for V_P/V_S and S_w the highest correlation occur at 0.99 at 39° and 0.445 at 43°)

The second step is generating EEI log for each target log at the premium angle of maximum correlation according to equation 2.3 (11) (EEI curves is parameterized by the project angle). In order to quality control and confirm that selected chi angle would work, we should plot EEI log attributes against equivalent well log derived attributes. If they track and well fit, it means that our project angle calculations are reliable.

Figure 4.3 and Figure 4.4 illustrate the EEI logs with target logs for well 11-8 and 11-9 respectively. It is apparent from these figures that, except for scaling factor (EEI log units are impedance); the EEI curves show satisfactory similarity with well log curves particularly in reservoir area. As figures show, the high correlation is with the Lambda-Rho, V_P/V_S ratio and bulk modulus in the zone of interest (ZOI) which confirms the capability of the EEI log at these angles. These results indicate that we can proceed one step further and use petrophysical volumes derived through EEI approach for quantitative interpretation. It is important to note that, under the situation of not satisfactory correlation, we should check our data quality and our parameters again then redo the process from starting point.

The EEI log spectrum method did not show good results for porosity in both wells. As Table 4.1 illustrates, the poor correlation coefficient associated with project angle, make it impossible to determine reliable chi angle for porosity from this method.

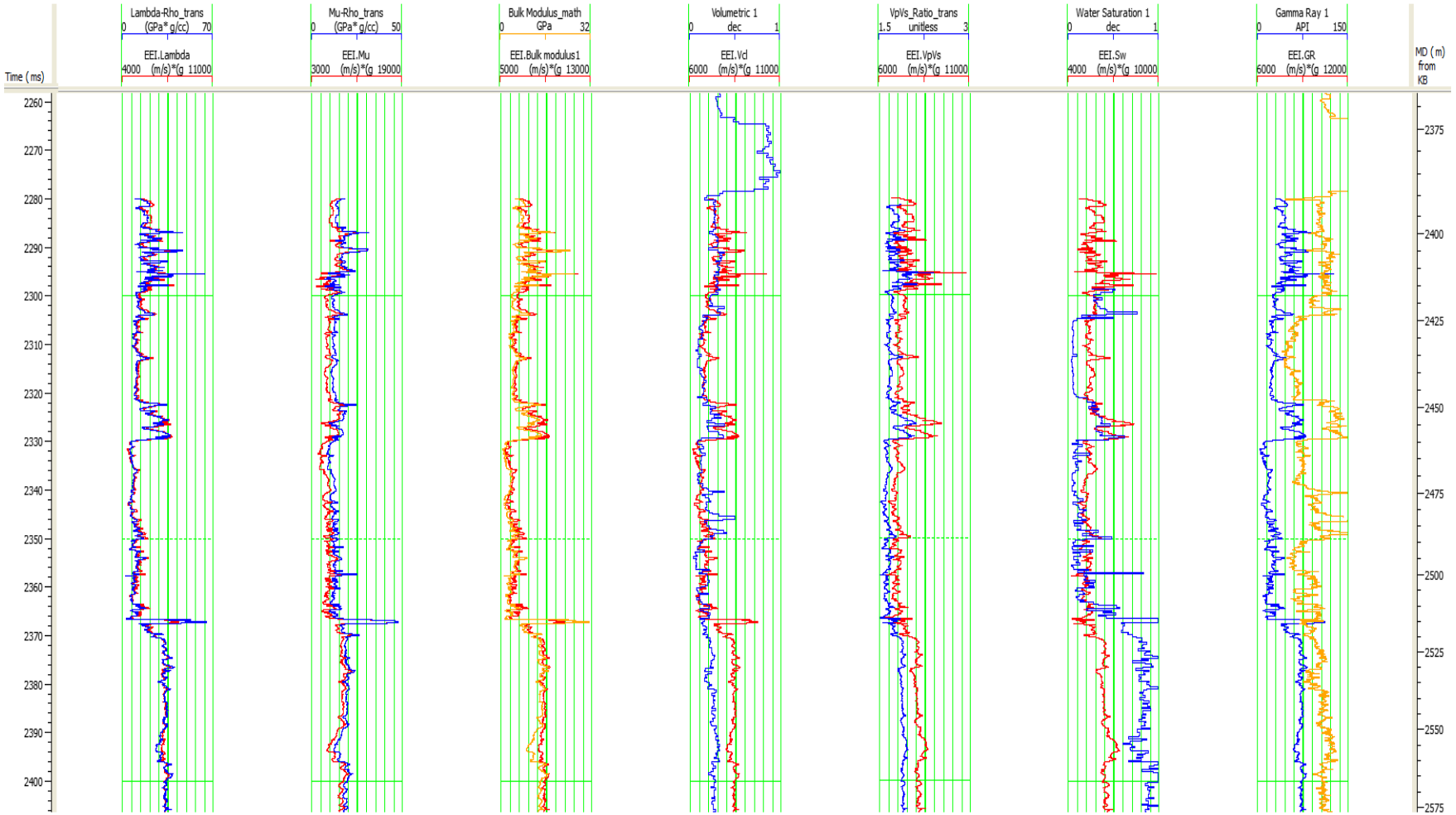

Figure 4.3: Calculated EEI logs superimposed on target logs for well 11-8. EEI log for Lambda-Rho, V_P/V_S ratio and bulk modulus closely resemble the attribute logs generated from the well but the units are impedance (from left to right: Lambda-Rho, Mu-Rho, bulk modulus, volume of shale, V_P/V_S ratio, water saturation and GR log).

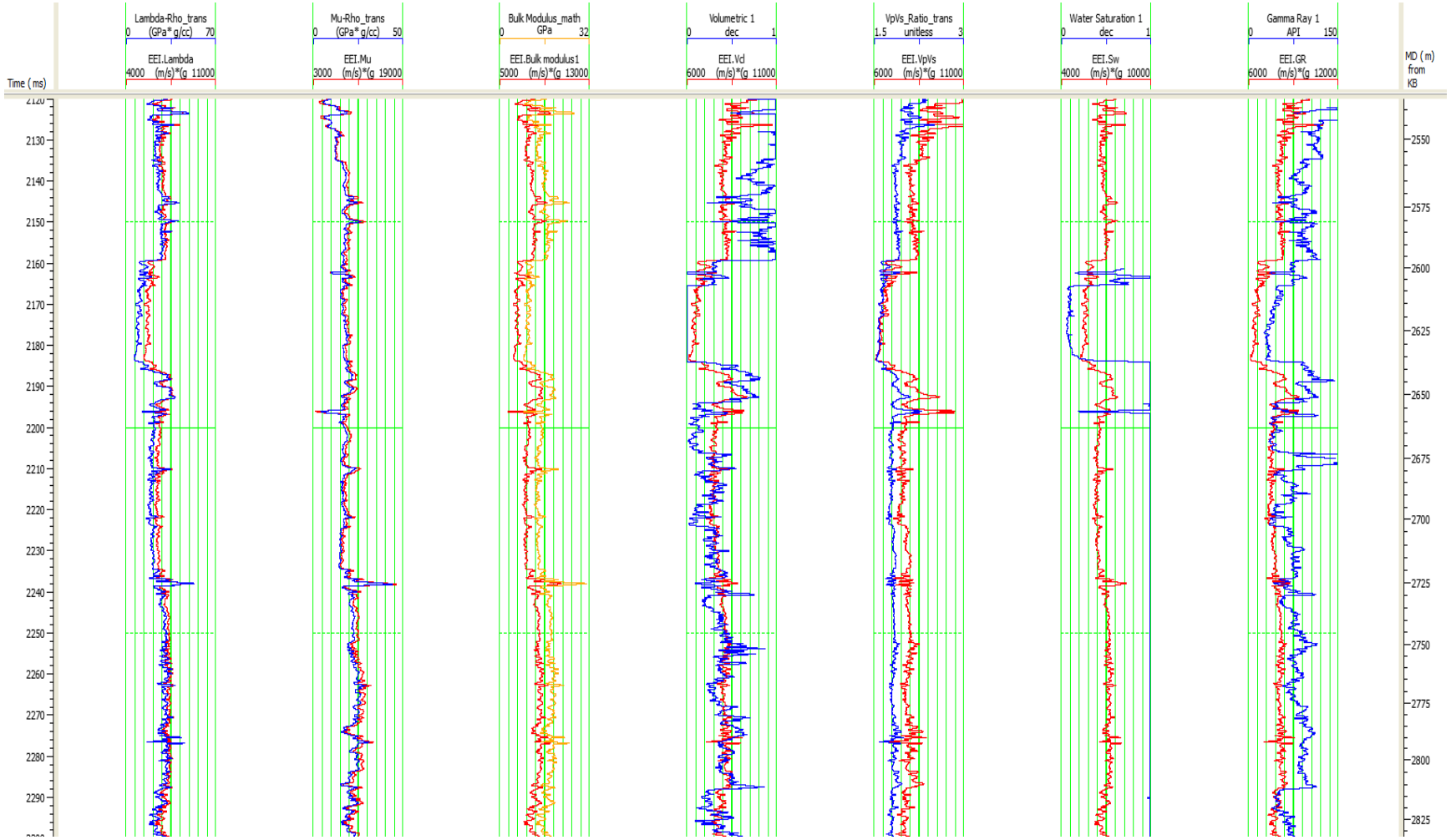

Figure 4.4: Calculated EEI logs superimposed on target logs for well 11-9. EEI log for Lambda-Rho, V_P/V_S ratio and Mu-Rho closely resemble the attribute logs generated from the well but the units are impedance (from left to right: Lambda-Rho, Mu-Rho, bulk modulus, volume of shale, V_P/V_S ratio, water saturation and GR log).

Another quality control method is EEI log spectrum analysis which shows the EEI computation for every angle between -90° and +90°. This approach allows us to see which angle value seems most reasonable. Figure 4.5 shows the EEI spectrum analysis for well 11-8.

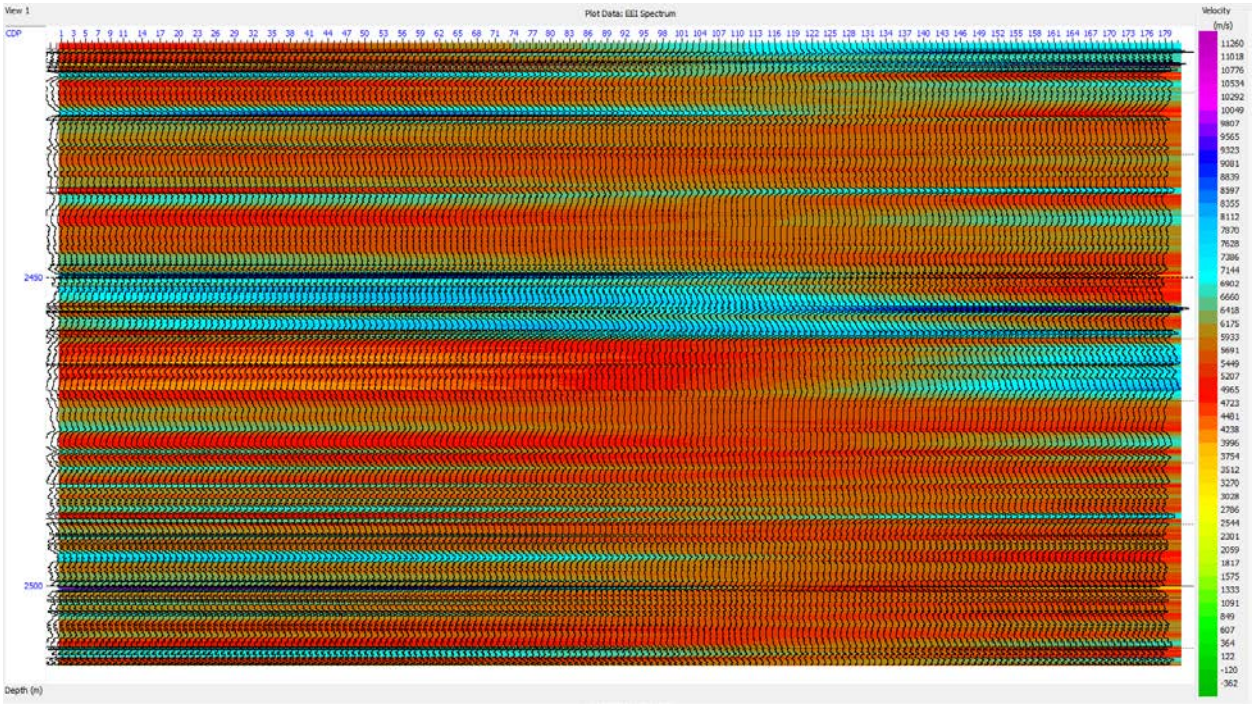

Figure 4.5: EEI log spectrum for well 11-8 shows the EEI computation for every angle between -90° and +90°. (There is no difference at ($\chi = 0°$)

In the next step, the EEI equation (equation 2.3, 11) was utilized again with the same chi angles found from cross correlation study and was applied on seismic inversion data to generate equivalent pseudo seismic volumes (EEI attributes). Implementation of extended elastic impedance to generate the desired volume attributes was performed using TraceMath scripts tool on Hampson-Russell software (HRS 9).

For this purpose, first seismic key volumes, V_P, V_S, ρ were derived from the input data volume (AI and V_P/V_S), then EEI equation (equation 2.3, 11) used to project new seismic volume corresponding to the chi angles designated for each elastic parameters described in the previous step. In order to obtain more accurate results, instead of using constant value 0.25, the K value was computed directly from the P-wave and S-wave velocity volumes (TraceMath scripts).

The products is EEI volumes corresponding to different elastic and petrophysical parameters such as bulk modulus, V_P/V_S ratio, LMR, S_w, etc. which are present in the following pages. The results indicate that chi angles obtained in cross correlation study can provide good separation between fluid and lithology on the zone of interest.

Check shot correction and log correlation were carried out for a well to seismic tie. By doing this, seismic attributes were studied in comparison with well log data. The present results are well defined and delineate gas sand reservoir.

Figure 4.6 shows the section view of EEI lambda volume ($\chi = 24°$). The equivalent log overlay on pseudo seismic volume (EEI volume) represents good fit and confirms inverted EEI result (Figure 4.7). It can be seen from the inverted result that the gas sand reservoir has low impedance (yellow) encased with high impedance shale (blue) at the well locations. The EEI lambda attribute is crisp and distinct within the gas zone encountered by the wells.

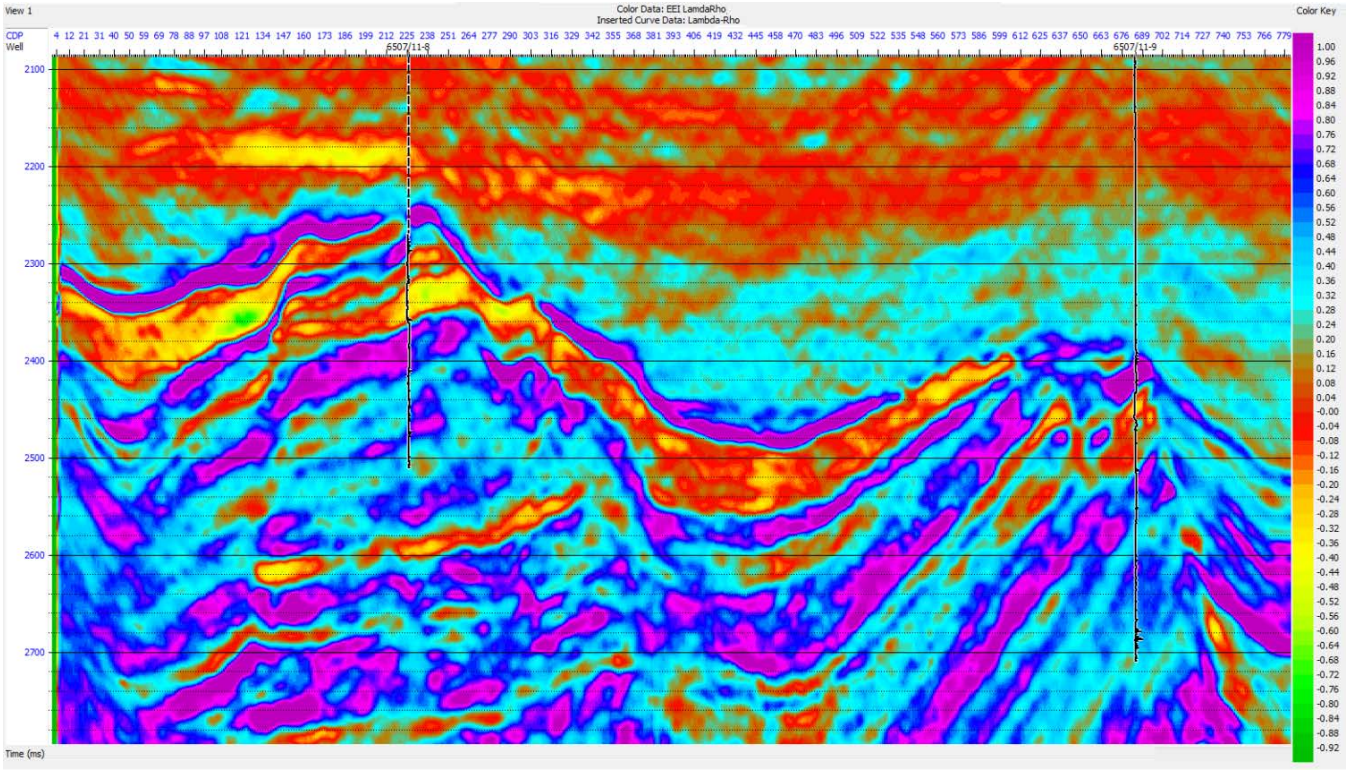

Figure 4.6: EEI lambda attribute ($\chi = 24°$)

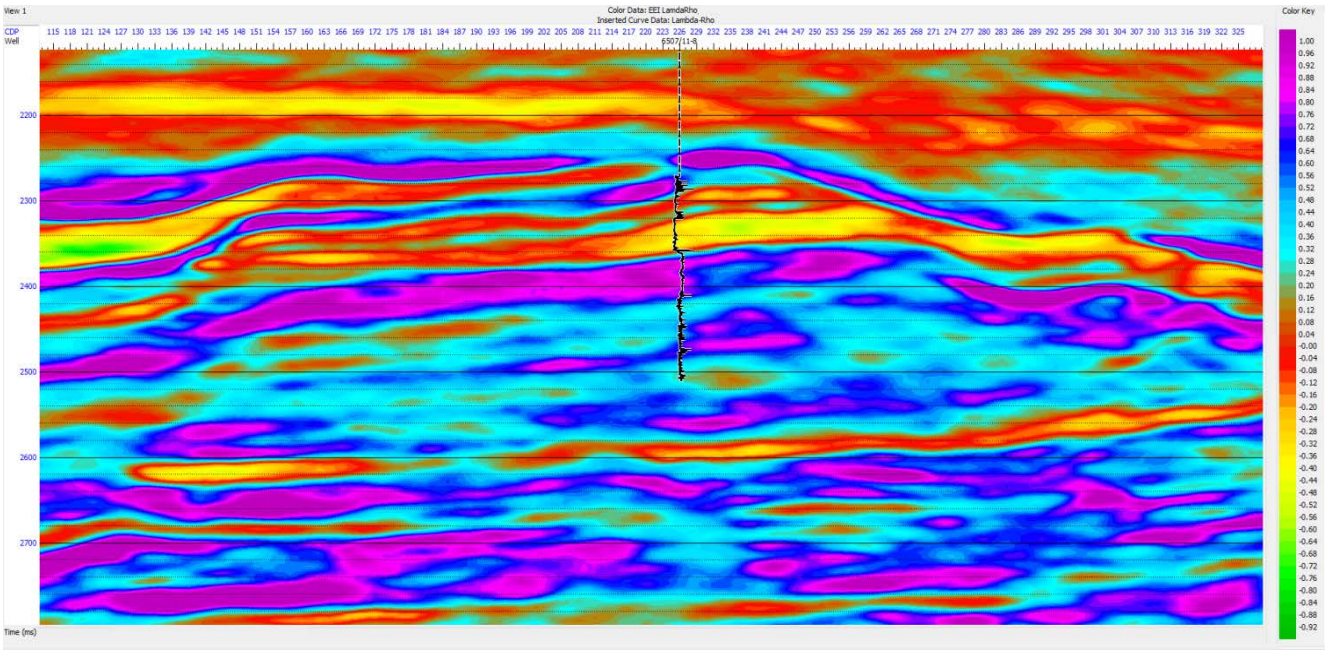

Figure 4.7: Expanded view of EEI lambda attribute around well 11-8 ($\chi = 24°$)

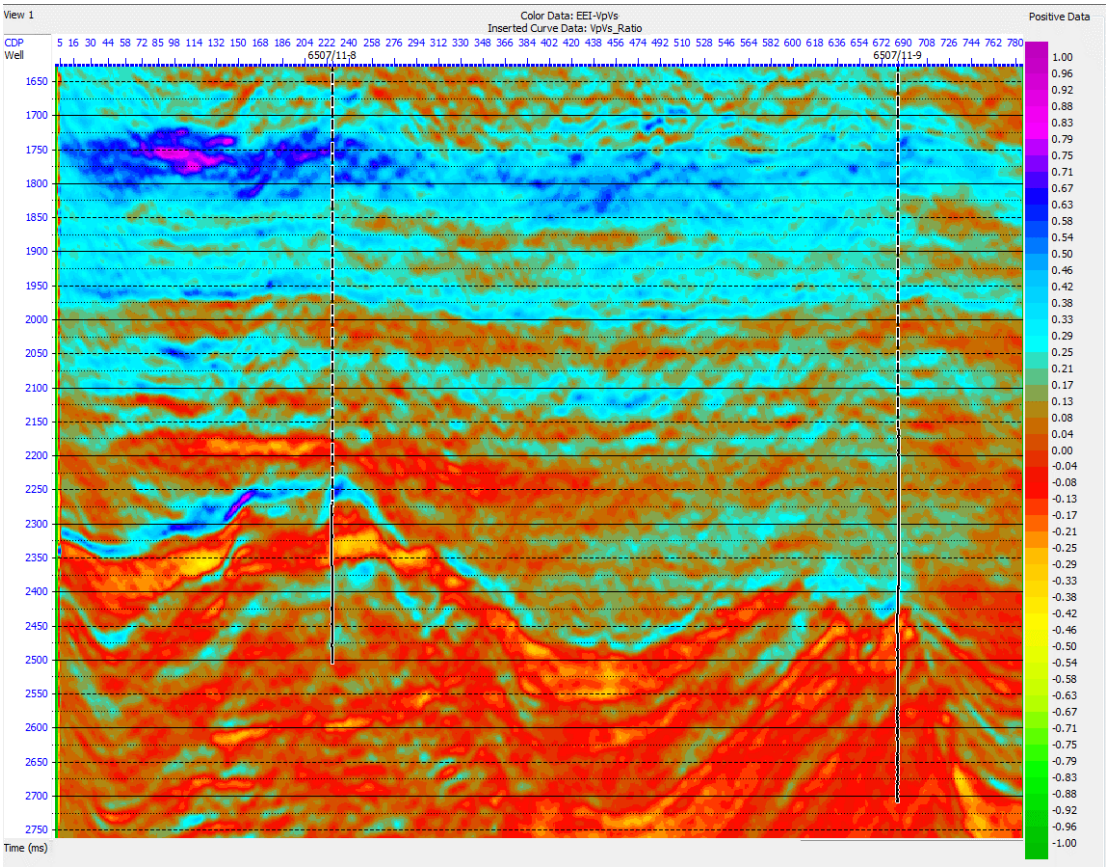

Figure 4.8: V_P/V_S EEI attribute ($\chi = 39°$)

EEI V_P/V_S volume ($\chi = 39°$) which shows excellent definition of the gas sand reservoir is presented in Figure 4.8. It is apparent from the figure that the correlation between EEI inversion result and V_P/V_S ratio log is interesting and gas sand zone is well defined.

Figure 4.9 shows the cross plot of acoustic impedance versus EEI V_P/V_S volume ($km/s * g/cm^3$).

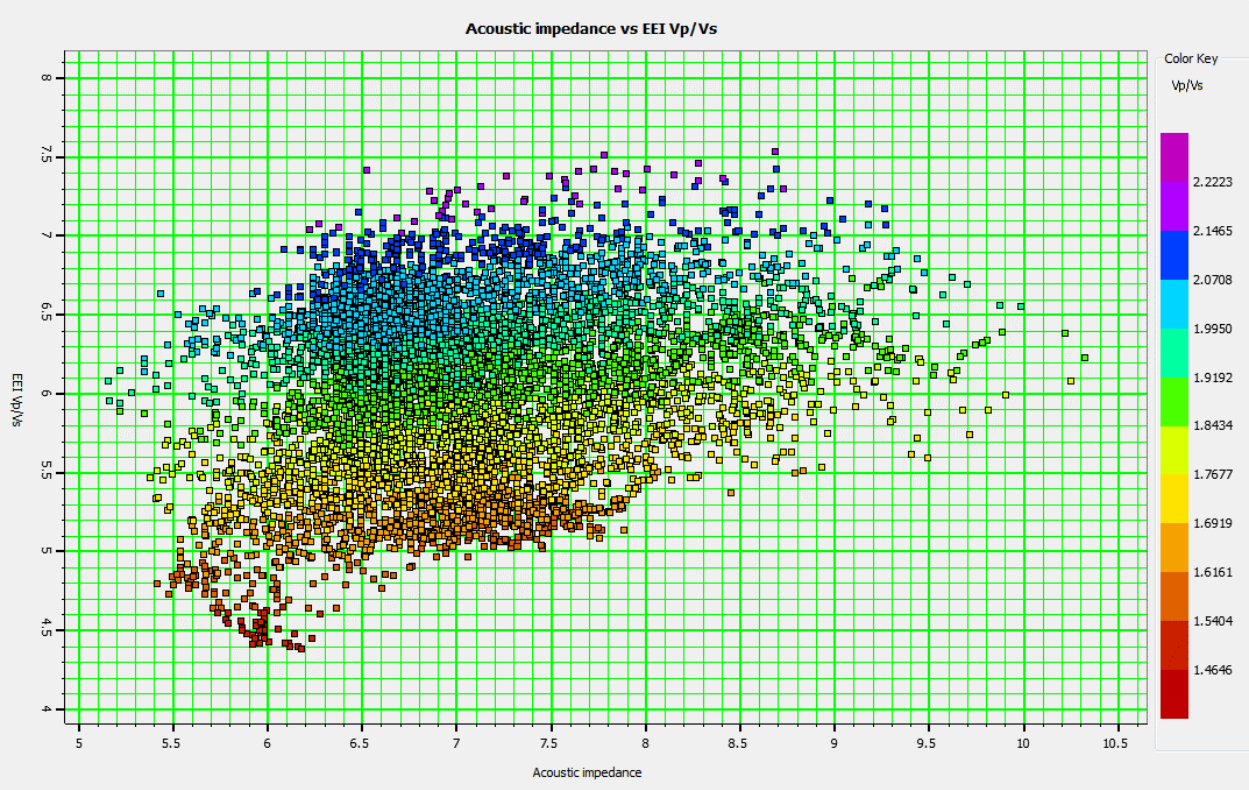

Figure 4.9: Acoustic impedance versus EEI V_P/V_S volume cross plot.

Figure 4.10 demonstrates a) The cross plot of EEI V_P/V_S volume versus EEI Lambda-Rho volume with cluster covering the gas sand reservoir. The attributes plotted as $km/s * g/cm^3$, the observed EEI values are in the range of 4-8 ($km/s * g/cm^3$) which is typical for moderately consolidated rocks (the cross plot is color coded by V_P/V_S ratio), and b) Cross section of selected polygon on seismic section which shows approximate location of hydrocarbon reservoir. Cross plotting enables us to enhance recognition of zone of interest and layer properties from the inversion data. These in turn could be useful to better understanding and definition of hydrocarbon reservoir.

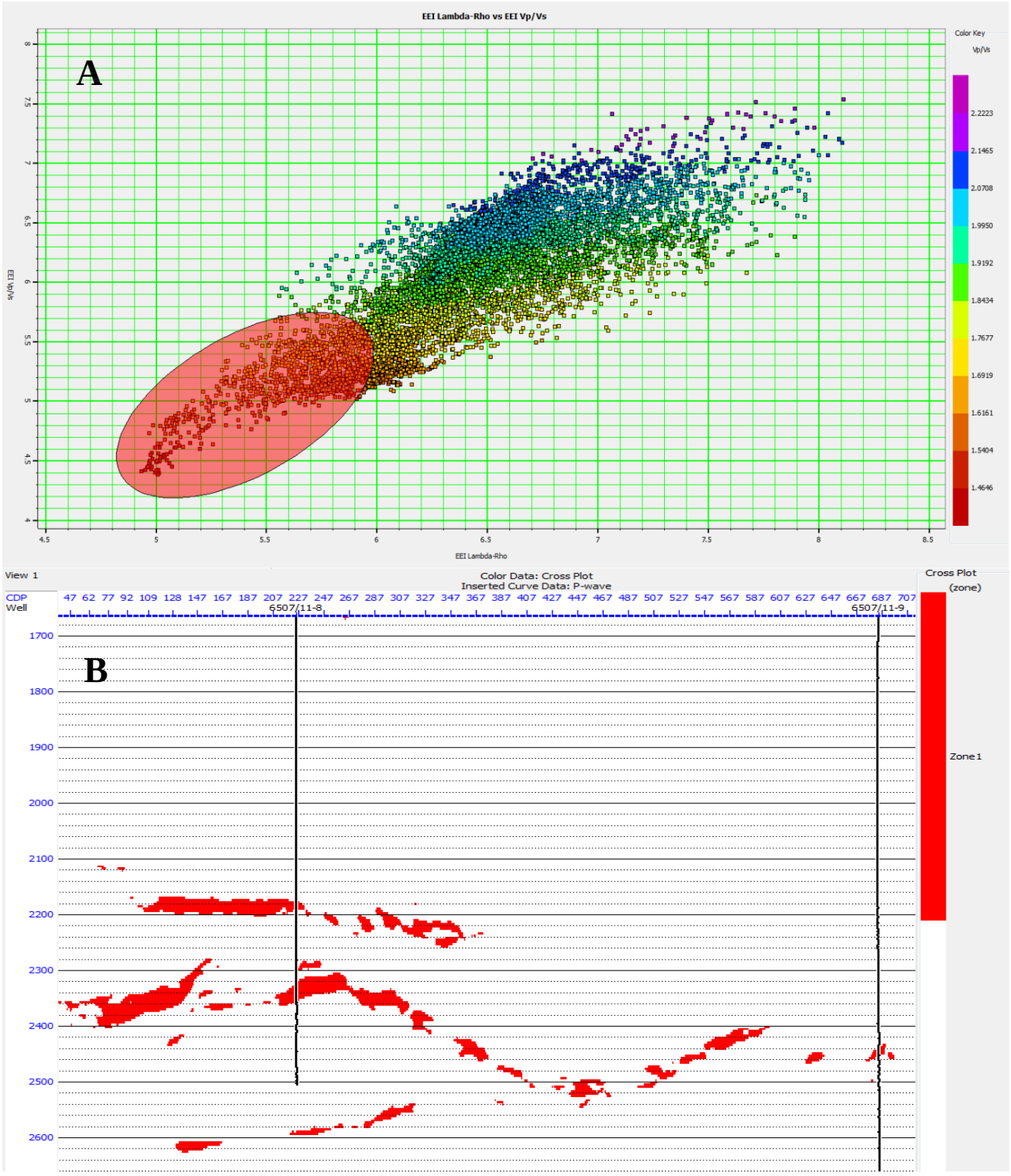

Figure 4.10: a) The cross plot of EEI V_P/V_S volume versus EEI Lambda-Rho volume with cluster covering the gas sand reservoir and b) Cross section of selected polygon on seismic section

Figure 4.11 shows inverted EEI bulk modulus ($\chi = 17°$) overlaid on bulk modulus log. As Figure 4.12 shows, the gas sand reservoir has the correct low EEI bulk modulus (yellow) values around well 11-8.

Figure 4.13 and Figure 4.14 illustrate the expanded view of V_{Shale} and S_w volumes obtained from EEI application respectively. From Figure 4.13 we can see that the inverted results showing good correlation with GR log around well 11-9. The target area shows low volume of shale as expected from well log analysis. Also as shown in Figure 4.14 we can clearly see the low EEI S_w around well 11-8 which is correlates well with water saturation log around well 11-8.

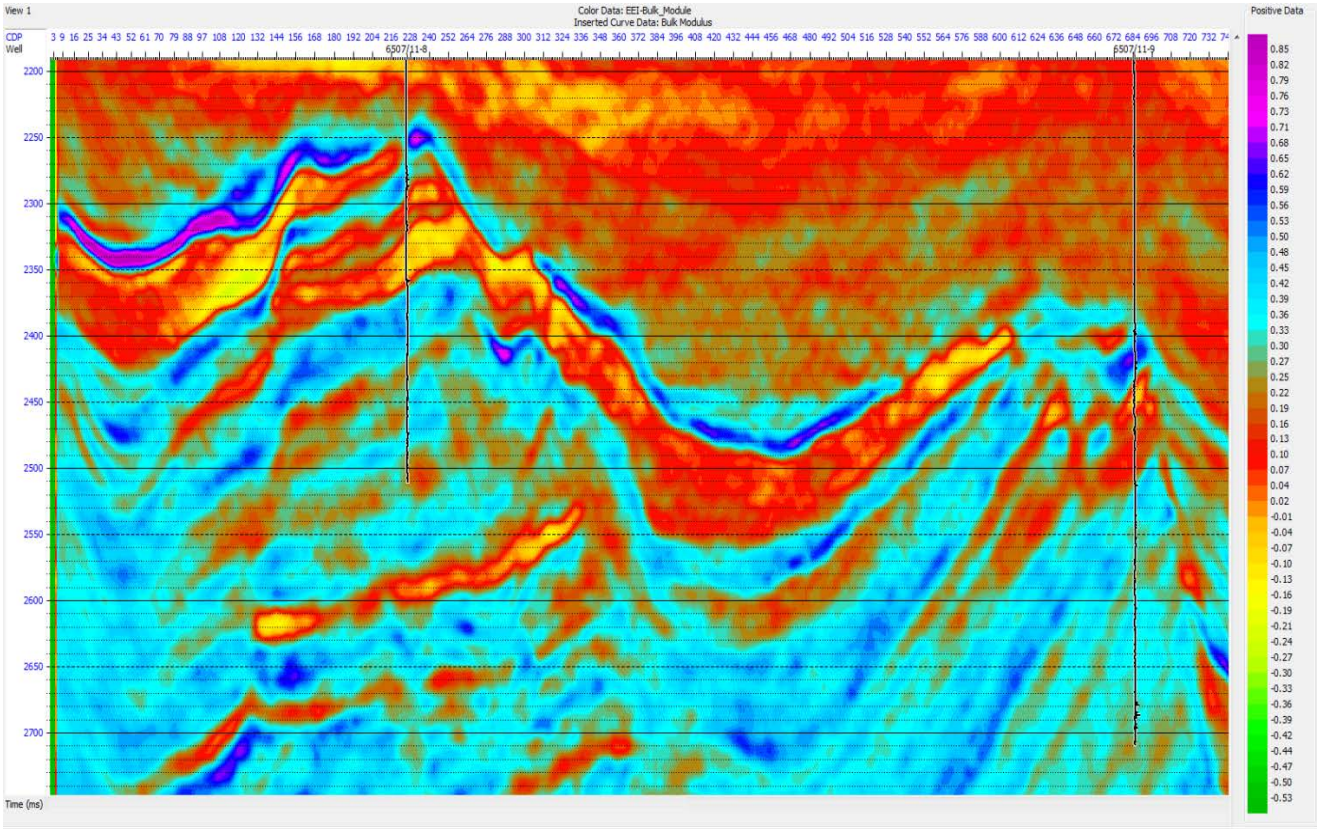

Figure 4.11: EEI bulk modulus attribute ($\chi = 17°$)

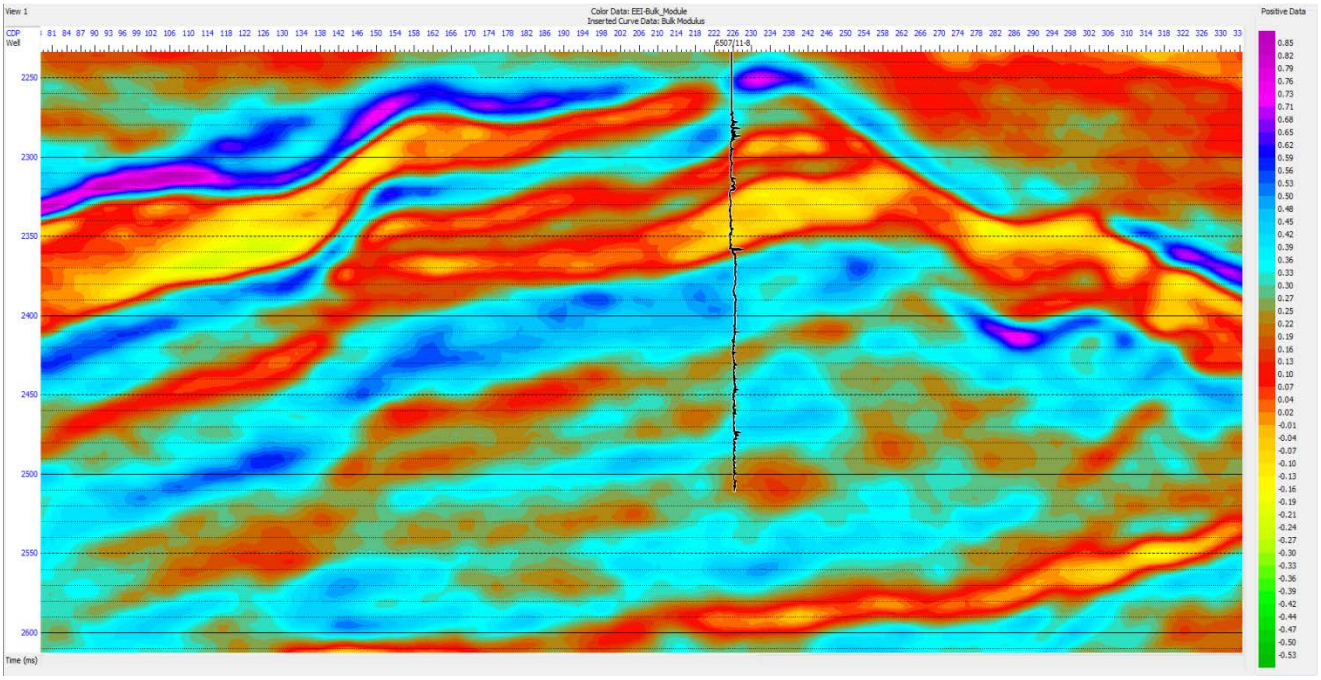

Figure 4.12: Expanded view of EEI bulk modulus attribute around well 11-8 ($\chi = 17°$)

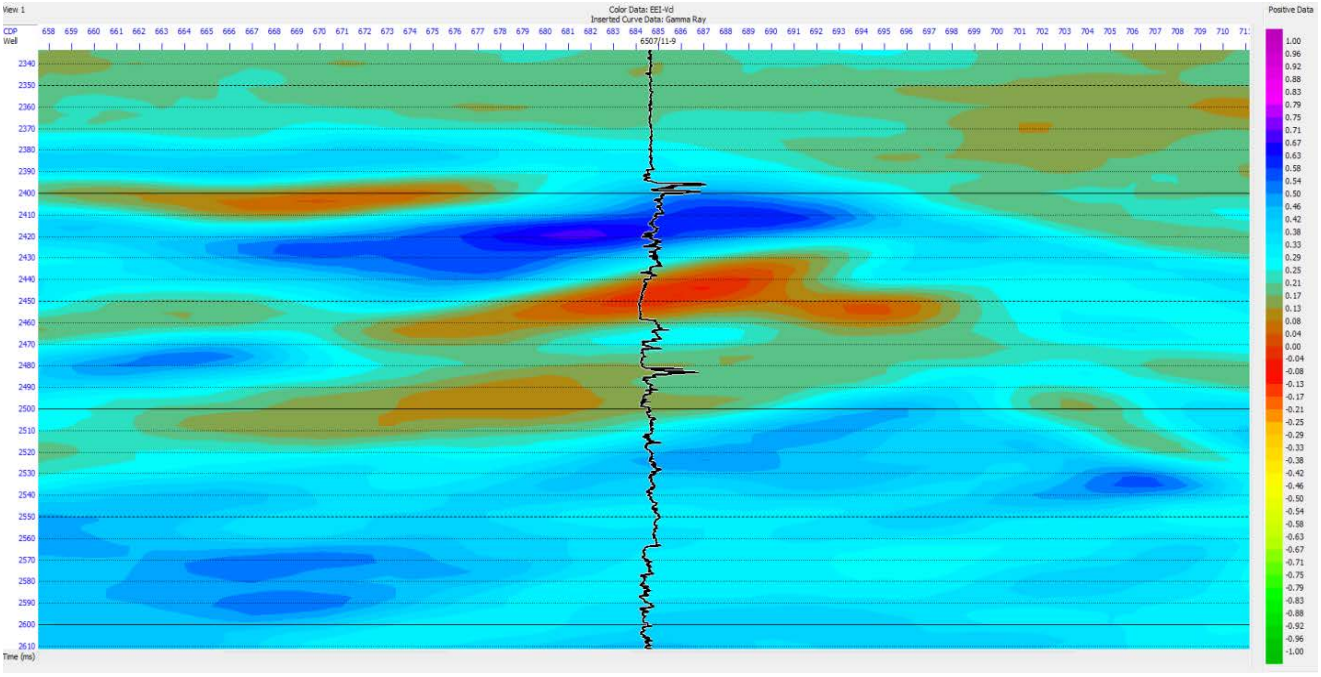

Figure 4.13: Expanded view of EEI V_{Clay} attribute around well 11-9 ($\chi = 13°$)

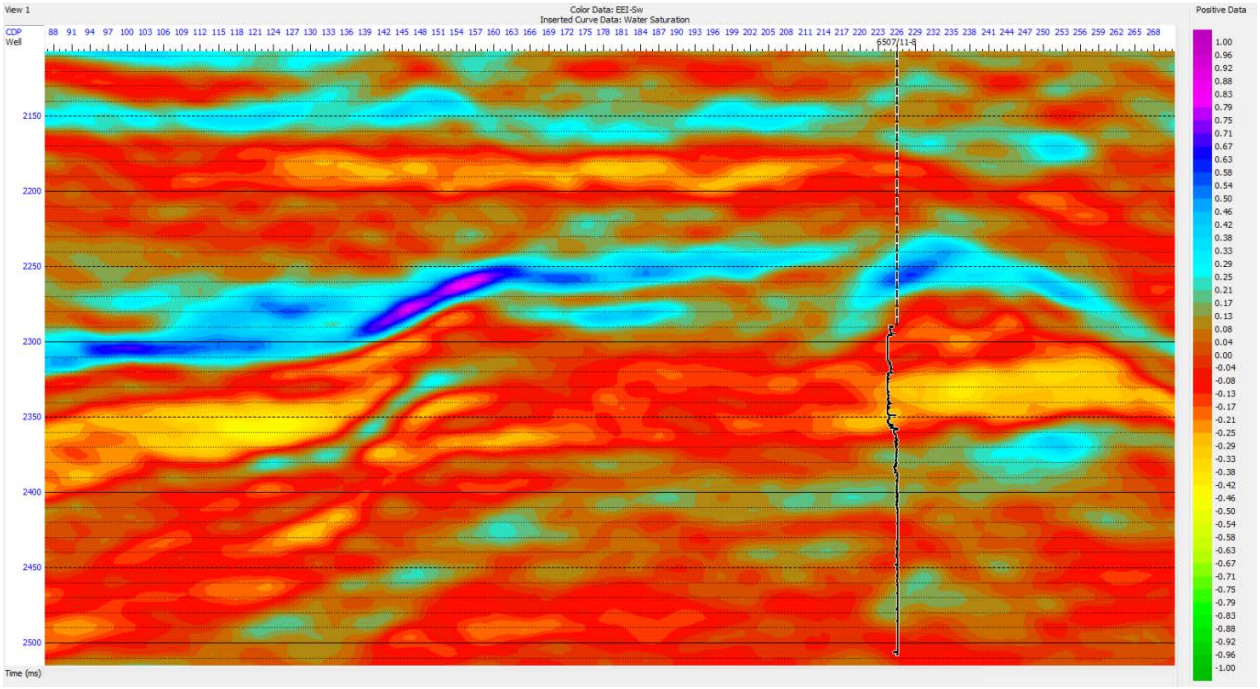

Figure 4.14: Expanded view of EEI S_w attribute around well 11-8 $(\chi = 43°)$

The EEI attributes for shear modulus at $(\chi = -53°)$ are presented on Figure 4.15 which correlate with shear modulus log (shear modulus is independent of fluid).

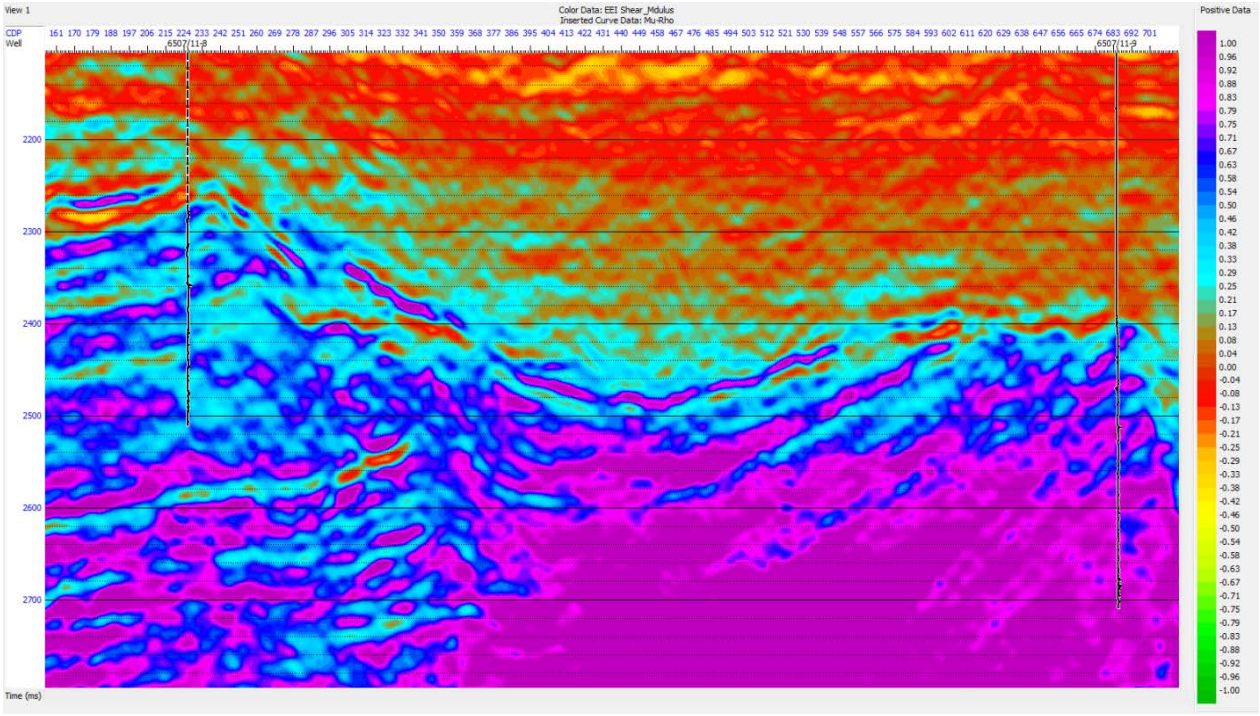

Figure 4.15: EEI shear modulus attribute $(\chi = -53°)$

5 Discussion

In this chapter the results of this study will be discussed and a further study with more focus on specific area will be suggested. As mentioned in the previous chapter, according to EEI volume results, the gas discoveries in the two wells were clearly identified in the EEI sections. Another important finding was that similar anomalies are above the reservoir or away from the well locations.

The single most striking observation to emerge from the Lambda and V_P/V_S EEI attributes is a probable prospect area with low V_P/V_S and Lambda-Rho has been identified close to well 11-8 location. Anomaly 1 indicates the location of drillable prospect zone (Figure 5.1). Gas accumulation is one possible reason for this anomaly, thereby creating an area of interest. This zone could, therefore, be recognized in its own right for potential gas production.

According to the available well report, the lithology down to sand reservoir (which occurs at ~2416 m) was mainly claystone with no reservoir quality (npd.no). One unanticipated finding was that, anomaly 2 was found in above the gas reservoir around well 11-8 location highlighted in Figure 5.1. Surprisingly this anomaly also captured by polygon in the cross plot of EEI V_P/V_S volume versus EEI Lambda-Rho volume (Figure 4.10). Lack of well log data has limited our interpretation ability and makes it difficult to explain this result.

The EEI lambda-Rho section has a normalized color scale. In a QI study we aim to relate, calibrate or connect some properties (quantitative) between our inversion products (in this case LR) to actual values calculated at well locations. The EEI inversion results could suggests that a weak link may exist between anomaly 2 and gas leakage from the reservoir. One possible explanation is due to some amount of gas movement from the sandstone reservoir to above formation causing this kind of anomaly. Gas leakage will yield deem seismic data (it means we are unable to see any reflectors in leakage area).

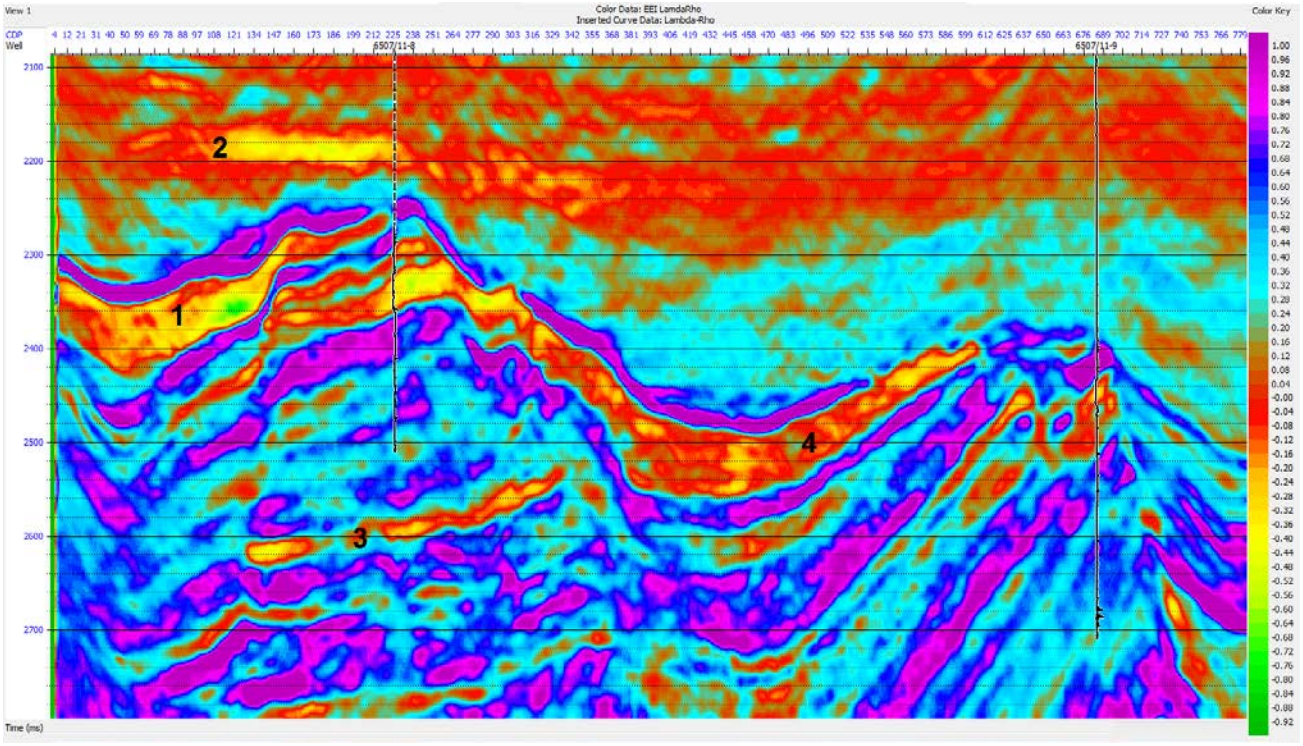

Figure 5.1: EEI Lambda-Rho (LR) at optimum chi angle

This type of anomalies should always be assessed in 3D seismic within the context of structure, however since 3D seismic was not available for this study, by only judging from the inverted section; it doesn't seem to be the leakage case. It is important to bear in mind that the interpretation of LR attribute alone is not easy since it can be interpreted as a range of lithologies or lithologies with different pore fluid material, hence caution must be applied, as the findings might not be transferable to facts. Anomaly 2 can be better interpreted if we compare it on MR (EEI Mu-Rho) values at the same place. There are, however, other possible explanations like lithology effect witch are discuss in the following pages as the most likely causes of anomaly number 2.

As can be seen from the Figure 5.1 a flat spot could be identified below the gas discoveries (well 11-8 location) (anomaly number 3). Generally "when a horizontal reflector crosses dipping stratigraphy we may have an instance of a horizontal fluid contact making an impedance contrast with the surrounding geology" (McQuillin, R., Bacon, M., Barclay, W, 1984). It seems possible from EEI inversion outcomes that this result is due to gas/water interface since, as discussed earlier, the velocity and density for gas filled reservoir are normally much lower than for water

filled reservoir. Therefore this anomaly could be related to circumstantial evidence for hydrocarbons accumulation. However this is weak interpretation again, according to Norwegian Petroleum Directorate (npd.no) and published wellbore report, since they have observed gas/water contact in the well, then we cannot expect flat spot deeper than the contact. Anomaly 3 follows the structural dips and is most likely due to geology aspects (stratigraphy). It might be related to presence of coal in Åre formation (oldest penetrated formation) which contains some amount of gas.

Another interesting anomaly is the one in the synclines adjacent to structure traps defining the reservoirs (anomaly number 4 in Figure 5.1). It seems the anomalies in the syncline are syntectonic (Alaei, 2013). This means that while the faults were moving the blocks the sediments deposited, so we can see the thickness variations which are not caused by erosion at the top because the reflectors are not truncated. It seems that this anomaly couldn't be directly related to hydrocarbon prospect and geology is the most likely cause of this occurrence.

One question that needs to be answered, however, is: are those similar anomalies above or below the gas sand reservoir area related to another reservoir, hydrocarbon accumulation/leakage, or they are caused by lithology effect or other sources? (Figure 4.6 and Figure 4.8). As discussed above, there are several possible explanations for this. Another one would be that presence of soft shale/hot shale, shallow overburden or digenetic effect that may have caused observed low values for lambda-Rho. We should also pay attention to the extent of the anomaly. Although we are looking on a 2D line but the anomaly (anomaly 2) is limited and usually shale lithologies extended spatially in larger areas than sands (Alaei, 2013). In addition, the reason for low V_P/V_S value outside the hydrocarbon reservoir may have something to do with layers which are well consolidated/cemented. In order to overcome the similar anomalies challenge we should study EEI attributes in combination with well log data. This combination provides some support for EEI attributes and well log property correlation.

In case of lack of well log data or when data do not match with EEI anomalies, we cannot trust inversion result. However this could provide abundant room for further progress and evaluate the risk factors for each of the uncertain area in the prospect zone. It is important to bear in mind the high uncertainty in these respond demand that data interpreted with great caution because of

probable pitfall. That is to say, the well logs should be used as quality control at the well location; if the well logs and associated EEI attributes reasonably match then we can confidently link the impedance to the reservoir quality. For instance, as shown in Figure 4.6 and Figure 4.8, our rock physic study represent that low V_P/V_S and Lambda-Rho correspond to gas discoveries which are perfectly fit with related EEI volumes.

Table 5.2 summarizes the finding results from extended elastic impedance study. From the Table 5.2 we can see that the gas discoveries in two wells are identified in most of the EEI sections. In addition, other anomalies which have discussed earlier are also repeated on some EEI sections.

	EEI V_P/V_S	**EEI Lambda-Rho (LR)**	**EEI Mu-Rho (MR)**	**EEI bulk modulus**	**EEI S_W**	**EEI V_{Clay}**
Gas discovery in well 11-8	*	*	*	*	*	*
Gas discovery in well 11-9	*	*	*	*	*	*
Anomaly 1	*	*	*	*	*	*
Anomaly 2	*	*		*		
Anomaly 3	*	*	*	*		*
Anomaly 4	*	*		*		

Table 5.1: Summarize presence or absence of gas discoveries and observed anomalies within different EEI inversion volumes.

This research has in turn raised many questions in need of further investigations. It is therefore, recommended that further research be undertaken in the following areas:

Further work needs to be carried out to establish scaled reflectivity seismic spectrum at each well location and cross correlate with the desired reservoir reflectivity parameter to determine the optimum χ angle. By comparing the scaled reflectivity method along with EEI spectrum method (method used in this work) we are able to evaluate the probable errors, fix possible lapse and obtain strongest anomaly at optimum fluid angle. To do this, we should have angle gather

volume and determine accurate intercept (A) and gradient (B). In addition, it might be possible to study on sensitivity of EEI outcomes when K values vary in the future investigations.

Future research should concentrate on the investigation of an algorithm generated from Gaussian statistical models of AVO intercept and gradient data for the purpose of determining the most anomalous seismic samples. Transformation of intercept and gradient to extended elastic impedance could potentially provide more insights for anomaly hunting and identification of the AVO background trend. It would be interesting to compare the anomalousness of EEI results with intercept and gradient outcomes.

Recent studies have revealed the weakness of EEI application for fluid discrimination in carbonate reservoir (Peng at el. 2008). It has been demonstrated that both gas bearing zone and water bearing zone have low EEI values in carbonate reservoir even under optimal project angle. A future study could assess and develop recently published approach called multi angle elastic impedance (MEEI) and investigate the change trend of EEI series within the range of incident angles for gas and water differentiation.

6 Conclusion

Well log data can provide valuable information in defining a reservoir and other important intervals in the well. Another key element is to understand the rock physics at the well locations. Integration of petrophysics with rock physics allows geoscientist to identify seismic anomaly associated with hydrocarbon accumulation or other reasons such as lithology effects and intelligently assess the risk and opportunities involved.

In recent years the inversion technique were well proven as worthy effort to justify placement of the well. Higher resolution outcomes with much less ambiguity resulting from integration study of extended elastic impedance (EEI) inversion along with additional pre stack attributes and different inversion techniques can give rise to a better reservoir valuation. More accurate results can lead to reducing the risk for successful field development by placing new wells in the most appropriate trajectory.

There are two main goals in interpreting inversion data: lithology and fluid identification (called QI or LFP), the main link for us to validate the interpretation or reduce uncertainty or address non-uniqueness of inversion is to link our interpretation to well data through rock physics.

In this study, well logs, rock physics cross plots and seismic inversion have been investigated for hydrocarbon and analyzed by extended elastic impedance method (EEI).

This study has given an account of and the reasons for the widespread use of extended elastic impedance (EEI) application for pre fluid and lithology prediction. The purpose of the current study was to assess how EEI inversion incorporates with petrophysical data and rock physics analysis to discriminate between lithology and fluid content and thereby improve reservoir characterization.

The results of this research support the idea that EEI can enhance interpretability and is a feasible approach to obtain detail reservoir delineation. EEI successfully identified and delineated gas sand reservoir in the study areas. Taken together, these results suggest the preference of using

multiples EEI attributes instead of single fluid and lithology attributes for the prospect assessment.

The most evident finding of this study would be that the robust EEI results suggest this approach as a really efficient and worthy effort for hydrocarbon differentiation and generating new prospects in calstic environment (anomalies away from the well locations); however, it is important to emphasize that for final decision making and more detailed prediction of specific reservoir properties, seismic inversion (simultaneous inversion) seems to be more appropriate. Also more detailed study with different techniques (e.g. AVO attributes) needs to be undertaken to evaluate possible options and authenticate EEI outcomes. In other words, EEI can be an excellent precursor for more detailed seismic inversion studies.

Finally, a number of caveats need to be noted regarding the present study. First, correlation coefficient study for different curves is a major step in EEI application and must be viewed with great care as any mistake in pervious calculation will ruin the correlation analysis. Second, the rapidly varying geology (both vertically and laterally) often makes the EEI interpretation as a difficult task. We should note that EEI inversion technique need additional information to enhance delineation of reservoir. Under this situation impedance value of the non-reservoir areas considerably overlap those of reservoir sand area and are easily misinterpreted. We should consider the EEI inversion technique cannot stand alone and to avoid probable pitfalls, additional information about rock physics of the area is required.

Bibliography

Alaei, B. (2013, June). Interpretation of extended elastic impedance (EEI) results. (S. A. Gharaee Shahri, Interviewer)

Arsalan, Syed., Yadav, Ashok. (2009). Application of extended elastic impedance: A case study from Krishna-Godavari Basin, India. *The Leading Edge, 28*(10), 1204-1209.

Avseth, P., Dvorkin, J., Mavko, G., and Rykkje, J. (2000). Rock physics diagnostic of North Sea sands: Link between microstructure and seismic properties. *Geophysical Research Letters, 27*(17), 2761-2764.

Avseth, P., Mukerji, T., Mavko, G. (2005). *Quantitative seismic interpretation: Applying rock physics tools to reduce interpretation risk.* Cambridge University Press.

Avseth, P., Ødegaard, E. (2004). Well log and seismic data analysis using rock physics templates. *First break, 22*(10), 37-43.

Awosemo, O. O. (2012). *Evaluation of elastic impedance attributes in offshore high island, gulf of Mexico (Master dissertation, University of Houston).* Houston: Universty of Houston.

Castagna, J. P. (1997). Principles of AVO crossplotting. *The Leading Edge, 16*(4), 337- 342.

CGGVeritas. (n.d.). *KnowledgeBase.* Retrieved March 2013, from CGGVeritas: http://www.cgg.com/knowledgebase.aspx?cid=861

Chi, Xin-Gang., Han, De-Hua. (2009). Lithology and fluid differentiation using rock physics template. *The Leading Edge, 28*(1), 1424-1428.

Connolly, P. (1999). Elastic impedance. *The Leading Edge, 18*(4), 438-452.

Connolly, P. (2010). Robust workflows for seismic reservoir characterisation. *CSEG Recorder, 35*(4), 7-10.

Connolly, P., Schurter, G. J., Davenport, M. (2002). Imaging and quantifying turbidites sand systems in deep water angola using extended elastic impedance. *Offshore Technology Conference.* Houston, Texas: Offshore Technology Conference.

David, C., Ravalec-Dupin, M. (2007). *Rock physics and geomechanics in the study of reservoirs and repositories.* The Geological Society of London.

Ezequiel, G., Tapan, M., Gray, M. (2003). Near and far offset P-to-S elastic impedance for discriminating fizz water from commercial gas. *The Leading Edge, 22*(10), 1012-1015.

Francis, A. M. (2002). Deterministic inversion: overdue for retirement? *PETEX 2002 Conference and Exhibition.* London, UK: PETEX.

Francis, A. M. (2003). Stochastic seismic inversion: solving large problem. *IAMG Conference.* Portsmouth, UK: IAMG.

Francis, A. M. (2006). Understanding stochastic inversion: part 1. *First Break, 24*(11), 69-77.

Francis, A., Hicks, G. J. (2006). Porosity and shale volume estimation for the Ardmore field using extended elastic impedance,. *EAGE.* Vienna: EAGE.

Goodway, B., Chen, T., Downton, J. (1997). Improved AVO fluid detection and lithology discrimination using Lamé petrophysical parameters; "λρ", "μρ", "λ/μ fluid stack", from P and s inversions. *SEG Technical Program Expanded Abstracts*, 183-186.

Grana, D., Dvorkin, J. (2011). The link between seismic inversion, rock physics and geostatistical simulations in seismic reservoir charracterization studies. *The Leading Edge, 30*(1), 54-61.

Greenberg, M. L. (1992). Shear-wave velocity estimation in porous rocks: Theoretical formulation, preliminary verification and applications. *Geophysical Prospecting, 40*(2), 195-210.

Gutierrez, Mario., Dvorkin, Jack., Nur, Amos. (2000). Rock physics characterization of a Tertiary fluvial reservoir, La Cira-Infantas oil field (Colombia). *SEG Expanded Abstracts*, 1643-1646.

Hazim, H., Al-Dabagh., Alkhafaf, Shireen. (2011). Comparison of Kρ and λρ in clastic rocks, A test on two wells with different reservoir-quality stacked sands from West Africa. *The Leading Edge, 30*(9), 986-994.

Hicks, G. J., Francis, A. (2006). Extended Elastic impedance and its relation to AVO crossplotting and Vp/Vs. *EAGE Vienna.* Vienna: EAGE.

Ishiyama, Tomohide., Ikawa, Hidemasa., Belaid, Kamel. (2010). AVO applications for porosity and fluid estimation of carbonate reservoirs offshore Abu Dhabi. *First Break, 28*(2), 93-100.

Kemper, M. (2010). Rock physics driven inversion: the importance of workflow. *First break, 28*(10), 69-81.

Kemper, M., Huntbatch, N. (2011). From inversion results to reservoir properties. *AAPG International Conference and Exhibition.* Milan, Italy: AAPG.

Krygowski, D. (2004). *Basic Well Log Analysis.* The American Association of Petroleum Geologists.

Latimer, Rebecca., Davison, Rick., Van Riel, Paul. (2000). An interpreter`s guide to understanding and working with seismic-derived acoustic impedance data. *The Leading Edge, 19*(3), 242-256.

Li, Xin-G., Han, D. H., Liu,J., McGuire, D. (2005). Inversion of Sw and porosity from seismic AVO. *SEG* (pp. 1307-1310). Houston, Texas: SEG Expanded Abstracts.

Mallick, S. (2001). AVO and Elastic Impedance. *The Leading Edge, 20*(10), 1094-1104.

McQuillin, R., Bacon, M., Barclay, W. (1984). *an introduction to seismic interpretation : Reflection seismic in petroleum exploration* (Second edition ed.). London: Graham & Trotman.

Naves, F.A., Mustafa, H.M., Rutty, P. M. (2004). Pseudo-Gamma Ray Volume from Extended Elastic Impedance Inversion for Gas Exploration. *The Leading Edge, 23*(6), 536-540.

npd.no. (n.d.). Retrieved from Norwegian Petroleum Directorate: http://www.npd.no/en/

Ostrander, W. J. (1984). Plane-wave reflection coefficients for gas sands at nonormal angle of incidence. *Geophysics, 49*(10), 1637-1649.

Pendrel, J. (2006). Seismic inversion - A critical tool in reservoir characterization. *Scandinavian oil-gas magazine, 5*(6), 19-22.

Promero Pelaez, A. S. (2012). *Prediction of reservoir quality with seismic attributes in Eocene sunmarine conglomerates, Mexico (Master dissertation, University of Oklahoma).* Oklahoma: University of Oklahoma.

Quakenbush, M., Shang, B., Tuttle, C. (2006). Poisson impedance. *The Leading Edge, 25*(2), 128–138.

Russell. (1999). AVO adds flavor to seismic soup. *AAPG Explorer, 18*(5), 112-117.

Russell, B. (1988). *Introduction to seismic inversion methods.* SEG Course Notes.

Russell, B. (2005). *Strata workshop: theory and exercises in seismic inversion and AVO.* Published Lecture Notes.

Russell, B., Hampson, D. (2006). The old and the new in seismic inversion. *CSEG Recorder, 31*(1), 5-11.

Russell, Brian., Hampson, Dan., Bankhead, Bradley. (2006). An inversion primer. *CSEG recorder, 31*(2), 96-103.

Russell, Brian., Hedlin, Ken., Hilterman, Fred., Lines, Laurence. (2001). Fluid-property discrimination with AVO: a biot-Gasmmann prespective. *CREWES research report, 13*(3), 403-419.

Schlumberger. (1972). *Log interpretation: Vol I, Principles.* Schlumberger.

Sharma, R. (2013, March). Extended elastic impedance application. (S. A. Gharaee Shahri, Interviewer)

Sharma, Ritesh., Chopra, Satinder. (2012). Determination of elastic constants using extended elastic impedance. *GeoConvention 2012: Vision.* Calgary, Canada: GeoConvention.

Singleton, Scott., Keirsted, Rob. (2011). Calibration of prestack simultaneous impedance inversion using rock physics. *The Leading Edge, 30*(1), 70-78.

Smith, T. C. (2011). Practical seismic petrophysics: the effective use of log data for seismic analysis. *The Leading Edge, 30*(10), 1128-1141.

Smith, Tad., Corporation, Apache. (2011). Practical seismic petrophysics: The effective use of log data for seismic analysis. *the leading Edge, 30*(10), 1128-1141.

Technical Note, Earthworks-reservoir.com. (n.d.). Retrieved from Earthworks-reservoir.com: http://www.earthworks-reservoir.com

Tian, Lixin., Zhou, Donghong., Lin, Gulkang., Jiang, Longcong. (2010). Reservoir prediction using Poisson Impedance in Quinhuangdao, Bohai Sea. *SEG 2010 Annual Meeting* (pp. 2261-2264). Denver, Colorado: SEG.

Walls, Joel., Dvorkin, Jack., Carr, Matt. (2004). Well logs and rock physics in seismic reservoir characterization. *Offshore technology conference.* Houston, Texas: Offshore technology conference,OTC 16921.

Whitcombe, D. (2002). Elastic impedance normalization. *Geophysics, 67*(1), 60-62.

Whitcombe, D. N., Connolly, P. A., Reagan, R. L., Redshaw, T. C. (2002). Extended elastic impedance for fluid and lithology prediction. *Geophysics, 67*(1), 63-67.

Whitcombe, D.N., Fletcher, J. G. (2001). The AIGI crossplot as an aid to AVO analysis and calibration. *SEG* (pp. 219-22). San Antonio: SEG 2001 Extende Abstracts.

Xu, Yong., Chopra, Satinder., Lines, Larry. (2009). Lithology differentiation and bitumen/water separation in Athabasca oil sands. *CSEG Recorder, 34*(1), 27-32.

Yi, Ni., Kui, Zhang. (2004). the elastic impedance inversion method and its application in SLG gas field. *SEG 74th annual meeting.* Denver, Colorado: SEG.

Zhen-Ming, Peng., Ya-Lin, Li., Sheng-Hong, Wu., Zhen-Hua, He., Yong-Jun, Zhou. (2008). Discriminating gas and water using multi-angle extended elastic impedance inversion in carbonate reservoirs. *Chinese journal of geophysics, 51*(3), 639-644.

Appendix A: Various equations for shale volume calculation

Linear response ($V_{Shale} = I_{GR}$):

$$V_{Shale} = I_{GR} = \frac{GR_{log} - GR_{min}}{GR_{max} - GR_{min}}$$

GR_{min}= minimum gamma ray reading within clean facies (sand unit)

GR_{max}= maximum gamma ray reading within clay rich facies (shale unit)

The nonlinear responses:

Larionov (1969) for Tertiary rocks :

$$V_{Sh} = 0.083\ (2^{2.7 I_{GR}} - 1)$$

Steiber (1970):

$$V_{Sh} = \frac{I_{GR}}{3 - 2 \times I_{GR}}$$

Clavier (1971):

$$V_{sh} = 1.7 - [(3.38 - (I_{GR} + 0.7)^2)]^{\frac{1}{2}}$$

Larionov (1969) for older rock:

$$V_{Sh} = 0.33 \times (2^{2 I_{GR}} - 1)$$

Appendix B:

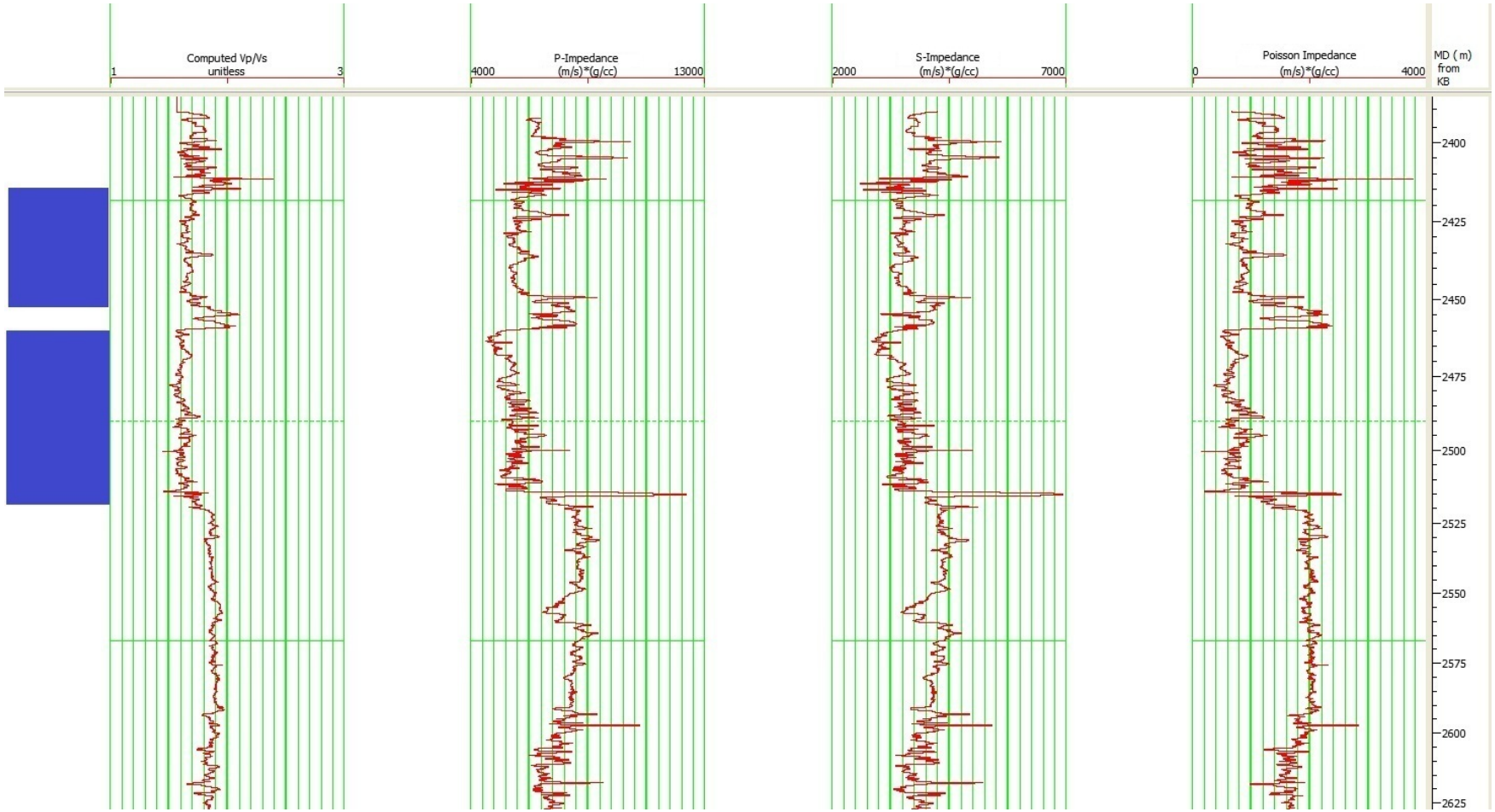

Figure B.1: From left to right:V_P/V_S, P-Impedance ,S-Impedance and Poisson Impedance log for well 11-8. Blue rectangles represent the hydrocarbon (gas) zones.

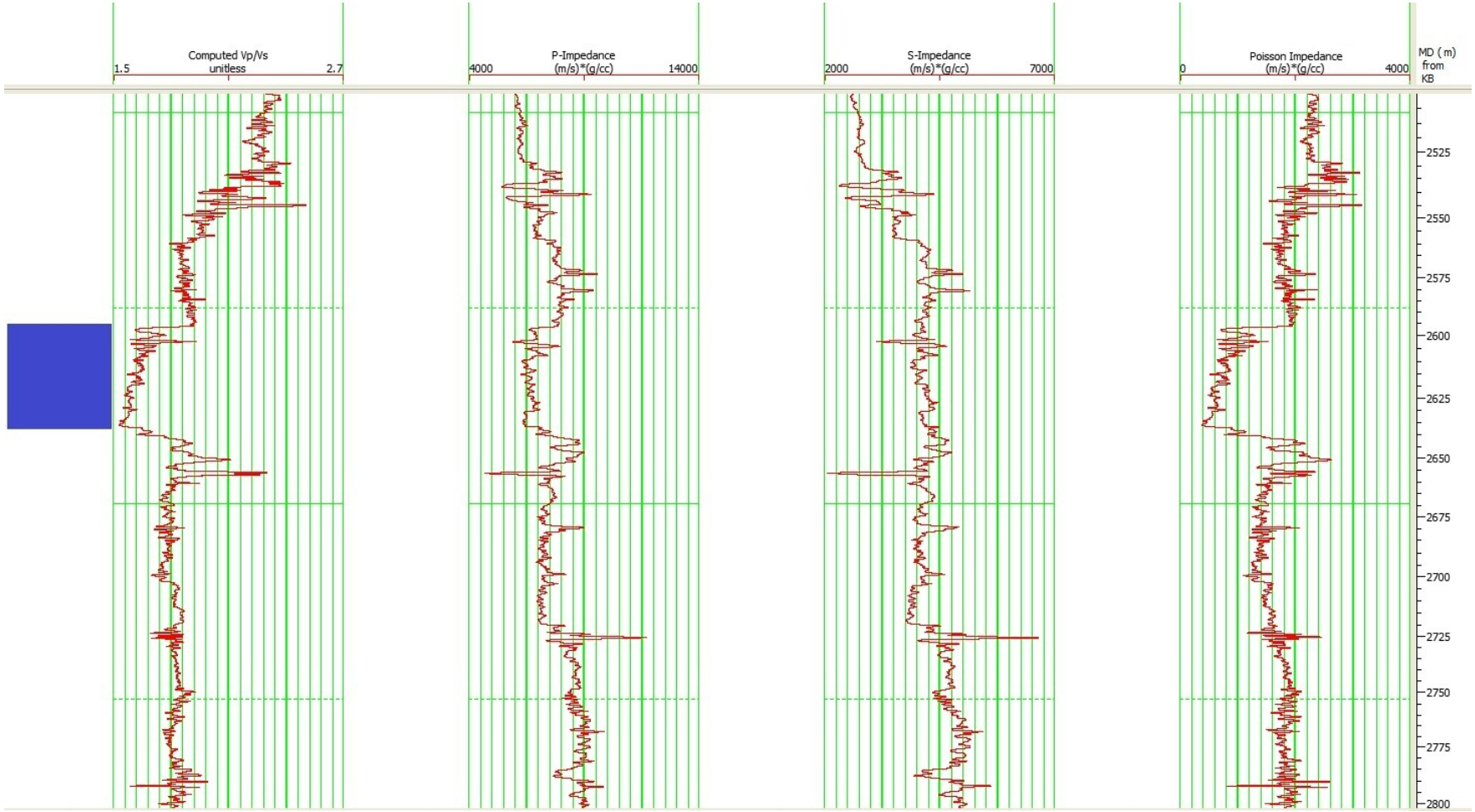

Figure B.2: From left to right:V_P/V_S, P-Impedance ,S-Impedance and Poisson Impedance log for well 11-9. Blue rectangle represents the hydrocarbon (gas) zones.

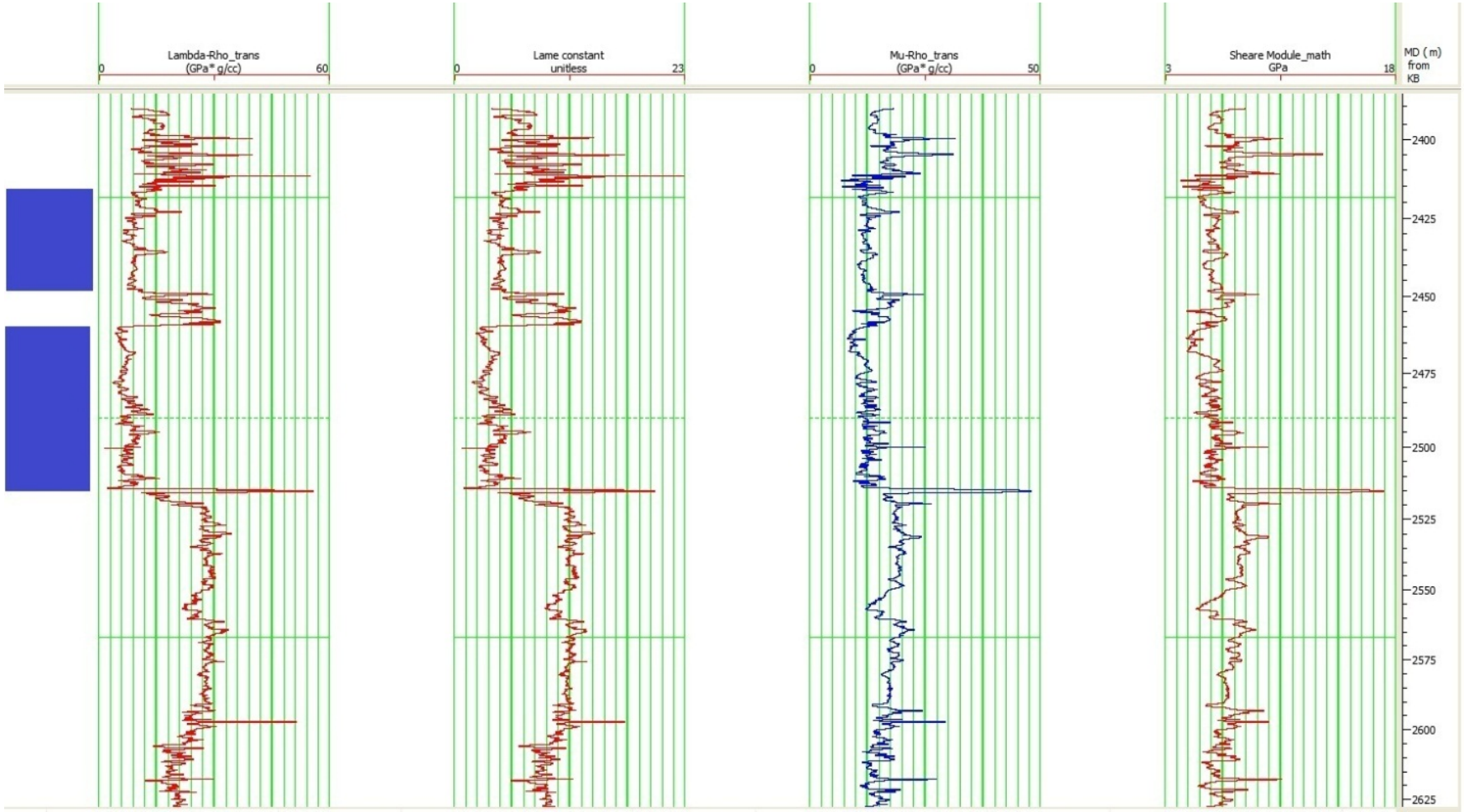

Figure B.3: From left to right: Lambda– Rho, lamé constant, Mu-Rho and shear module log for well 11-8. Blue rectangles represent the hydrocarbon (gas) zones

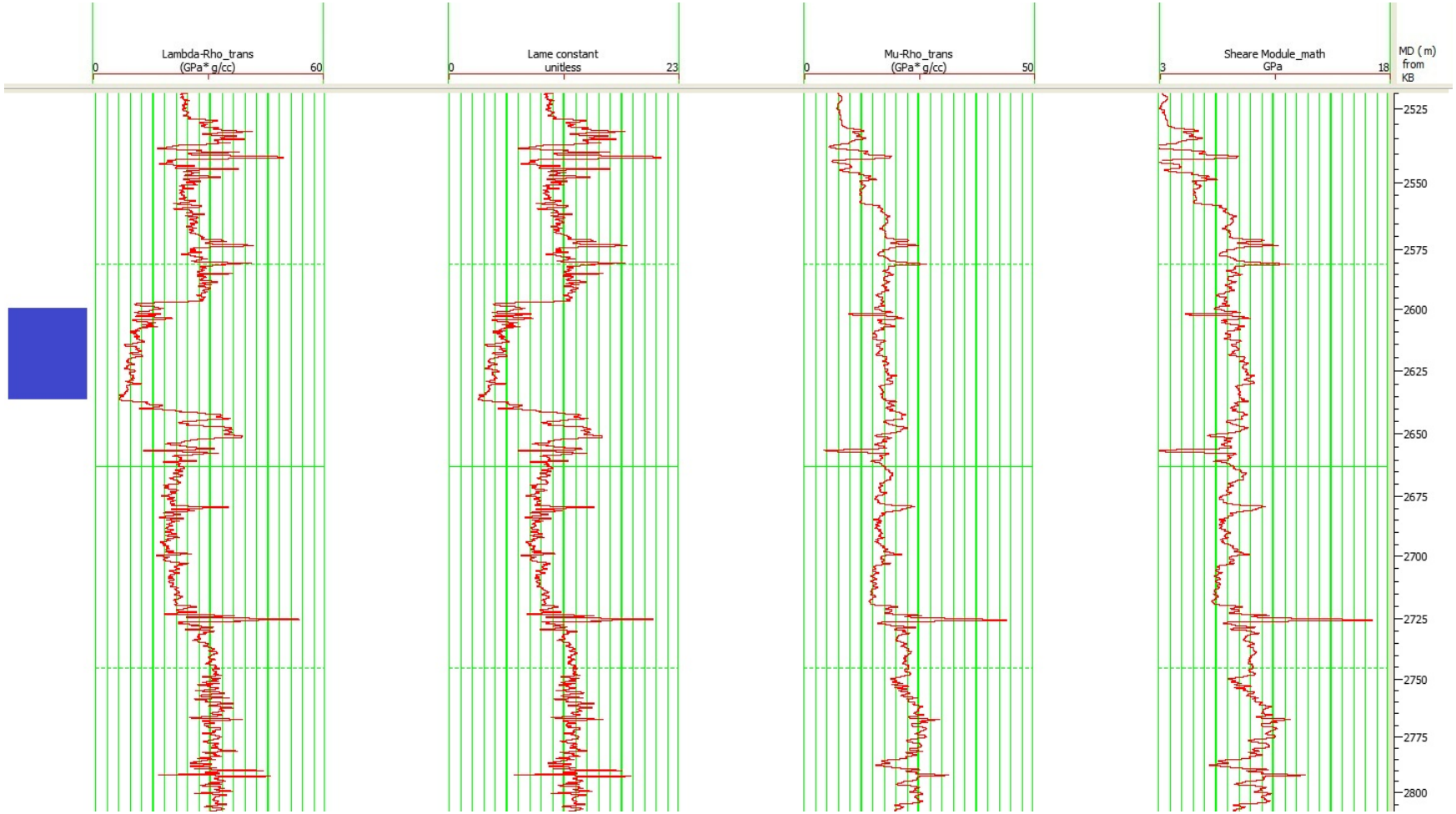

Figure B.4: From left to right: Lambda– Rho, lamé constant, Mu-Rho and shear module log for well 11-9. Blue rectangle represents the hydrocarbon (gas) zones.

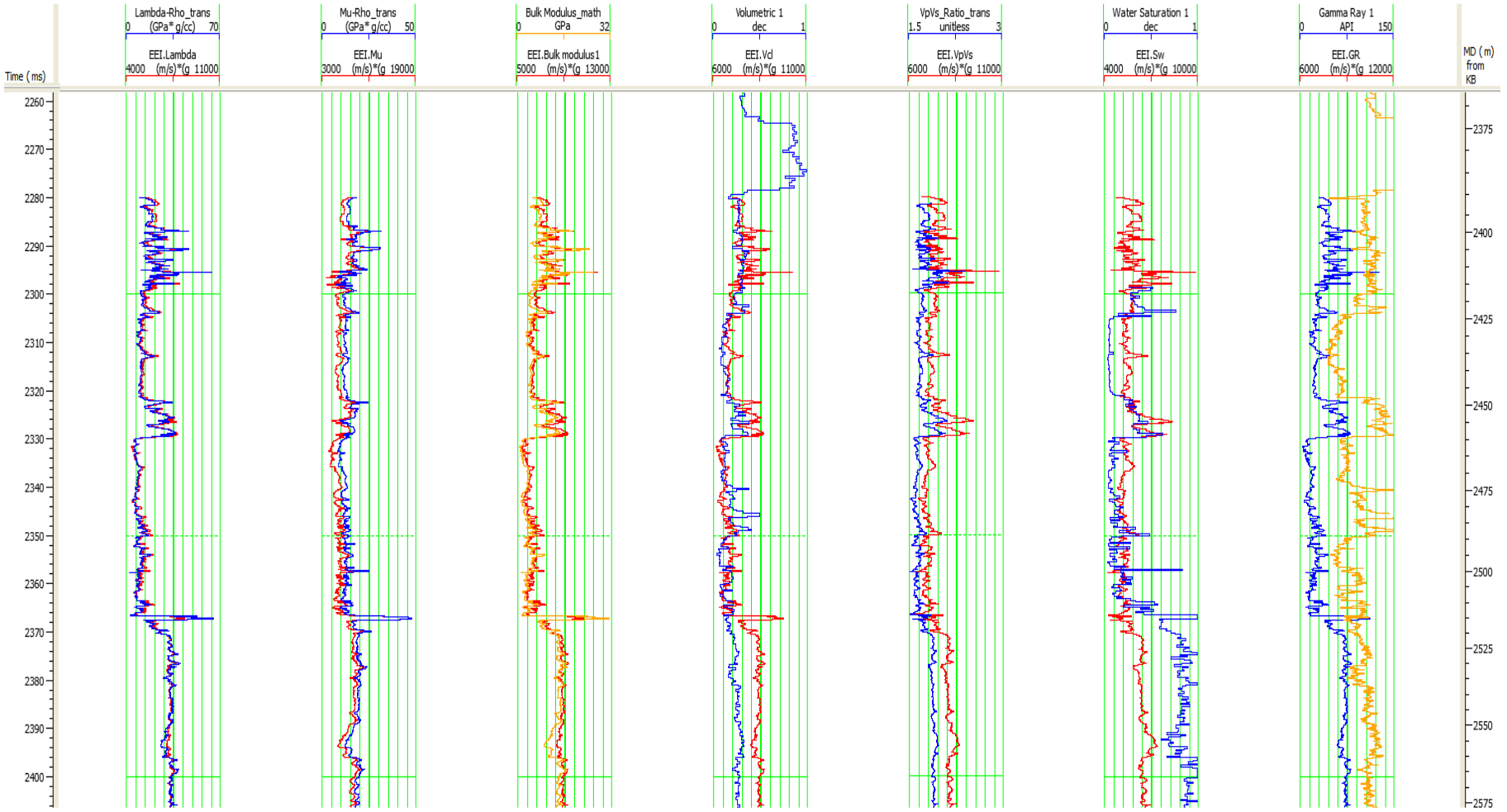

Figure B.5: Calculated EEI logs superimposed on target logs for well 11-8.

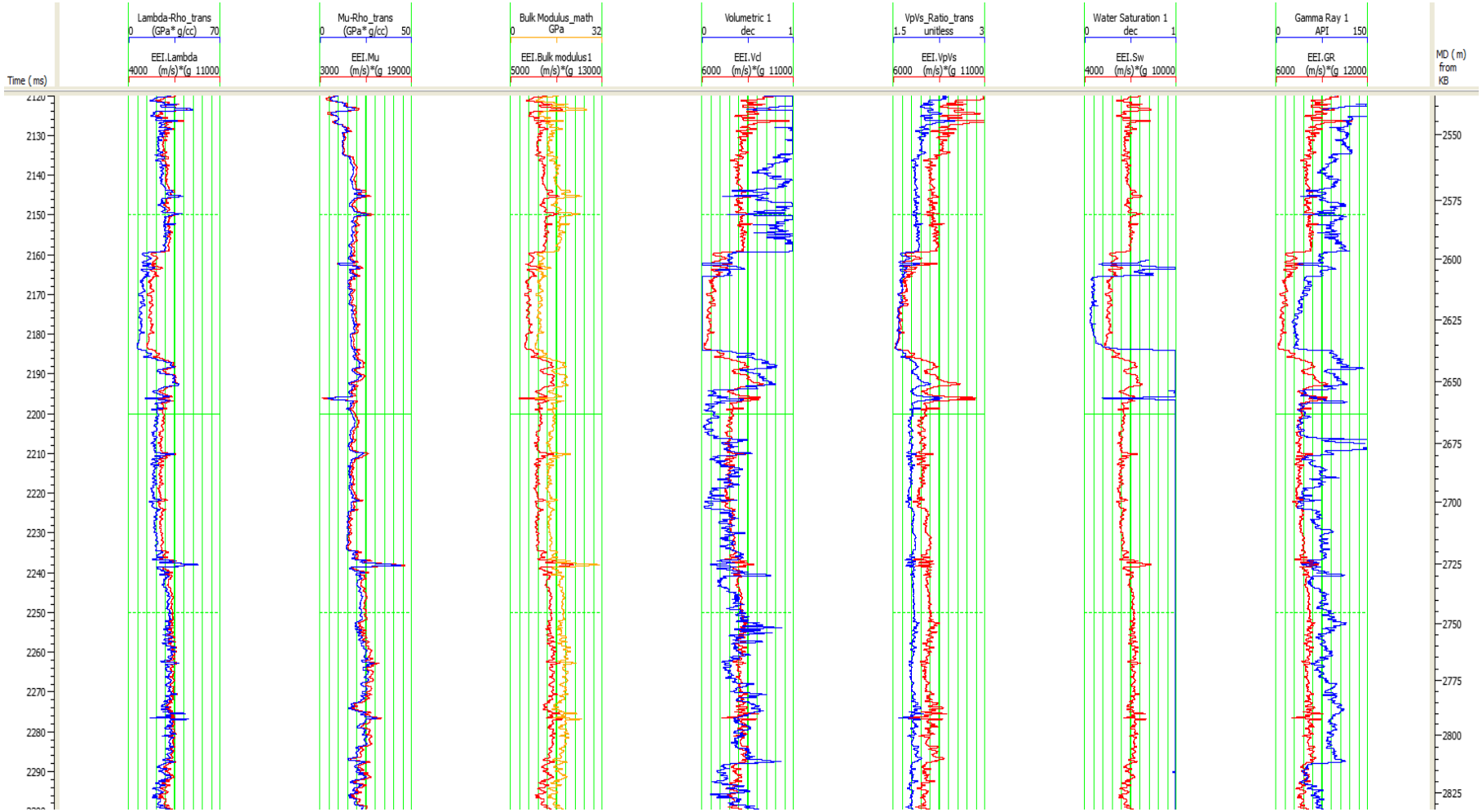

Figure B.6: Calculated EEI logs superimposed on target logs for well 11-9.